THE PERFORMANCE OF MEMBRANES IN A NEWLY PROPOSED RUN-AROUND HEAT AND MOISTURE EXCHANGER

A Thesis Submitted to the College of

Graduate Studies and Research

In Partial Fulfillment of the Requirements

For the Degree of Master of Science

In the Department of Mechanical Engineering

University of Saskatchewan

Saskatoon

By

Michael David Larson

PERMISSION TO USE

In presenting this thesis in partial fulfilment of the requirements for a Postgraduate degree from the University of Saskatchewan, I agree that the Libraries of this University may make it freely available for inspection. I further agree that permission for copying of this thesis in any manner, in whole or in part, for scholarly purposes may be granted by the professor or professors who supervised my thesis work or, in their absence, by the Head of the Department or the Dean of the College in which my thesis work was done. It is understood that any copying or publication or use of this thesis or parts thereof for financial gain shall not be allowed without my written permission. It is also understood that due recognition shall be given to me and to the University of Saskatchewan in any scholarly use which may be made of any material in my thesis.

Requests for permission to copy or to make other use of material in this thesis in whole or part should be addressed to:

Head of the Department of Mechanical Engineering

University of Saskatchewan

Saskatoon, Saskatchewan S7N 5A9

ABSTRACT

The growing cost of energy combined with the increasing energy demand has driven the need for more efficient energy use. Air-to-air energy recovery in buildings has been shown to provide substantial energy savings in many cases. A new type of air-to-air energy recovery system, known as a run-around energy exchanger (RAEE), and which has excellent potential for the retrofit market, has been proposed and numerically modelled for heat and moisture exchange by Fan et al. (2006). This thesis focuses on the material properties of semi-permeable membranes required for each RAEE exchanger core.

Two commercially available membranes are considered in this thesis: a spunbonded polyolefin manufactured by DuPont™ with the trade name Tyvek®, and a two layer polypropylene laminate material manufactured by the 3M™ Company with the trade name Propore™.

The moisture transfer effectiveness of the RAEE system depends mostly on the ability of its membrane to transfer water vapour. This effectiveness is investigated by measuring the vapour diffusion resistance of Tyvek® and Propore™ using a dynamic moisture permeation cell (DMPC). For Tyvek®, the average vapour diffusion resistance is 440 s/m, which corresponds to an expected typical RAEE energy recovery effectiveness of 52%. For Propore™, the average vapour diffusion resistance is 140 s/m, which corresponds to an RAEE effectiveness of 62% in the same exchanger system.

The air permeability is also measured using the DMPC with Tyvek® having a Darcy air flow resistance of 27 nm^{-1} and Propore™ having a Darcy air flow resistance of 111 nm^{-1}. The lower air flow resistance of Tyvek® is undesirable since air transfer is undesirable in the RAEE system.

The liquid penetration pressure is determined using a modified standard method that resembles the geometry of a membrane in the RAEE exchanger. It is found that the Propore™ has a liquid penetration pressure beyond the measurement capabilities of the apparatus (276 kPa); while the Tyvek® membrane has a liquid penetration pressure of 18 kPa which agrees well with published values.

The elastic moduli of the membranes are required to predict the membrane deflection under typical operating pressures and to properly size a support screen. The elastic modulus is determined using two tensile standards and a bulge test. The bulge test results are used in the design since the geometry of the bulge test better represents the situation of a pressurized membrane in the RAEE. The elastic modulus of Propore™ is found to be 20 ± 3 MPa and the elastic modulus of Tyvek® is found to be 300 ± 45 MPa. The values are used in subsequent calculations for sizing the square screen, where it is found that a screen with square openings of 12.7 mm (0.5 in.) is required to support the membrane.

The degradation of Tyvek® and Propore™ with UVC exposure is also investigated. It is found that both materials deteriorate when exposed to UVC radiation, and that the degradation is primarily a function of the exposure time and not the exposure intensity.

Considering all material properties tested, it is concluded that the Propore™ membrane is a better membrane choice for the RAEE than the Tyvek® membrane.

ACKNOWLEDGMENTS

I would like to foremost acknowledge my supervisors, C.J. Simonson and R.W. Besant for their time and continuing support throughout this research. Without their assistance and motivation this work would not have been possible.

I acknowledge the invaluable assistance of Chris James, Dave Deutcher, Dave Crone and Hans Steinmetz in facilitating the experimental component of this research.

I acknowledge Phil Gibson of the U.S. Army Soldier Systems Center for performing all dynamic moisture permeation cell (DMPC) tests and Jason Maley of the Saskatchewan Structural Sciences Center (SSSC) for performing all Raman spectroscopy and atomic force microscope measurements.

I acknowledge the Department of Mechanical Engineering, the Natural Sciences and Engineering Research Council of Canada and Venmar CES Inc. for their generous and much appreciated financial support.

.

This thesis is dedicated to my parents, Ron and Conni Larson, and to my loving fiancé, Deanna Fast.

Thank you for your continued love and support throughout my studies.

TABLE OF CONTENTS

page

LIST OF TABLES

LIST OF FIGURES

NOMENCLATURE

A	Area [m^2]
a	Membrane radius or half width [m]
b	Diameter of the sun 6.96 x 10^5 [km]
B	Mean distance from the sun to the earth's upper atmosphere 1.5 x 10^8 [km]
C	Concentration [kg/m^3]
c_p	Specific heat capacity [J/(g K)]
Cr^*	Heat capacity ratio
C_{sat}	Saturation concentration [kg/m^3]
C_v	Vapour concentration [kg/m^3]
$C_{v,sat}$	Saturation vapour concentration [kg/m^3]
ΔC	Concentration difference across the membrane [kg/m^3]
δC	Concentration difference from the inlet to outlet of the DMPC cell [kg/m^3]
$\Delta \overline{C}$	Log mean concentration difference across the DMPC cell [kg/m^3]
ΔC_a	Concentration difference across the membrane at side a of the DMPC cell [kg/m^3]
ΔC_b	Concentration difference across the membrane at side b of the DMPC cell [kg/m^3]
D_h	Hydraulic diameter [m]
D_m	Diffusion coefficient of the membrane [m^2/s]
Δp	Pressure difference [Pa]
D_{UVC}	Dose of the UVC bulb [kWs/m^2]
ΔW	Humidity ratio difference [$g_{water\ vapour}/kg_{dry\ air}$]
Δz	Membrane thickness [m]
E	Elastic modulus [MPa]
$E_{atm,250\rightarrow258}$	Emissive power of the sun at the earth's upper atmosphere between 250 nm and 258 nm wavelengths [W/m^2]
$E_{10\%}$	10% secant modulus [MPa]
$E_{2\%}$	2% secant modulus [MPa]
E_b	Emissive power of a black body [W/m^2]
$E_{b,atm}$	Emissive power of the sun at the earth's upper atmosphere [W/m^2]
$E_{b,sun}$	Emissive power of the sun [W/m^2]
E_{bulb}	Emissive power of the UV bulb [W/m^2]
e_f	Final gauge length of a tensile sample [mm]
e_o	Initial gauge length of a tensile sample [mm]
$F_{0\rightarrow\lambda}$	Fraction of energy up to the wavelength λ
g	Convective heat transfer coefficient [W/ (m^2 K)]
g_m	Convective mass transfer coefficient [kg/ (m^2 s)]
h	Deflection height [m]

H	Enthalpy [kJ/kg]
h_{fg}	Heat of vaporization [kJ/kg]
k	Thermal conductivity [W/ (m K)]
K_1	Curve fit constant - linear method
K_2	Curve fit constant - energy minimization method
k_d	Darcy permeability [m^2]
k_m	Vapour permeability of the membrane [kg/(m s)]
$\dot{m}''$	Mass flux [kg/(m^2 s)]
$\dot{m}$	Mass flow rate [kg/s]
M_r	Mass flow rate ratio
M_w	Molecular weight of water (kg/kmole)
N	Number of samples
NTU	Number of heat transfer units
NTUm	Number of mass transfer units
p	Pressure [Pa]
P_{atm}	Atmospheric pressure [Pa]
p_p	Liquid penetration pressure [Pa]
p_{sat}	Saturation pressure[Pa]
p_v	Vapour pressure [Pa]
$p_{v,sat}$	Saturation vapour pressure [Pa]
q	Heat transfer [W]
Q	True volume flow rate [cm^3/min]
Q_s	Indicated volume flow rate [cm^3/min]
R	Membrane bulge radius of curvature [m]
R	Universal gas constant [J/(kg kmole)]
R_{bl}	Vapour diffusion resistance of boundary layer [s/m]
R_D	Darcy air flow resistance [1/m]
Re	Reynolds number
R_m	Vapour diffusion resistance of membrane [s/m]
s	Arc length [m]
s_o	Initial arc length [m]
t	Membrane thickness [m]
T	Temperature [K]
t_{exp}	UV exposure time [days]
T_s	Reference temperature 273.15 [K]
t_s	Two tailed student t value for the 95% confidence interval
t_{solar}	Equivalent solar exposure time [days]
U	Overall heat transfer coefficient [W/(m^2 K)]
U_m	Overall mass transfer coefficient [kg/(m^2 s)]
U_x	Uncertainty of parameter x (where x is any calculated or measured value)

$U_{\bar{x}}$	Uncertainty of the mean of parameter x (where x is any calculated or measured value)
V	Velocity [m/s]
W	Humidity ratio [$g_{water\ vapour}/kg_{dry\ air}$]
x	Co-ordinate of the RAEE core parallel to the air flow [m]
X	Ratio of water mass to desiccant mass [kgw/kgd]
$\bar{x}$	Mean of parameter x (where x is any calculated or measured value)
x*	Dimensionless x co-ordinate
x_o	Dimension of the RAEE core in the x co-ordinate direction [m]
Y	Biaxial Modulus [MPa]
y	Co-ordinate of the RAEE core parallel to liquid flow [m]
y*	Dimensionless y co-ordinate
y_o	Dimension of the RAEE core in the y co-ordinate direction [m]
z	RAEE co-ordinate perpendicular to the membrane [m]
z_o	Dimension of the RAEE core in the z co-ordinate direction [m]

Greek Symbols

α	Dimensionless pre-stress
β	Dimensionless membrane thickness
γ	Bulge arc angular co-ordinate
δ_E	Standard deviation of E
$\delta\phi$	Humidity difference from the inlet to the outlet of the DMPC cell [%]
δ_m	Membrane vapour permeability [kg/(Pa s m^2)]
ε_a	Axial strain [mm/mm]
ε_γ	Strain in the γ direction [mm/mm]
ε_{lat}	Latent effectiveness
ε_o	Pre-strain [mm/mm]
ε_{sen}	Sensible effectiveness
ε_T	Total strain[mm/mm]
ε_t	Transverse strain [mm/mm]
ε_{tot}	Total effectiveness
η	Dimensionless deflection height
θ	Membrane in plane angular co-ordinate
λ	Wavelength [nm]
μ	Dynamic viscosity [kg/(m s)]
ν	Poisson's ratio
ξ	Dimensionless pressure
ρ	Air density [kg/m^3]
σ_γ	Stress in γ direction [MPa]
σ_o	Pre-stress [kPa]
σ_{sb}	Stefan-Boltzmann constant 5.67×10^{-8} [$W/(m^2\ K^4)$]

ϕ	Relative humidity [%]

Acronyms

AATCC	American Association of Textile Chemists and Colorists
AFM	Atomic force microscope
AHU	Air handling unit
ANSI	American National Standards Institute
ARI	Air-conditioning and Refrigeration Institute
ASHRAE	American Society of Heating Refrigerating and Air-conditioning Engineers
ASME	American Society of Mechanical Engineers
CAN/CGSB	Canadian General Standards Board
CFM	Cubic feet per minute [ft^3/min]
DAQ	Data acquisition system
DMPC	Dynamic moisture permeation cell
ePTFE	Expanded polytetrafluoroethylene
FPM	Feet per minute [ft/min]
HDPE	High density polyethylene
HVAC	Heating ventilating and air-conditioning
IAQ	Indoor air quality
ISO	International Standards Organization
JIS	Japanese Industrial Standards
LVDT	Linear variable displacement transducer
NASA	National Aeronautics and Space Administration
PC	Personal computer
PP	Polypropylene
PTFE	Polytetrafluoroethylene
PU	Polyurethane
RAEE	Run-around energy exchanger
RH	Relative humidity
SSSC	Saskatchewan Structural Sciences Centre
UTS	Ultimate tensile strength [MPa]
UV	Ultraviolet
UVA	Ultraviolet light from the 320 nm to 400 nm wavelengths
UVB	Ultraviolet light from the 290 nm to 320 nm wavelengths
UVC	Ultraviolet light from the 200 nm to 290 nm wavelengths
UVEC	Ultraviolet exposure chamber
UV-PCO	Ultraviolet photo-catalytic oxidation
VOC	Volatile organic compound
WVTR	Water vapour transmission rate [$kg/(m^2\ s)$]

CHAPTER 1
INTRODUCTION

Energy efficiency is becoming increasingly important in today's society. As a society, we spend a majority of our time indoors and therefore energy efficient buildings are at the forefront of an energy efficient future. The energy efficiency of a building is governed by many factors including, building materials, building use and building systems. A key to maximizing the energy efficiency in a building when mechanically conditioning air is the recovery of waste energy from exhaust air. Since both the temperature and relative humidity are controlled in buildings, recovery of both the thermal or sensible energy and moisture or latent energy is important. Energy and heat recovery systems using energy wheels, cross flow plates and heat pipes have been widely used to lower heating and cooling costs for buildings when the supply and exhaust ducts are adjacent (Besant et al., 2003). New applications in the heating ventilation and air-conditioning (HVAC) industry involving semi-permeable membranes for humidity control have also been recently developed. A unique liquid-to-air application has been presented by Scovazzo et al. (1998) and the use of semi-permeable membranes in an evaporative cooling application has been presented by Johnson et al. (2003). The numerical investigation of a plate-type air-to-air exchanger using semi-permeable membranes has been presented by Zhang et al. (1999); however, the author is not aware of any commercially available systems that use a completely contained run-around fluid to transfer both moisture and heat between remote exchangers.

A selection of the currently available systems is summarized in Figure 1.1 which is divided into four quadrants. Above and below the abscissa axis represents energy recovery and heat recovery systems respectively. Heat recovery refers to only sensible or heat transfer and energy recovery refers to combined sensible and latent or heat and mass transfer. The left and right sides of the ordinate axis represent systems with adjacent ducting and non-adjacent ducting respectively.

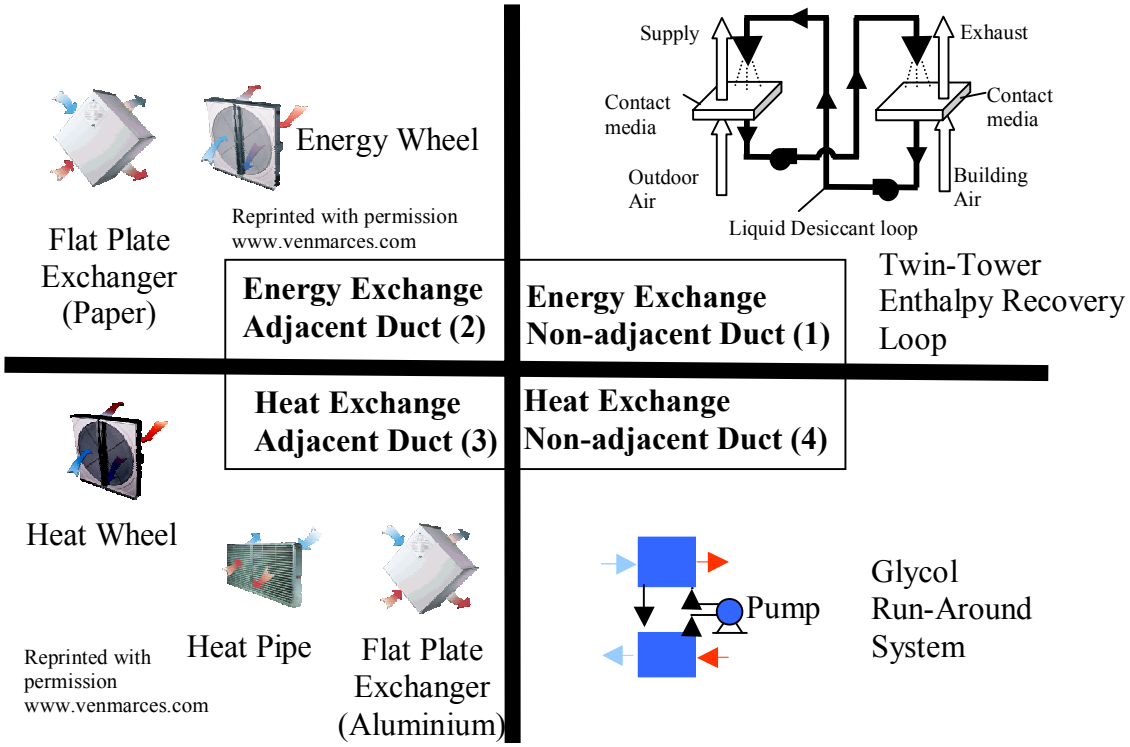

Figure 1.1. Schematic of available exchanger technologies highlighting the need for the RAEE system.

All of the exchangers shown in Figure 1.1 are commercially available technologies. The exchangers in quadrant 3 are the most common and are used in situations where the duct work is adjacent or passes through a common air handling unit (AHU). Plate type exchangers are made from common materials, such as aluminium or plastic and are

relatively inexpensive to manufacture. The run around exchanger of quadrant 4 comprises two liquid-to-air exchangers that are coupled by a fluid. This coupling fluid is typically glycol, and can be pumped throughout a building to facilitate the sensible exchange between two airstreams that are non-adjacent. The exchangers of quadrant 2 are newer technologies with the membrane plate exchanger having few manufacturers and relatively unknown performance (ASHRAE, 2004). The energy wheel is a well established technology that transfers both heat and moisture; however, it has the limitation of needing two side-by-side airstreams to pass through each side of a wheel. The twin tower energy recovery loop shown in quadrant 1 is the only system that provides total energy recovery and has the flexibility of non-adjacent duct placement. The disadvantages of this system include the need for demister pads to contain the salt solution, and its lack of performance data (ASHRAE, 2004).

When the supply and exhaust streams of an energy or heat recovery system need to be together it presents limitations on the placement of ducting in new building and limits the use of these systems in retrofit applications. This drawback of duct positioning can be overcome in the heat exchanger case by using a run around loop such as in quadrant 4 of Figure 1.1. However, the energy savings of a total energy recovery system such as those in quadrant 2 of Figure 1.1 are significantly greater than the savings of heat recovery alone. A new system with the placement versatility of the run-around and the performance characteristics of the energy recovery systems is considered in this thesis and is given the name: run around energy exchanger, or RAEE. A schematic of the combination of these two technologies is shown in Figure 1.2

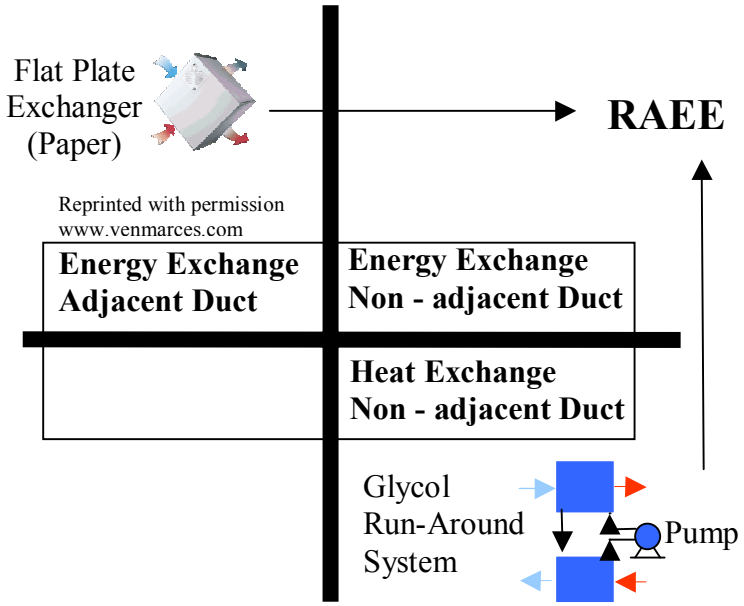

Figure 1.2. Schematic of the flat plate energy exchanger and glycol run-around system being combined to create the new RAEE system.

This configuration offers an alternative to the twin tower energy recovery loop of quadrant 1 in Figure 1.1. In contrast to the twin tower energy recovery loop, the RAEE system is fully enclosed so the salt solution is safely contained and no mist elimination is required. The contained salt solution means that there will be no cross contamination of the individual air streams, thus making the RAEE ideal for situations where cross contamination is critical. The exchanger core could also be more easily implemented into air handling units that currently use other plate type exchangers. In addition, the total effectiveness of the RAEE is predicted to be higher than the twin tower energy recovery loop (Fan et al., 2006).

The RAEE system is shown schematically in Figure 1.3. The system consists of two exchanger cores placed in the existing ducting of a building, one in the supply air stream and one in the exhaust air stream. The two cores are connected by a liquid desiccant

which flows in pipes and is controlled by a single pump that can be placed anywhere in the closed liquid system.

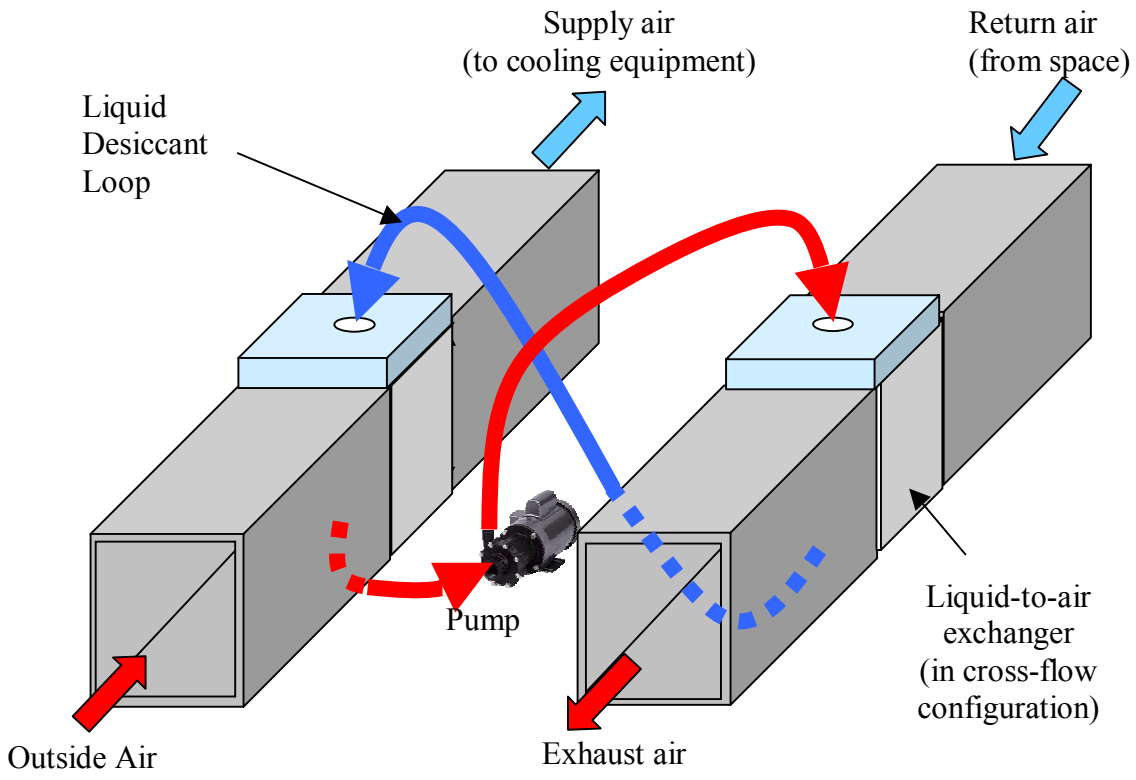

Figure 1.3. Schematic of the proposed RAEE system.

The closed desiccant loop that connects the individual exchangers facilitates the transfer of moisture as well as heat between the air streams, unlike the traditional run-around which exchanges heat only. To exchange this moisture between the air and solution the individual exchanger cores are made of a water vapour permeable membrane material. The moisture transfer is achieved through the vapour pressure gradient associated with the relative humidity difference between the salt solution and the air stream. This transfer of moisture reduces the latent load on the HVAC system.

Of interest in this thesis is an individual core from the RAEE system and more specifically the membrane used within the core. The properties and type of membrane used affect the design and performance of the completed system.

1.1 Background of the RAEE project

The exchanger described above has been numerically modeled by Fan et al. (2006) and Fan (2005). This numerical model allowed the calculation of the temperature and humidity contours within the individual exchangers, as well as the sensible, latent and total effectiveness of the individual exchangers and the overall system at a variety of operating conditions. Based on the success of the numerical simulation, plans were made to design a prototype of the RAEE. During the summer of 2004, the initial process of selecting a membrane for a prototype of the exchanger was completed (Larson, 2004). An initial prototype was built in the spring of 2005 and was tested in the thermal sciences laboratory at the University of Saskatchewan (Hemmingson, 2005). A picture of the first prototype, showing the flow directions, is shown in Figure 1.4

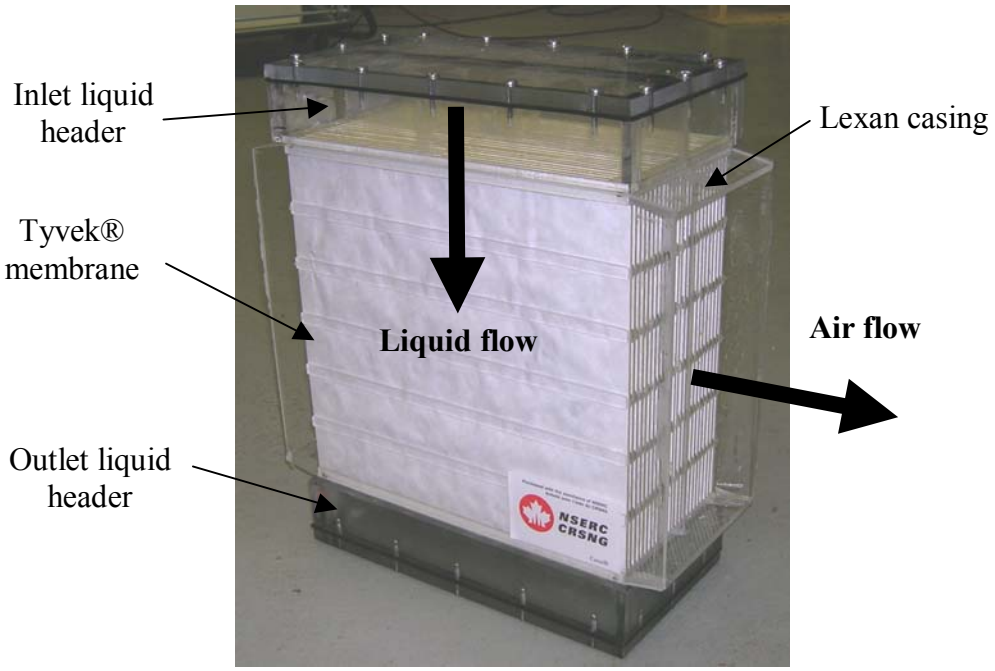

Figure 1.4. Picture of the initial RAEE prototype exchanger that was built in the spring of 2005.

The results of the testing of the first prototype were compromised due to unforeseen problems. One problem was that the liquid pressure caused the membrane to deflect and partially block the air flow channels. This deflection was due to slack in the membrane material and an insufficient support structure. To compensate for the large deflections, the exchanger was only operated at very low liquid pressures. At low liquid pressure there was poor liquid flow distribution throughout the liquid side of the exchanger. As a consequence, the heat and mass transfer were limited and the overall performance was poor.

The low pressure configuration also resulted in air flow through the membrane material (Tyvek®) from the air side to the liquid side. This air flow into the liquid side had detrimental effects on the system performance. Air permeation through the membrane is a situation that must be avoided by maintaining a larger pressure on the

liquid side. In addition to air flow permeability, a small amount of liquid was able to leak through the membrane. Liquid penetration of the membrane must be avoided at the operating liquid pressure of the exchanger by selecting a membrane with higher liquid penetration resistance.

These problems with the first prototype are addressed by examining the material properties associated with the deflection of the membrane, the air permeability and the liquid penetration. The results of this research were then used to design and construct two exchangers. These were mounted in an RAEE test facility and tested in the thermal sciences laboratory at the University of Saskatchewan (Erb, 2006).

Figure 1.5 shows the 3D CAD drawing of the core for the second prototype exchanger, which gives the overall size data.

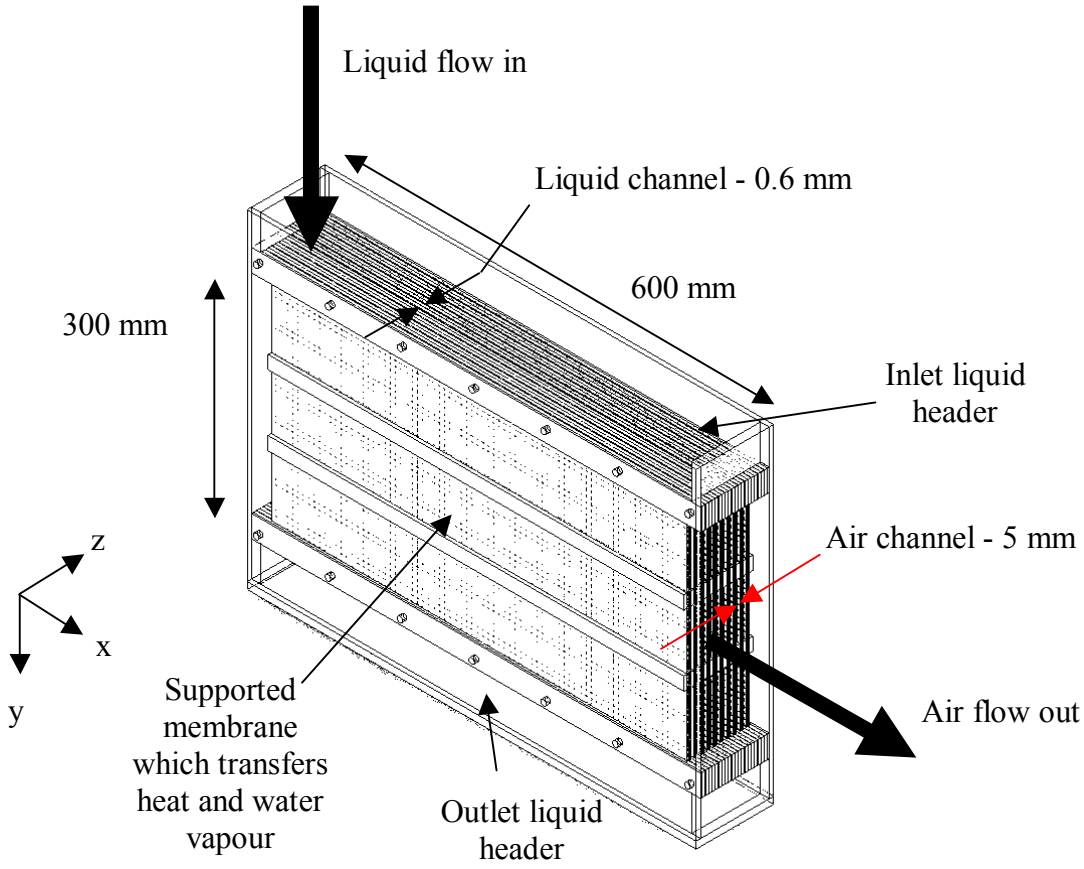

Figure 1.5. CAD drawing of the second prototype exchanger.

1.2 Introduction of critical properties

The properties that are of significant interest are determined from the experience of the first prototype exchanger and the numerical work of Fan et al. (2006). The water vapour permeability of the membrane has been shown by Fan et al. (2006) to be crucial to obtain a high latent effectiveness of the exchanger. The air permeability, liquid penetration pressure and the elastic properties of the membrane are all properties that were not adequately considered before the construction of the first prototype and need to be investigated. Resistance to ultraviolet (UV) degradation is an additional property that is only crucial to the function of the RAEE when UV radiation is used to kill microbial

growth as in applications where high indoor air quality (IAQ) is required. The following gives a brief introduction of the properties that are considered in this thesis.

1.2.1 Water vapour permeability

The critical element in the success of the RAEE is the ability of the membrane to effectively transmit water vapour yet remain a barrier to the aqueous salt solution. The property that quantifies the transfer of water vapour is known as the water vapour permeability or alternatively expressed as the vapour diffusion resistance.

The water vapour permeability is a constant of proportionality between the water vapour mass flux and the vapour pressure gradient (humidity difference) across the specimen. This one-dimensional mass flux, normal to the membrane surface, is governed by the following simplified equation based on Fick's Law of mass diffusion,

$$\dot{m}'' = \delta_m \frac{\Delta p}{\Delta z} \qquad [1.1]$$

where $\dot{m}''$ is the mass flux through the specimen [kg/(m^2 s)], δ_m is the vapour permeability of the material [kg/(Pa s m)], Δp is the vapour pressure difference across the specimen [Pa], and Δz is the thickness of the specimen [m] (Kumaran, 1998).

Equation [1.1] shows that as the water vapour permeability, δ_m, increases, the mass flux increases. At any given operating condition, or pressure difference, a higher mass flux through the membrane will result in a higher effectiveness of the exchanger. It should be noted that the permeability is a property of the material and is independent of thickness. The permeance of a particular material is obtained by dividing the permeability by its thickness (Δz) (i.e. permeance = $\delta_m / \Delta z$) and the vapour diffusion resistance, R_m, is the inverse of the permeance (i.e. $R_m = \Delta z / \delta_m$). In industry, the

permeability of a material will be quantified by the mass flux and is commonly referred to as the water vapour transmission rate (WVTR) and given in units of kg/(m^2·day). These values can only be converted to material properties if the conditions of the testing (i.e. Δp_v) are known.

1.2.2 Liquid penetration resistance

Another key feature of the membrane is that it must remain a barrier to the flux of the salt solution. If the liquid is able to flow through the membrane, the functionality of the exchanger would be lost. Only materials that are a barrier to liquids are being considered for use in the exchanger design; however, these materials will have a critical pressure at which liquid is forced through the membrane. This property is commonly referred to as: the hydrostatic head, liquid penetration pressure, or "waterproofness". The liquid penetration pressure is generally determined by measuring the pressure difference at which liquid water transfers through the membrane. This liquid penetration pressure is observed when drops of water become visible on the dry side of the membrane.

Water vapour diffusion resistance and liquid penetration pressure will increase as the thickness of a membrane increases. The minimum value of liquid penetration pressure must be greater than the typical operating pressure of the system. Since it is desirable to have low water vapour diffusion resistance and high liquid penetration pressure, it can be seen that the membrane must have a unique set of characteristics to be considered for the RAEE system.

1.2.3 Elastic properties

One of the most important properties in the design of the exchanger core is the elastic properties of the membrane. The primary concern is the deflection of a membrane into

the adjacent air channel at the operating pressure of the RAEE system. This deflection must be limited by a structural support system for the membrane. This structural support system must be as small as practical so that heat and mass transfer surface area is not significantly diminished. In order to calculate the deflections of the membrane in the exchanger the elastic modulus and the Poisson's ratio of the membrane materials are required.

1.2.4 Short wave ultraviolet degradation

Typical energy wheels have air leakage rates between the supply and exhaust of 1 to 5% (ASHRAE, 2004). Due to the configuration of the RAEE, the air leakage rate will theoretically be zero, which makes the RAEE system an excellent candidate for energy recovery is situations where leakage is not acceptable, such as hospitals, clean rooms etc. HVAC systems in these clean environments sometimes use UV light to help keep moist components of the HVAC system (typically cooling coils) free from microbial growth. The RAEE may be a potential site of microbial growth or it may be near a component exposed to UV light. The investigation of the degradation of the membrane materials with UV allows the useful life of the core under UV exposure to be determined.

1.3 Membrane materials

Only membranes that are commercially available are considered for the RAEE exchanger core. An initial search of membranes resulted in eight manufacturers with materials that were considered for the RAEE system. A preliminary investigation into the eight membranes, with only the manufacturers data considered, narrowed the membrane selection to two primary candidates: DuPont™ Tyvek® and 3M™ Propore™ (Larson, 2004). The following is a description of these membrane materials. Also

included for comparison is a description of expanded polytetrafluoroethylene (ePTFE). It is used as a reference material in the vapour diffusion resistance and air permeability tests. Other membrane materials that were considered are also given.

1.3.1 DuPont™ Tyvek®

DuPont™ Tyvek® is a spunbonded membrane made of high density polyethylene (HDPE) fibres. The fibrous composition of Tyvek® results in a microporous structure that has high water vapour permeability yet it remains a barrier to liquid penetration at low pressures.

HDPE is a common polymer found in many applications from plastic bags and bottles to toys and tools. In 1955, a researcher at DuPont™ noticed fluff being wasted at an experimental lab. Over the next four years a program was put in place to develop the fluff into a product and as a result a patent was filed for a long yarn polyethylene and a proprietary flash spinning technology was developed. During the manufacturing of the new product the HDPE waste fluff was spun into fine strands and then randomly distributed using this flash spinning technique to create Tyvek® (DuPont™, 2006). Figure 1.6 shows an atomic force microscope image of the microstructure of Tyvek®. The image shows a 20 by 20 micron area where crossing strands of the HDPE yarn can be seen.

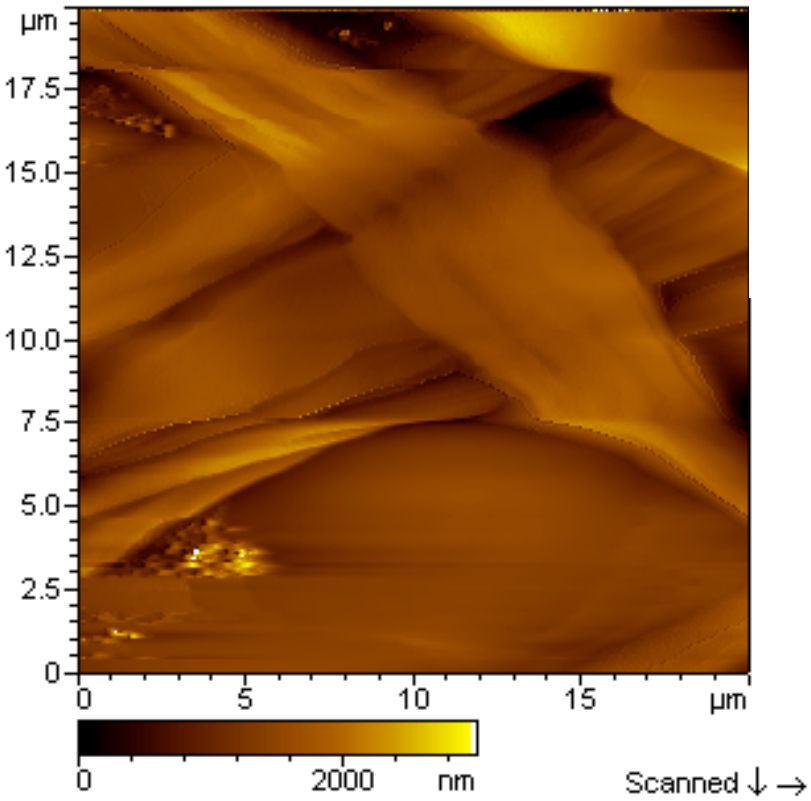

Figure 1.6. Atomic force microscope image of Tyvek® (20 x 20 µm).

Tyvek® material is currently used in many applications. Tyvek® HomeWrap® is used as an exterior wind barrier for homes. It is used in exterior walls and attics to prevent liquid penetration while it allows vapour diffusion. Tyvek® envelopes offer protection of their contents from liquids and are significantly more tear resistant than traditional paper envelopes. Tyvek® protective clothing allows water vapour to escape yet keeps liquids from penetrating to the user.

Tyvek® is readily available in the form of a large roll from the manufacturer. The Tyvek® used in this thesis was obtained directly from the manufacturer and the specific Tyvek® tested is made for the Japanese market. All reference to Tyvek® in this thesis refers to the Japanese Tyvek® product. In comparison to the readily available Tyvek®

HomeWrap® which has a typical thickness of approximately 0.2 mm, the Japanese Tyvek® has a thickness of approximately 0.16 mm and has a smoother finish. This smooth finish is a result of the Japanese Tyvek® being bonded over its entire surface area. The Tyvek® HomeWrap® is only bonded at specific points, which gives it a rougher embossed texture.

1.3.2 3M™ Propore™

Polypropylene (PP) is a polymer that is common in many household applications such as microwave tolerant plastics and indoor/outdoor carpeting. 3M™ has developed a proprietary technique to create a microporous PP membrane. This microporous PP membrane has high water vapour permeability and is a barrier to liquid penetration. It is very elastic, but it is available in a two layered laminate. Propore™ is the name given to the two-layer composite material consisting of the proprietary microporous polypropylene (PP) membrane which is thermally laminated to a non-woven PP fabric. The non-woven fabric acts as a support for the highly elastic PP membrane. Figure 1.7 shows an atomic force microscope image of the microstructure of the Propore™ membrane on the microporous PP face.

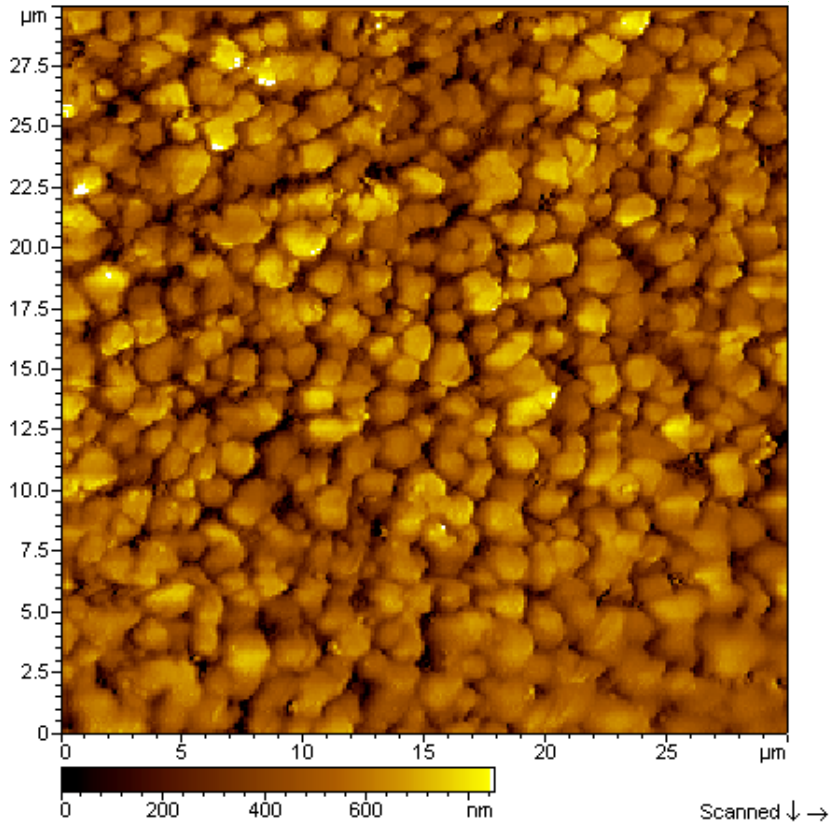

Figure 1.7. Atomic force microscope image of Propore™ (30 x 30 µm).

Propore™ material is available in the form of large rolls and it too was obtained directly from the manufacturer. Current uses of Propore™ include light duty rainwear, medical packaging and disposable mattress and pillow case covers for hospitals and care facilities.

1.3.3 Polytetrafluoroethylene (PTFE)

PTFE was also developed by a researcher at DuPont™ and is more commonly known by the DuPont™ trade name of Teflon®. Teflon® is not known for its water vapour permeability; however, a researcher at W.L. Gore and Associates stretched the Teflon® material and discovered that it is exceptionally permeable to water vapour. The new material was known as expanded PTFE (or ePTFE). This new membrane material has

many of the characteristics of Teflon®, with greatly increased water vapour permeability. Gore's proprietary technique for creating ePTFE allowed them to create products that were permeable to water vapour, but impermeable to liquid water, such as Gore-tex® brand outerwear. Expanded PTFE is the most vapour permeable hydrophobic membrane available with vapour permeability that is comparable to that of cotton. In ASTM F 2298 (2003) ePTFE is considered as the benchmark for the water vapour permeability of waterproof membranes. It is used as a comparison material for all other materials because it can be used to calibrate the instrument for measuring water vapour permeability.

ePTFE is very fine and difficult to handle, it is extremely elastic, tends to stick to itself, and has low tensile strength (similar to Teflon® tape that is widely used by plumbers). This problem is easily remedied by laminating the membrane to another material for support. The new laminated membrane will then have a permeability limited by the laminate material, and the laminating method. An example of an ePTFE laminate is the standard Gore-tex® membrane which is composed of an ePTFE membrane with a polyalkyleneoxide polyurethane-urea coating that is laminated to a woven nylon (Gibson, 2000a). The coating is hygroscopic and it is this layer that governs the overall resistance to moisture transfer. The eVent® membrane made by BHA technologies is another example of an ePTFE laminate. The eVent® membrane consists of an ePTFE membrane with a proprietary coating that is laminated to a nylon textile material. Both eVent® and Gore-tex® membranes are used primarily for outerwear although both companies also produce filtrations products.

In general, ePTFE is known to have exceptional water vapour permeability and is therefore well suited to the RAEE; however, the cost of ePTFE and its laminates is especially high as will be discussed in Section 1.3.5.

1.3.4 Other materials

Two other materials that were considered for the first prototype are also introduced. The properties of these materials are not considered in all chapters; however, results are presented for comparative purposes in Chapters 2 and 4.

The Entrant™ GII membrane, manufactured by Toray Industries, is created by applying a polyurethane coating to a nylon yarn. The thin polyurethane coating provides moderately good water vapour permeability while the membrane maintains the tensile strength of the nylon yarn. The disadvantage of the Entrant GII membrane is that the coating can wear off in time.

Sympatex® membrane is manufactured by Sympatex® technologies and is composed of a monolithic polymer layer composed of a hygroscopic copolymer of polyester and polyether. Sympatex® is not microporous and thus the moisture transfer occurs through molecular diffusion through the membrane. This moisture transfer is dependent on the water content of the membrane.

1.3.5 Cost of membranes

While many materials and material properties are examined to help improve the design and performance of the RAEE exchanger, a very important factor for commercial implementation of the RAEE system is the cost. The cost of the membranes eliminates many options for their use in industry. However, the membranes are not permanently rejected for the RAEE since future pricing may change this situation.

To be a competitive energy exchange product, the cost of the exchanger core must be limited to approximately $0.85 per L/s ($0.40 per cubic foot per minute (CFM)) of airflow. Assuming a typical flow rate of a light commercial ventilation unit of approximately 235 L/s (500 CFM) gives a target price of $200 for the core. Since the membrane is only part of the cost of the core, the membrane material must cost significantly less than $200. Figure 1.8 shows the price of the membrane required to make the second prototype exchanger having a membrane surface area of 40 m^2. All membrane prices are obtained from the manufacturer.

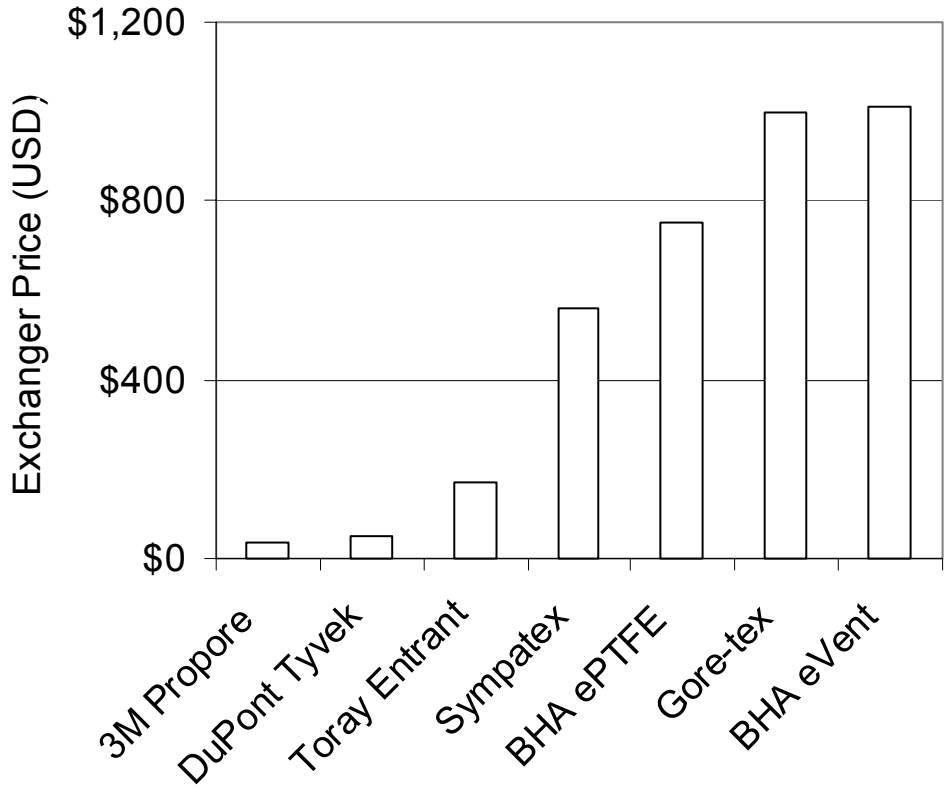

Figure 1.8. Membrane cost for a single exchanger core with a surface area of 40 m^2 for a number of possible membranes.

Considering the target cost of $200, the only membranes that are cost competitive at this time are 3M™ Propore™ and DuPont™ Tyvek®. These two materials are the focus

of this thesis although the other membranes will be occasionally discussed for comparison and completeness.

1.4 Research objectives

The objective of this thesis is to choose a membrane to be used in the RAEE system. This is accomplished by the following specific objectives.

- To measure the water vapour permeability of membranes that may be used in the RAEE.
- To use the measured values of water vapour permeability and the model of Fan et al. (2006) to predict the performance of the RAEE.
- To measure the air permeability of membranes that may be used in the RAEE.
- To measure the liquid penetration pressure of membranes that may be used in the RAEE.
- To measure the elastic properties required to calculate the deflection of the membranes in the exchanger for a range of operating conditions.
- To determine the feasibility of using UV light to clean the membranes, through testing the membranes degradation with UV exposure.
- To use the above data to recommend the membrane that is best suited for the second RAEE prototype and any future prototypes.

The determination of the aforementioned properties also includes investigating the current measurement techniques and associated standards used to determine the properties, evaluating them and choosing the most suitable measurement technique.

CHAPTER 2
EFFECTIVENESS, WATER VAPOUR AND AIR PERMEABILITY MEASUREMENTS

The latent effectiveness of the RAEE system is dependent on the water vapour permeability of the membrane. This relationship was shown in the research of Fan (2005). This relationship between effectiveness and water vapour permeability is very sensitive for water vapour diffusion resistances greater than 20 s/m which is the case for most membranes (see Section 2.6). This sensitivity implies that the water vapour permeability of the membrane must be thoroughly examined. It should also be noted that in order to comply with ASHRAE standard 90.1 (2004), an effectiveness of at least 50% is required for an energy exchanger.

The published ranges of water vapour permeability for many materials have a large variation. These differences are due to the differences in test methods, test conditions, and sources of data. Figure 2.1 shows the variation of permeability data with test method for a number of membranes. The data are obtained from the manufacturers' specifications, from McCullough et al. (2003) and from test results performed by Phil Gibson. Note that the results of Figure 2.1 are on a log scale so the differences between each test method are large.

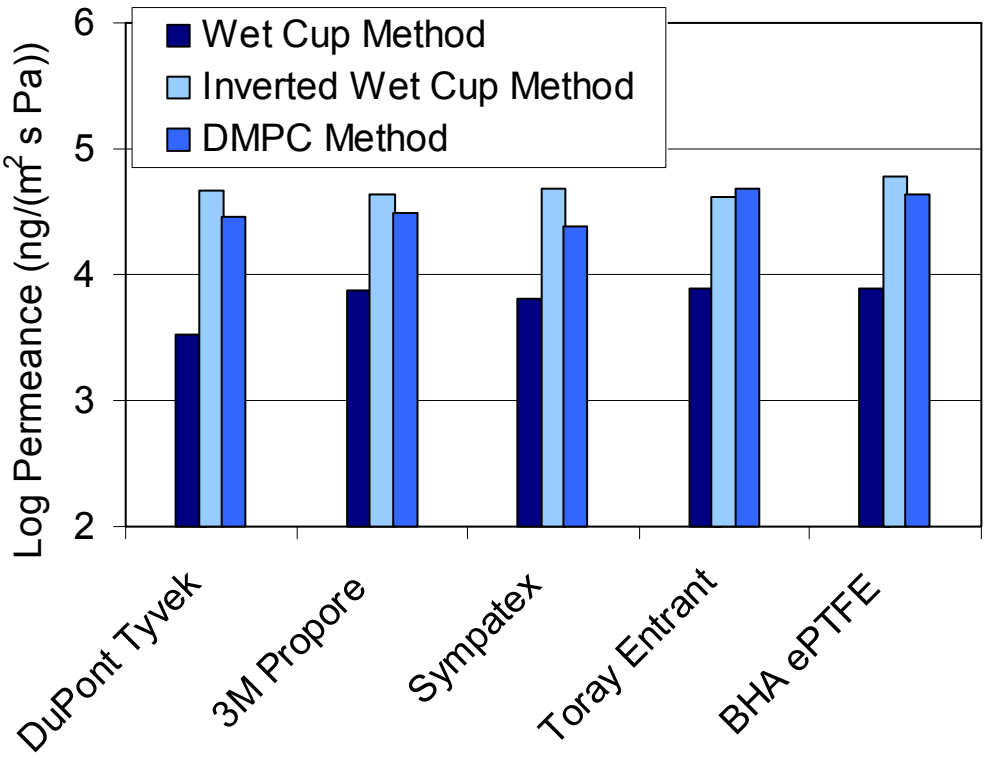

Figure 2.1. Log permeance of membranes using three different test methods: wet-cup, inverted wet-cup and dynamic moisture permeation cell.

The water vapour permeability of a material is a complex function of temperature, humidity, orientation and microstructure. For design purposes, the water vapour permeability of a given material is often given a single value such as in the ASHRAE Fundamentals handbook (2005), when in fact the value is sensitive to the test conditions.

Different methods of testing often result in different values of water vapour permeability, and due to the low resistance of the membrane relative to that of air, it is difficult to accurately calculate the water vapour permeability of just the membrane. Several test methods are currently in use; however, they often yield different results because the uncertainties may be large. The data of these tests result in a large range of water vapour permeability values for a given material over a range of test conditions.

This permeability measurement problem is of special interest in this thesis, because accurate values of water vapour permeability are required to input into the numerical model of Fan et al. (2006) so that the latent effectiveness of the RAEE can be accurately simulated.

2.1 Test methods

This section outlines the most common water vapour permeability test methods used for membranes and lists the advantages and disadvantages of each method. The methods are divided into two categories, with each having several associated test methods. The first category is gravimetric methods, which includes any method that determines the moisture transfer flux through a specimen by measuring the change in mass over a period of time. The second category is dynamic methods, which measures the moisture transfer flux by measuring the air flow rate and the humidity difference across a test cell.

2.1.1 Gravimetric method

Water vapour permeability has traditionally been determined using a gravitational method known as the cup test. The cup test was introduced by Joy and Wilson and first used in 1954 (Kumaran, 1998). There are two well known standards for performing the cup test, ASTM E 96 (2000) and ISO 12572 (1997). Test specimen dimensions and tolerances vary slightly between the two standards, but the basic procedure is the same for each. Both standards describe two different test conditions, referred to in the ASTM standard as the dry cup method and the wet cup method. The former uses a desiccant providing 0% relative humidity in the cup while the latter uses water, providing 100% relative humidity in the cup. In both cases the cups are placed in a chamber providing 50% relative humidity and a constant temperature. The cups are weighed using a mass balance at regular intervals until a constant or steady state mass flux is obtained. The

ASTM standard also outlines the inverted cup method which follows the same procedure as the wet cup method only that the cup is inverted to allow the water to sit directly on the test material. A schematic of both the standard cup test (wet cup) and the inverted cup test is shown in Figure 2.2. Laboratory studies have shown that this inverted cup can yield results up to 10 times greater than the wet cup (McCullough et al., 2003).

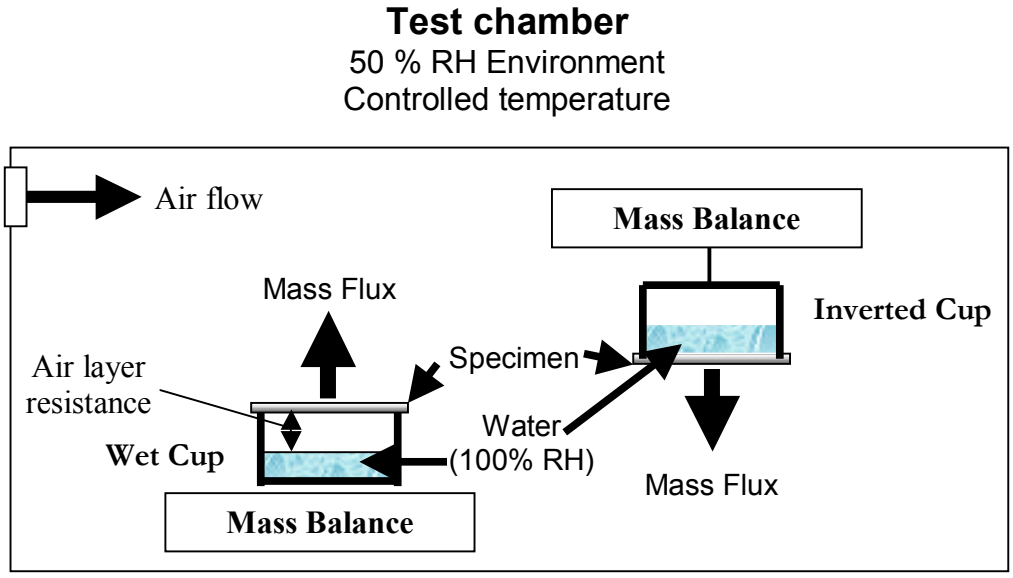

Figure 2.2. Schematic of the cup test method showing the wet cup test and the inverted cup test in a common test chamber.

The standard has remained relatively unchanged for the last six decades. Inter-laboratory studies from North America and Europe have shown a standard deviation in the results ranging from 11% to 21% (Kumaran, 1998), which corresponds to 95% uncertainties of 22% and 44%, respectively. These standards leave many different parameters in the hands of the tester; some elements that are not strictly defined include: the shape and size of the specimens, the sealing method, a correction for the overlap of the specimen on the cup, a correction for the buoyancy effects, and a correction for the

air and surface resistances. It is at the discretion of the tester as to what the dimensions of the cup will be, and in the case of the ASTM standard, whether or not any or all the corrections will be used. This ambiguity in test procedure may result in a wide distribution of values of permeability for a given material when measured by different laboratories. However, the repeatability within a single laboratory can also be poor even when the same procedure is followed. Tye (1994) suggested that the worst-case scenario is an error of 25% to 30% while 10% is considered acceptable, and in early years errors of ten times the worst-case scenario were not uncommon. The consensus is that this standard method of determining permeability needs to be revisited and improved (Kumaran, 1998). While the method has flaws, it is still widely used because it is very easy and inexpensive to perform, and gives reliable results for materials with high vapour diffusion resistance such as many building materials.

As a result of the known issues with the cup test many modified techniques have been developed. One of the dominant sources of error in the cup test is the vapour diffusion resistance of the air layer between the sample and the salt solution. A common solution is to place the liquid directly onto the specimen as in the inverted cup method of ASTM E 96 (2000). This is not always possible due to the nature of the specimen (e.g. paper or wood). An alternative proposed by Svennberg et al. (2003), Dolhan (1987), and in the alternative standards, ISO 15496 (2004), ASTM D 6701 (2001), and CAN/CGSB – 4.2 No. 49-99 (1999) is to place a vapour permeable guard film (e.g. an ePTFE membrane) between the sample and the liquid salt solution. In this method the salt solution is in contact with the ePTFE membrane while the specimen is exposed to moving air. A schematic of this modified test method in shown in Figure 2.3.

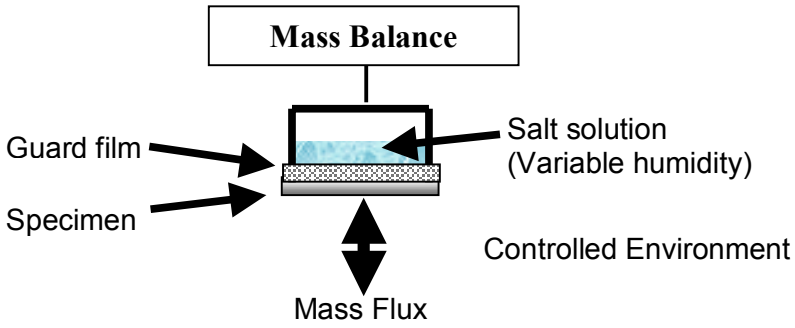

Figure 2.3. Schematic of an alternative cup test using a guard film.

This method requires that the resistance to vapour diffusion of the guard film be subtracted from the results, which can cause large errors if the sample being tested has a resistance of the same order of magnitude as the guard film.

Galbraith et al. (2003) proposed a low pressure technique in which the traditional cup test takes place in a vacuum chamber. This method greatly decreased the time of a test, from days to hours; however, many problems with the cup test are still present and due to the test setup being unique there are no data for inter-laboratory comparison.

2.1.2 Dynamic method

The dynamic method has the common attribute with the gravitational method of a controlled humidity on both sides of a sample specimen. In the dynamic method a stream of air is passed on one or both sides of the sample and the change in water vapour concentration is detected in one of the flow streams. A schematic of the dynamic moisture permeation cell (DMPC) is shown in Figure 2.4. This schematic shows separate flows on each side of a test cell; however, only one side need have flow in some alternatives of the dynamic test method.

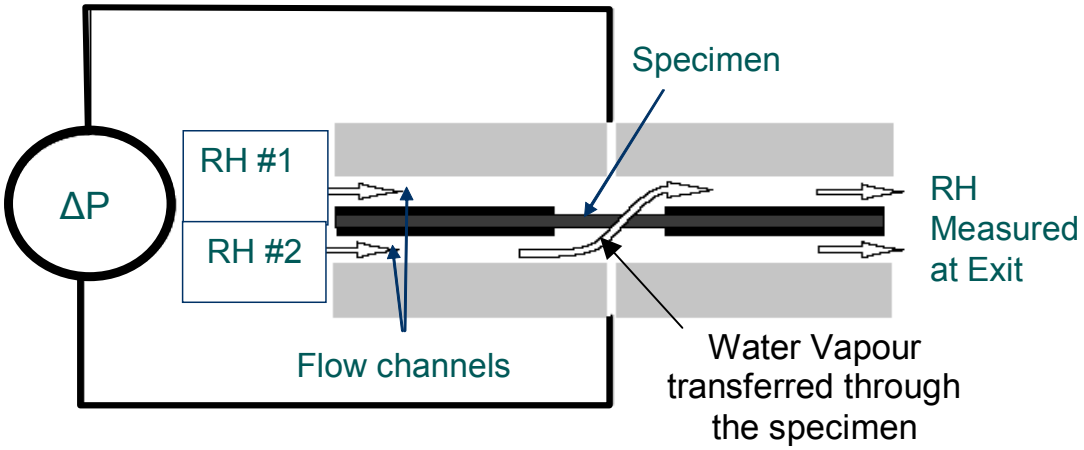

Figure 2.4. Schematic of the dynamic moisture permeation cell (DMPC) test method (Reprinted with permission Gibson, 2000a).

In the ASTM F 1249 (2001) infrared test method, the sample is sealed in a diffusion cell with a wet side and a dry side. The wet side is maintained at a constant temperature and humidity. The dry side has a flow of dry air (0% RH) entering the cell. As the dry gas leaves the diffusion cell it contains a trace amount of water vapour that has diffused through the sample. This dry side gas passes by an infrared sensor which detects the fraction of water vapour in the air. This concentration of water vapour in the air can then be compared to the concentration created by a calibration material of known vapour flux. From this known value, the vapour flux through the current specimen can be obtained (ASTM F 1249, 2001). Variations of this standard can also be performed where the detection technique of an infrared sensor is replaced by a capacitance type humidity sensor or a chilled mirror hygrometer. These types of test facilities are commercially available but the accuracy is often poor since they are intended for quality control of manufactured materials rather than research.

Recently, a vapour permeability test method known as the dynamic moisture permeation cell (DMPC) was designed specifically for textiles and thin membranes. The

method was designed for materials research and a new standard has been developed (ASTM F 2298, 2003). The apparatus for this method was designed by the Materials Science Team at the U.S. Army Soldiers Systems Center in the mid 1990's. This method is similar to the Infrared method of ASTM F 1259 (2001) except it has greater flexibility and better control of the test conditions. In particular, the humidity of the gas streams on each side of the sample can be controlled independently as can the test temperature of the sample. In addition, the DMPC is the only method which recognizes the fact that there may be an air pressure difference across the samples so it implements differential pressure control. This control also allows the DMPC to measure the air permeability of a specimen.

2.1.3 Selected test method

As indicated previously, the gravitational methods are not well suited to measure the water vapour permeability of thin membranes. Another concern not addressed by any known gravitational techniques is the effect of air permeability of the specimen. In materials which have high air permeability, the advective flow of water vapour can easily be misinterpreted as vapour transfer due to diffusion. For this reason alone any method that does not control the pressure difference across the specimen is not suited for materials with high air permeability. The gravitational methods are best suited for low air permeable building materials such as plywood, gypsum and air retarders.

Another advantage of the dynamic methods over the gravimetric methods is the speed with which results can be obtained. The time for a traditional cup test to reach equilibrium can be days, while the time for a dynamic measurement is usually measured in minutes.

Of the dynamic methods investigated, the DMPC is the only method available that addresses the issue of advective mass transfer through the membrane. The DMPC's flexibility includes measurements of vapour diffusion resistance over a range of humidities and temperatures and with the added ability to measure the air permeability. Since the membranes studied in this thesis are somewhat air permeable, the control of air pressure is crucial and the DMPC method is used to obtain permeability data. Since DMPC measurements are not currently available at the University of Saskatchewan, all data were obtained from Dr. Gibson's DMPC at the U.S. Army Soldier System Centre in Natick, MA. Dr. Gibson tested the Tyvek® and Propore™ membranes as well as a pure (non-laminated) ePTFE membrane.

2.2 DMPC apparatus

Figure 2.5 shows a schematic of the dynamic permeation cell from Gibson (2000a). The schematic of Figure 2.5 shows the components and connections of the DMPC system.

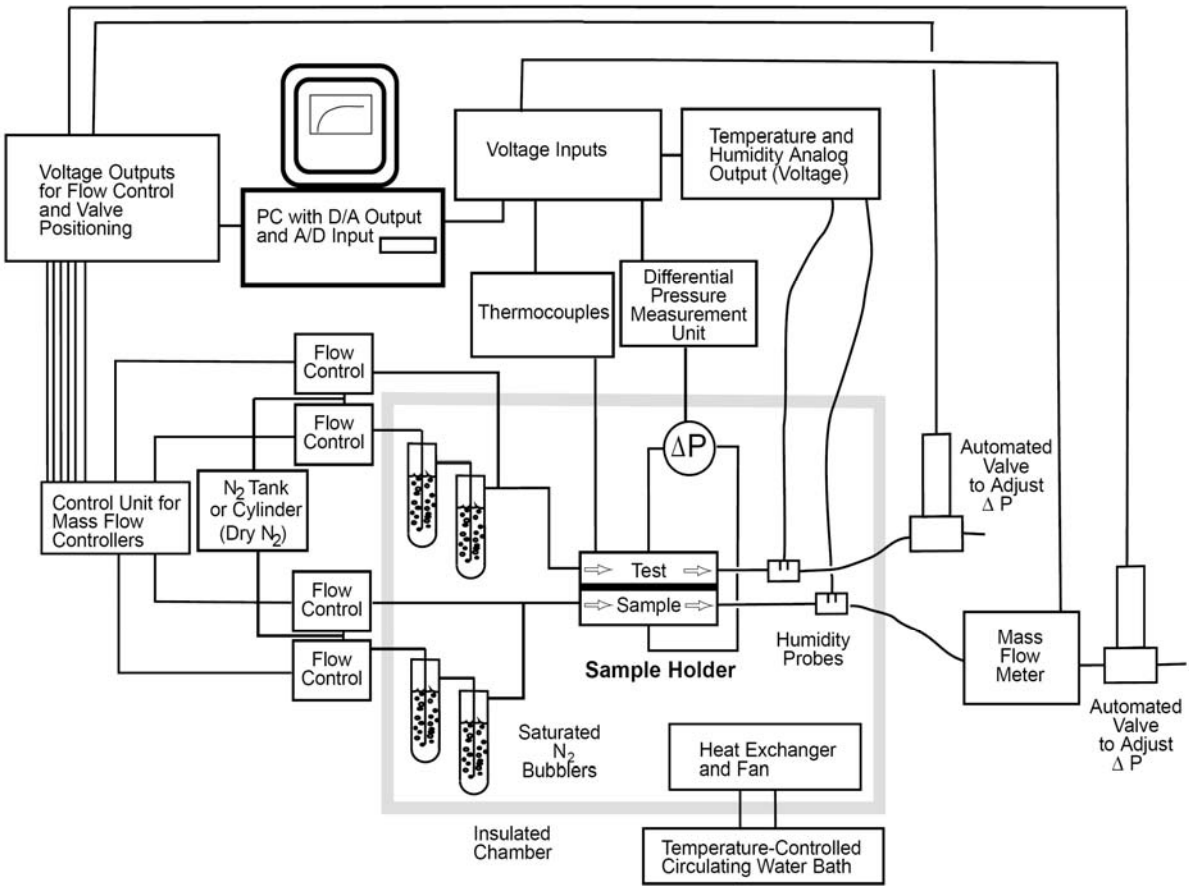

Figure 2.5. Schematic of the dynamic moisture permeation cell (DMPC) (Reprinted with permission, Gibson, 2000a).

In the DMPC, the specimen is placed between two different sides of a container known as a permeation cell or sample holder which is shown in more detail in Figure 2.6. Two nitrogen gas flows of known temperature and water vapour concentration are created using MKS model 1259C flow controllers which proportionally mix dry nitrogen (0% RH) and saturated nitrogen (100% RH). The saturated streams are created by passing the source nitrogen stream through a series of water tanks. These two streams are then individually passed over the respective sides of the specimen in the sample holder. The set points for the mass flow controllers are given by the user and are input via a personal computer (PC) with an onboard digital to analog converter. The

temperature of the insulated chamber is measured using a thermocouple and maintained with a circulating water bath and heat exchanger assembly. The relative humidity is measured at the top and bottom of the specimen in the outgoing streams using Vaisala HMP capacitance type sensors. The flow rate at the outlet of the bottom portion of the permeation cell is measured using an 822 Top-Trak mass flow meter. The pressure difference across the sample is measured using an MKS Baratron Type 398 differential pressure transducer with a type 270B signal conditioner. All voltage signals from the measurement devices are input into the PC. All of the measurements are controlled by the PC using a program written by the U.S. Army Soldier System Center. The program requires an input file which contains the desired set points for a test (or series of tests) and the length of time to run each test. Equilibrium is assumed to be reached at the end of the test where the final data point is recorded and then used to calculate the mass flux, and water vapour diffusion resistance of the specimen (Gibson et al., 1997).

Figure 2.6 shows a schematic of the permeation cell used in the DMPC apparatus of Gibson (2000a)

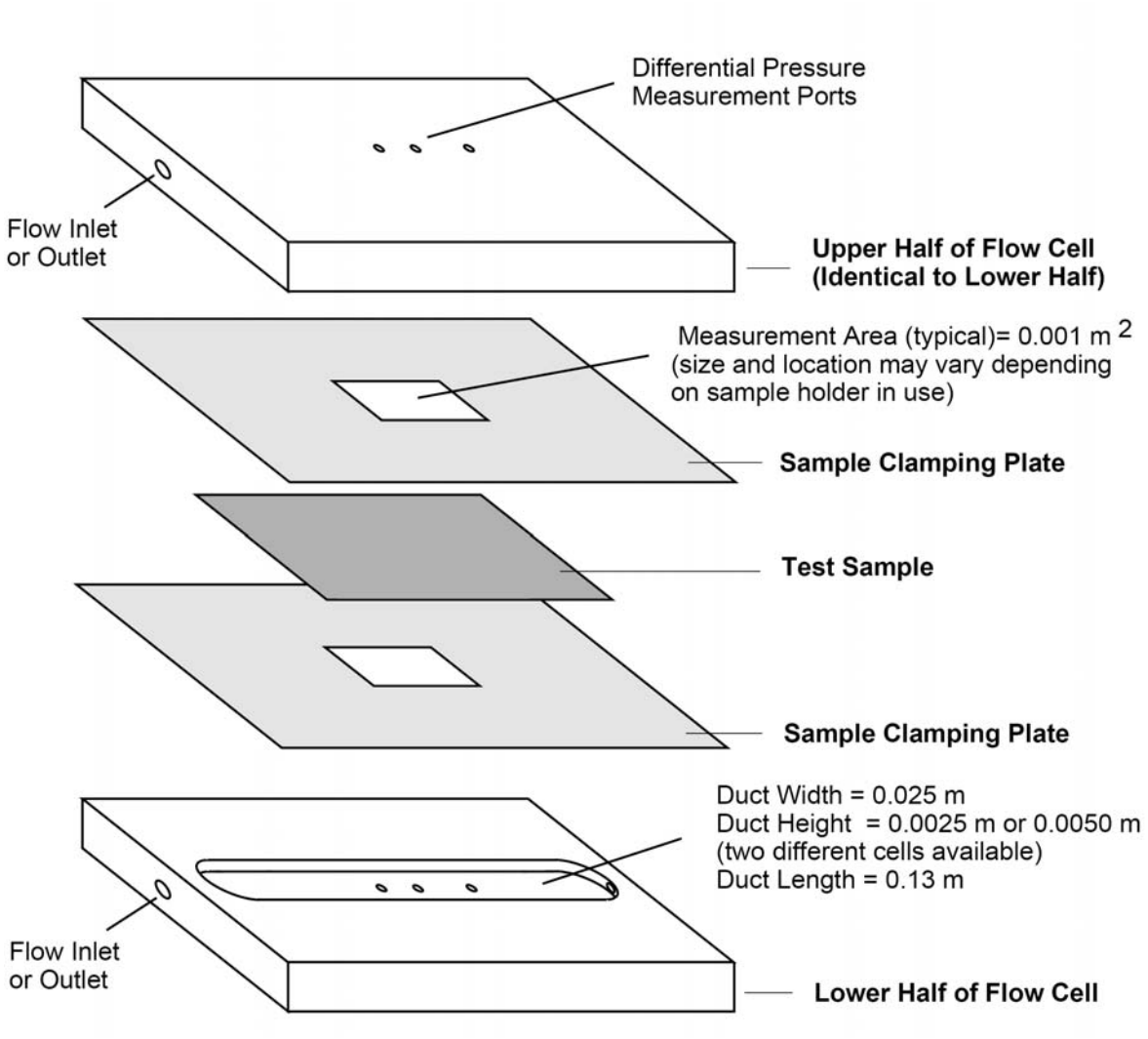

Figure 2.6. Permeation cell pieces and relevant dimensions (Reprinted with permission Gibson, 2000a).

The cell is made up of two halves that are clamped together with bolts (not shown). Each half has a flow inlet and outlet as well as a port in the middle where the differential pressure is measured. The sample is clamped between the two halves of the cell with clamping plates to restrict the measurement area. The dimensions of the cell are such that the distance from the inlet to the sample provides adequate spacing for the flow to become fully developed at all flow speeds of the DMPC. The developing length and fully developed velocity profile can be calculated analytically. Gibson et al. (1995) used

a numerical simulation to model the flow and the results agreed very well with the analytical solution.

The water vapour diffusion resistance as a function of humidity is obtained by performing a series of consecutive tests at increasing mean humidity, while maintaining the same humidity gradient across the sample. The result is a plot of vapour diffusion resistance versus mean humidity. The trend of this plot has been shown to be highly significant in hydrophilic materials and materials with highly hygroscopic laminates and gives insight into the vapour diffusion resistance of the material over the range of conditions experienced in the RAEE (Gibson et al., 1995). Since the test cell and flow control is enclosed within an insulated chamber (see Figure 2.5), the vapour diffusion resistance as a function of temperature can also be investigated. Gibson (2000a) showed that the vapour diffusion resistance variation over the temperature range of 0 to 40 ^{o}C is insignificant for microporous materials. Thus, any temperature dependence of the membrane's water vapour permeability in this thesis is assumed to be negligible and any dependency is left for future work.

Vapour diffusion resistance data at below freezing temperatures are limited to a few tests due to the difficulty in testing at temperatures below zero. Data for some membranes have been measured at temperatures as low as -10^{o}C by Gibson by replacing the nitrogen bubblers with ice chips in the DMPC (Gibson, 2000a). Osczevski (1996) tested Gore-tex® permeability at temperatures as low as -25^{o}C using an independent method involving direct contact with super cooled ice. Morillon et al. (2000) have published data as low as -18^{o}C on packaging membranes such as cellophane and polyethylene. These tests were performed using the traditional cup test with sucrose

solution that would not freeze. The results of Morillon et al. (2000), Osczevski (1996), and Gibson (2000a) show that the mass flux through a specimen decreased with decreasing temperature. Morillon et al. (2000), Osczevski (1996) and Gibson (2000a) conclude that the water vapour permeability decrease with temperature is due to the relationship of the saturation vapour pressure with temperature and not necessarily due to a variation in a material property. Gibson (2000a) concludes that there is negligible vapour diffusion resistance change due to temperature for temperatures above 0^{o}C. The RAEE system may experience temperatures below zero; however, vapour diffusion resistance data in this range are left for future work.

In the DMPC method the air pressure difference across the sample is controlled and is set to zero which ensures that only mass transfer due to diffusion is occurring. Alternatively, the air pressure differential may be varied and the vapour diffusion resistance as a function of pressure difference is obtained. The shape of this plot gives insight into the relationship between diffusion and advective mass transfer and enables the air permeability of the material to be calculated (Gibson et al., 1997). The separation of advective and diffusion mass transfer is particularly important in microporous materials and thin membranes where there may be significant advective mass transfer.

2.3 DMPC analysis

The analysis of the DMPC method is presented by Gibson (1995, 1997, 2000a, and 2000b). The details of this analysis are given in Appendix A and a summary is given here.

The mass flux through the specimen is measured and is then used to calculate the vapour diffusion resistance. The mass flux is given by,

$$\dot{m}'' = \frac{\delta\phi \cdot Q_s \cdot p_{v,sat} \cdot M_w}{A \cdot R \cdot T_s} \qquad [2.1]$$

where $\delta\phi$ is the humidity difference from the inlet to the outlet on the top of the test cell [% RH], Q_s is the indicated flow rate [cm^3/min], $p_{v,sat}$ is the saturation vapour pressure [Pa], M_w is the molecular weight of water [kg/kmole], A is the specimen area [m^2], *R* is the universal gas constant [J/(kg kmole)] and T is a reference temperature of 297.15 K.

Since the mass flux of water vapour through the membrane will change with humidity gradient it is convenient to give the results of the DMPC test as a vapour diffusion resistance which includes the effects of a changing humidity gradient in the log mean concentration difference across the sample and is given by,

$$R_m = \left[\frac{\overline{\Delta C}}{\dot{m}''}\right] - R_{bl} \qquad [2.2]$$

where $\overline{\Delta C}$ is the log mean concentration difference [kg/m^3] and R_{bl} is the boundary layer resistance [s/m]. The boundary layer resistance is known for the flow cell based on the work of Gibson et al. (1995).

The Darcy air permeability is used to quantify the air permeability of the membrane and is given by the following equation,

$$k_D = \left(\frac{\mu \cdot \Delta z}{A}\right)\left(\frac{Q}{\Delta p}\right) \qquad [2.3]$$

where Q is the volume flow rate [m^3/s], Δz is the thickness of the membrane [m], μ is the dynamic viscosity of the fluid [kg/(m s)], Δp is the pressure difference across the material [Pa] and k_D is the Darcy permeability of the material [m^2].

The first term of equation [2.3] consists of constant properties and the second term is equal to the slope of the flow rate versus pressure graph obtained in the convective test. The flow rate is measured at the exit of the bottom of the cell and encompasses the flow entering the cell and any additional flow (or loss) through the material.

2.4 DMPC uncertainty

The uncertainties in the DMPC results are calculated using the techniques outlined in ANSI/ASME 19.1 (1998). In this method, the uncertainty is divided into two contributions: the precision and the bias. The precision and bias of the measurement devices are obtained from calibration and the uncertainties of the calculated parameters are determined. The uncertainty calculated using this method is referred to as the measurement uncertainty. In addition to this calculated uncertainty, inter-laboratory studies have been performed (ASTM F 2258, 2003) and values of repeatability of a given measurement and the reproducibility of a measurement between laboratories are reported. The values of the inter-laboratory study are given in Table 2.1.

Table 2.1. Summary of the uncertainty values from Inter-laboratory studies using the DMPC (ASTM F 2258, 2003).

Mean water vapour diffusion resistance (s/m)	Repeatability standard deviation (%)	Reproducibility standard deviation (%)	95% Repeatability limit (%)	95% Reproducibility limit (%)	Humidity gradient (%)	Flowrate (cm^3/min)	Material
172.6	1.8%	8.6%	5.1%	24.0%	90%	2000	Fabric 1
262.7	2.3%	9.1%	6.5%	25.5%	90%	2000	Fabric 2
509.7	2.4%	7.8%	6.7%	21.7%	90%	2000	Fabric 3

The data in Table 2.1 are taken from the ASTM F 2298 (2003) standard and are based on the measurements of 4 independent laboratories. Therefore, the 95% confidence intervals are 2.8 times the standard deviations. The detailed explanation and equations used to calculate the measurement uncertainty are found in Appendix B. The

values at a selection of conditions for both materials are summarized in Table 2.2 to give a perspective of the range of uncertainty. All results from the tests conducted by Dr. Gibson for this thesis are based on the average of three measurements. The 95% repeatability limit is based on these three samples tested by Gibson and the total uncertainty limit is the root sum square of the repeatability limit and the measurement uncertainty. All values of Table 2.2 are for a mean humidity of 50% and the vapour diffusion resistance includes the resistance of the boundary layer.

Table 2.2. Summary of the uncertainty for both Propore™ and Tyvek® at a variety of operating conditions.

Mean water vapour diffusion resistance (s/m)	95% Measurement uncertainty (%)	Humidity difference at inlet (%)	Flowrate (cm^3/min)	Material	Conditions	95% repeatability limit (%)*	95% total uncertainty limit (%)
161	3.5%	90%	2000	ePTFE	Standard test conditions	n/a	n/a
276	5.3%	90%	2000	Propore		6.7%	8.5%
568	8.5%	90%	2000	Tyvek		15.6%	17.8%
695	92.6%	10%	2000	Tyvek	Gradient dependence	38.9%	100.4%
698	46.8%	20%	2000	Tyvek		14.6%	49.0%
579	15.5%	50%	2000	Tyvek		15.4%	21.9%
283	42.0%	10%	2000	Propore	Gradient dependence	15.4%	44.8%
298	22.4%	20%	2000	Propore		13.8%	26.3%
274	8.4%	50%	2000	Propore		7.2%	11.0%
597	9.8%	90%	1000	Tyvek	Flow rate dependence	14.1%	17.2%
660	17.1%	90%	300	Tyvek		11.7%	20.7%
304	6.3%	90%	1000	Propore	Flow rate dependence	4.9%	8.0%
382	15.0%	90%	300	Propore		2.8%	15.3%

* based on three samples

It can be seen that the uncertainty of the measurement is highly dependent on the flow rate, the material and humidity gradient. The greatest contribution to the uncertainty is from the measurement of the humidity difference from the inlet to the outlet of one side of the test cell. For materials with low vapour diffusion resistance such as the ePTFE the difference in the humidity from inlet to outlet is greater and therefore the uncertainty is lower. Similarly, as the flow rate is decreased, less vapour will enter

the air stream as it flows over the sample and therefore the humidity difference is less and the measurement uncertainty increases. The greater the humidity difference between the inlet air streams, the greater the mass flux through the specimen. This larger mass flux results in a greater humidity change in the measured humidity and therefore a lower uncertainty. The values at 10% humidity gradient result in very little mass transfer and therefore the uncertainty in these measurements are very high. The uncertainty values shown in the plots of Section 2.5 are the 95% total uncertainty limits.

2.5 DMPC results

The overall effectiveness of the RAEE system is governed by the vapour diffusion resistance results. The application of the results is presented in Section 2.6. This section presents the vapour diffusion resistance results for the Propore™ and Tyvek® membranes. Where possible the results of an ePTFE membrane are also included for comparison. The results are all obtained from Dr. Gibson of the U.S. Army Soldiers System Center. All tests are performed at a constant temperature of 30^{o}C. A sample area of 25 cm^2 is used in all tests except for the modified testing where a sample area of 10 cm^2 is used. Unless otherwise stated, average test result refers to the average of three different specimens cut from the same sheet of material.

Figure 2.7 shows the vapour diffusion resistance for several materials as a function of humidity. The data for Tyvek® and Propore™ are from the tests performed by Gibson for this thesis and data for all other materials are obtained from previously published tests performed by Gibson. Note that the vapour diffusion resistance is given on a log scale.

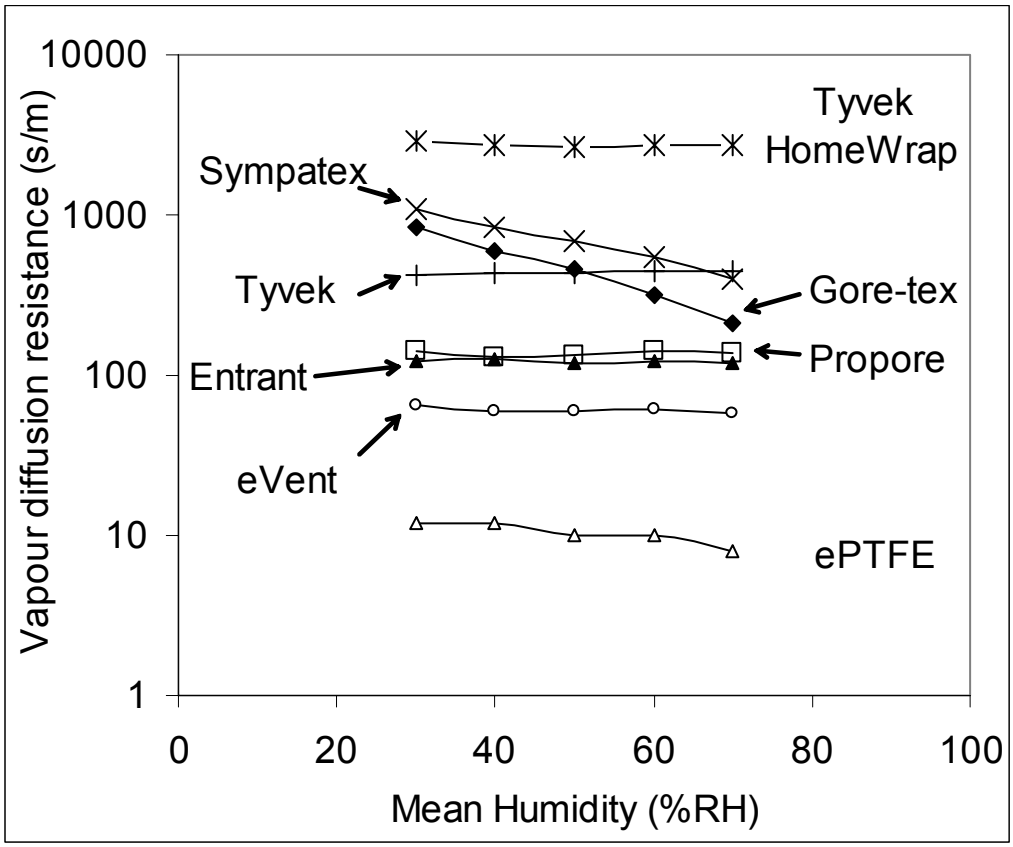

Figure 2.7. Comparison of vapour diffusion resistance for several membranes as a function of relative humidity.

It can be seen that the ePTFE membrane has the lowest vapour diffusion resistance and it is used as a standard reference material in all of Gibson's testing. The Propore™ material has similar properties to the Toray Entrant™ membrane and is not quite as water vapour permeable as the BHA eVent® material which is a laminate using an ePTFE membrane. The Tyvek® membrane has over twice the resistance of the Propore™ but has six times less resistance than the more common Tyvek® HomeWrap®. The Gore-tex® and Sympatex® membranes are the only two membranes that are not microporous. These membranes have hygroscopic properties and their vapour diffusion resistance is therefore governed by their adsorbed water content. At higher humidities they have higher moisture contents resulting in capillary moisture

transfer in addition to vapour diffusion. As a result their resistance decreases with humidity. At low humidities the moisture transfer is essentially by vapour diffusion alone and therefore the resistance is higher at low humidities.

2.5.1 Vapour diffusion resistance

The vapour diffusion resistance is shown in Figure 2.8 as a function of mean humidity across the specimen, with the humidity gradient held constant at 50% RH. For example, at a mean relative humidity of 30% RH, the inlet conditions are 5% RH on the dry side of the cell and 55% RH on the wet side.

(a) (b)

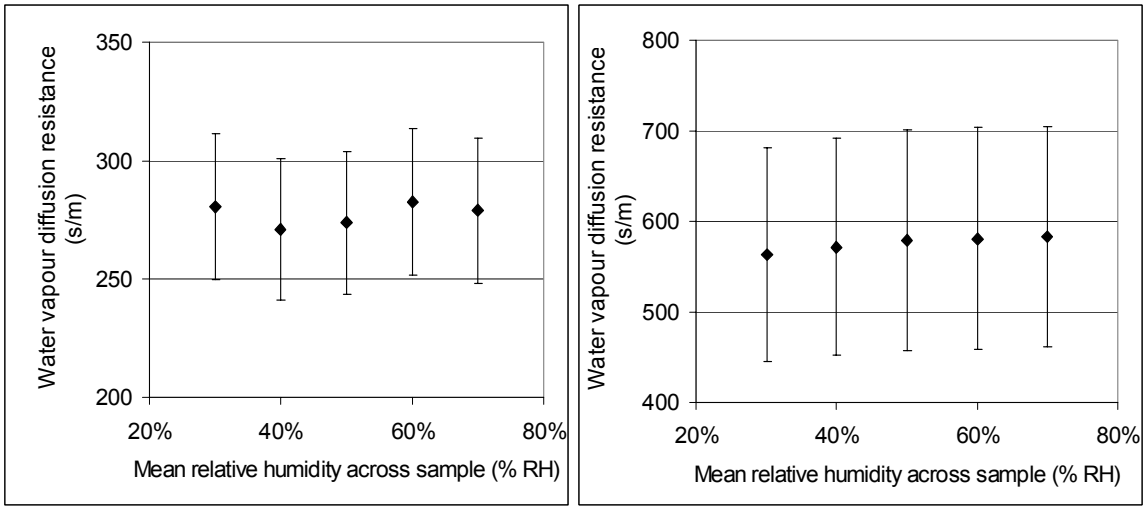

Figure 2.8. Vapour diffusion resistance as a function of humidity for (a) Propore™ and (b) Tyvek®.

It can be seen that the vapour diffusion resistance is not sensitive to the mean humidity for the Propore™ and Tyvek® membranes. This is generally the case for hydrophobic microporous materials in which adsorbed water does not play a significant role in the diffusion process (Gibson, 2000b).

The effects of the humidity gradient are investigated by performing tests with the same mean humidity but with different humidity gradients. The results are of interest in this thesis since the humidity gradient across the membrane in the exchanger will constantly be changing and will often be relatively small. The results are shown in Figure 2.9

(a) (b)

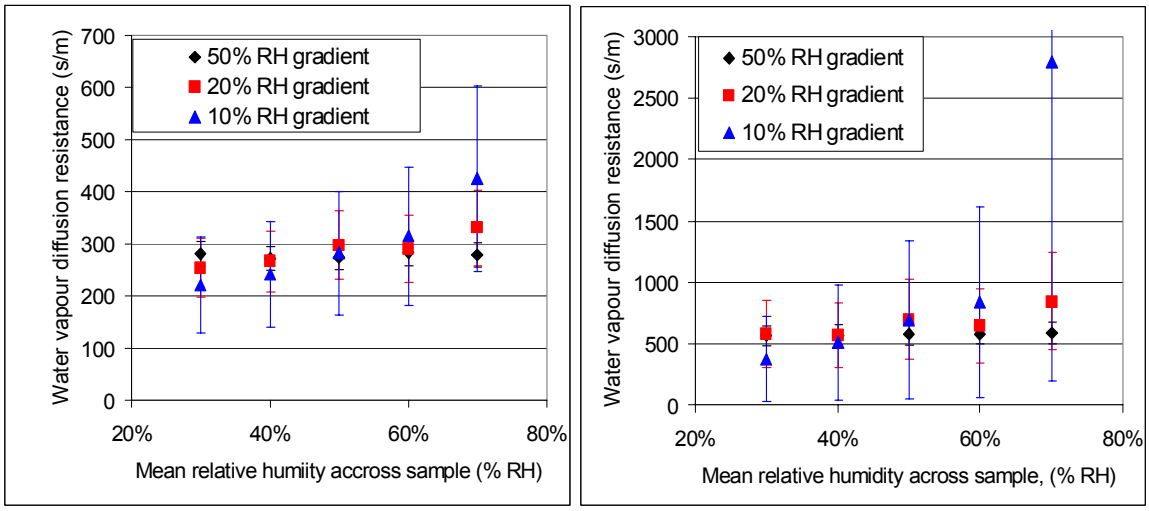

Figure 2.9. Effect of humidity gradient on vapour diffusion resistance for (a) Propore™ and (b) Tyvek®.

It can be seen that as the humidity gradient decreases, the vapour diffusion resistance becomes more sensitive to the mean humidity of the test. However, the uncertainty in the measurement at the low humidity gradients is quite large and therefore this dependence is not conclusive. It is possible that there is a small dependence of the vapour diffusion resistance on the sorption properties of the material that can only be seen at relatively low concentration gradients. If this is the case, then the performance of the RAEE system may be decreased when the humidity differences are small and the

operating conditions are humid. The effect is likely caused by the humidity sensors used in the DMPC apparatus which have increased error at high humidity.

The effect of air flow rate on the vapour diffusion resistance is important because the air flow rates used in the model of Fan et al. (2006) of the RAEE system are larger compared to the flow rates of the DMPC. To study the effect of air flow rate, the vapour diffusion resistance is presented as a function of the air flow rate in Figure 2.10. In Figure 2.10 the averaged total resistance is shown along with the corrected resistance. The corrected resistance is equal to the total measurement minus the boundary layer resistance or the ePTFE resistance.

(a) (b)

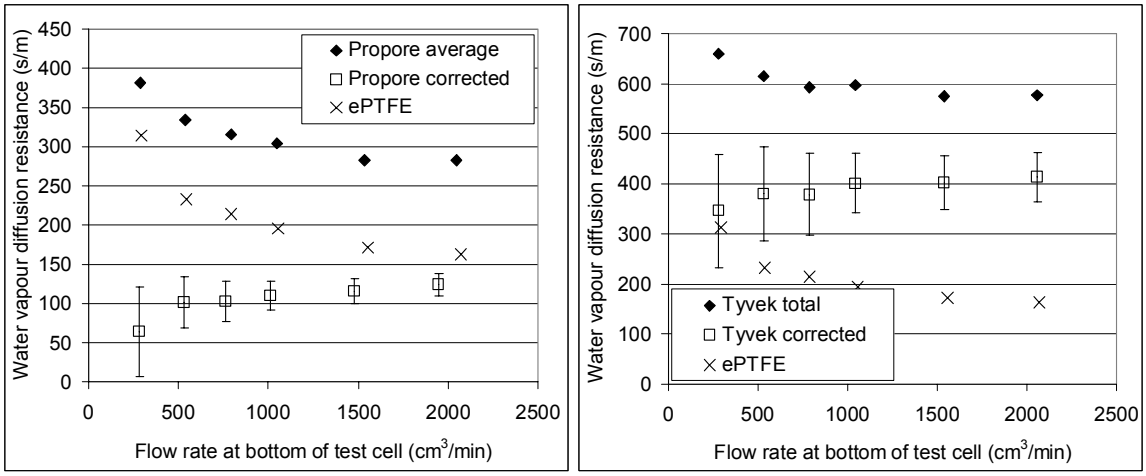

Figure 2.10. Effect of flow rate on vapour diffusion resistance for (a) Propore™ and (b) Tyvek®.

The results of Figure 2.10 show that the corrected vapour diffusion resistance increases as the flow rate increases. The range of flow rates in the test cell give laminar and fully developed flow conditions over the sample in the test cell and therefore the convective mass transfer coefficient, and consequently the airflow boundary layer resistance, should remain constant. If the flow is not fully developed, the convective

mass transfer coefficient would be greater and the total resistance would decrease. As the flow rate increases the flow takes longer to become fully developed and a drop in the total resistance is seen. The corrected resistance should eliminate any effect of a developing boundary layer in the test cell since only the material vapour diffusion resistance is desired. Although the corrected resistance is lower at low air flow rates, the vapour diffusion resistance is constant within the uncertainty of the measurement.

The flow conditions of the test cell have been presented by Gibson et al. (1995) in the form of analytical calculations as well as numerical modelling. Laminar flow conditions are maintained in the DMPC at all times. The test cell of the DMPC was designed with a distance of 0.07 m between the flow entrance and the sample. Calculations show that the entrance length of the flow will be less than 0.07 m for all cases. Contradictory to the calculations of Gibson et al. (1995) the results of Figure 2.10 indicate that flow may not be fully developed at the higher flow rates.

In calculating the vapour diffusion resistance of a membrane, the log mean concentration difference is used to quantify the concentration difference across a sample. A log mean concentration difference is used across a sample to account for the changing concentration from the inlet to the outlet on one side of the specimen. The measurements in this thesis are all taken with the air flows in parallel flow. To investigate the effect of air flow arrangement, the test of Tyvek® as a function of humidity with a 50% relative humidity gradient is repeated with counter flow arrangement and the results are shown in Figure 2.11.

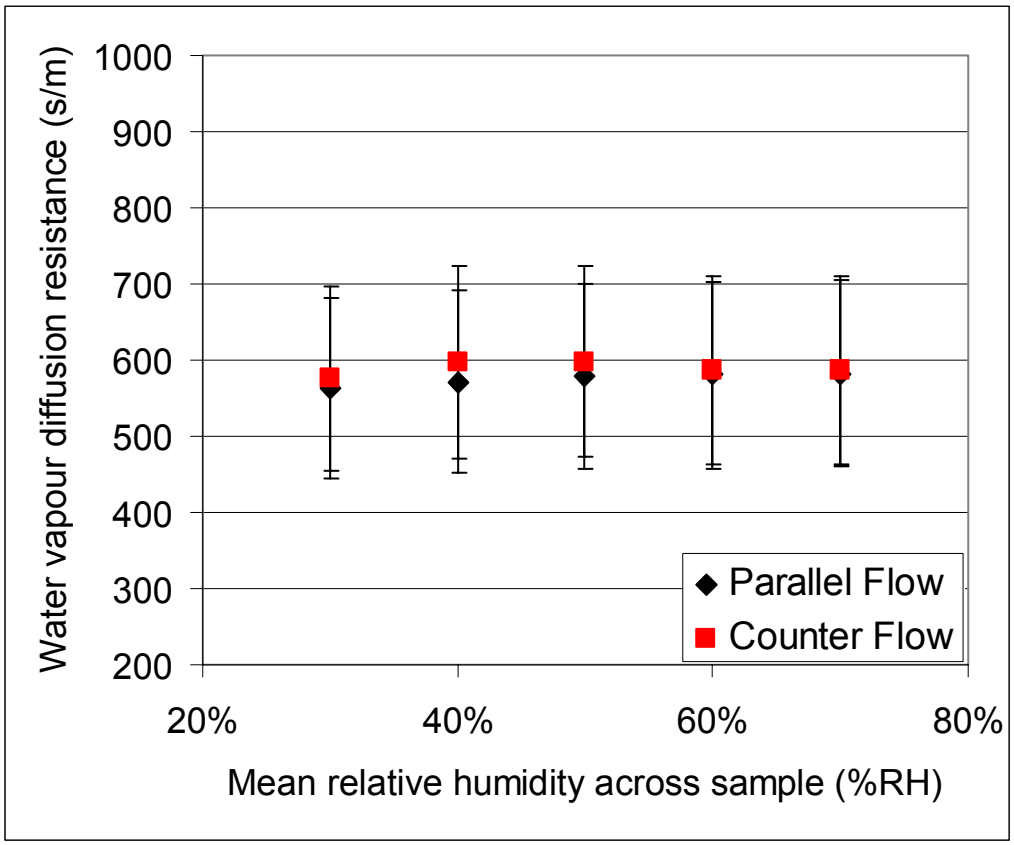

Figure 2.11. Effect of counter flow versus parallel flow in the test cell for Tyvek®.

It can be seen that the flow orientation has a negligible effect on the results, especially considering the uncertainty bounds of the measurements. Although a counter flow arrangement would result in a more uniform concentration difference across the sample than a parallel flow, the effects are not measurable within the uncertainty of the apparatus.

2.5.2 Air permeability

Figure 2.12(a) shows the vapour diffusion resistance as a function of pressure differential across the membrane. For this test, the humidity gradient is held constant at 90% RH, the volume flow rate is held at 2000 cm^3/min and the pressure differential across the sample is varied. Figure 2.12(b) shows the variation of the flow rate at the

bottom of the test cell as a function of the pressure differential across the sample. The plots of Figure 2.12 are used to calculate the air permeability values of Tyvek® and Propore™ that are summarized in Table 2.3. The equations used to obtain the air flow resistance are given in Appendix A. The plots of Figure 2.12 are the average measurements of three samples.

(a) (b)

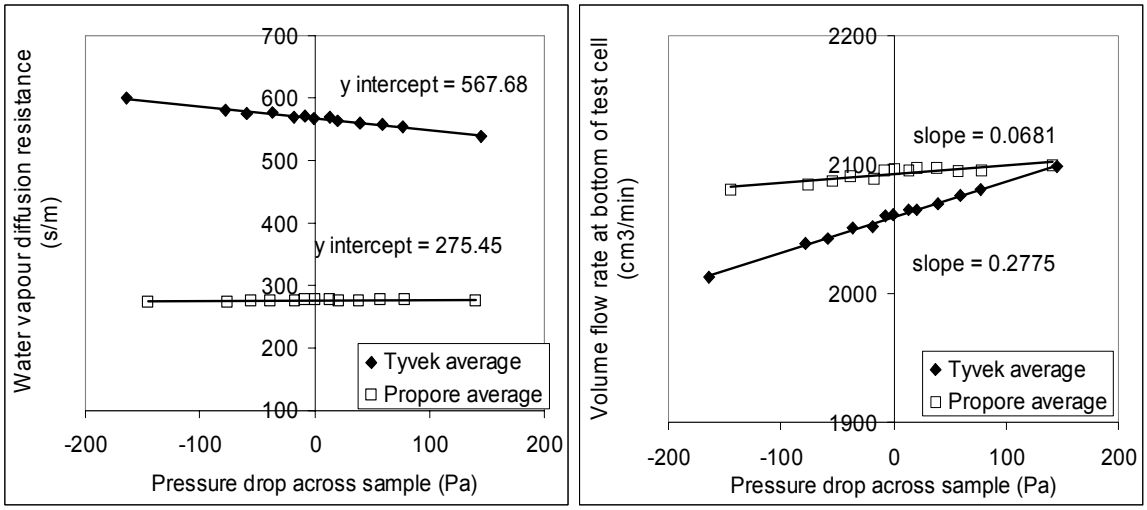

Figure 2.12. (a) The vapour diffusion resistance of Propore™ and Tyvek® given as a function of the pressure drop across the sample and (b) the total flow rate at the bottom of the test cell as a function of the pressure drop across the sample for both Propore™ and Tyvek®.

A material with no air permeability will have zero slope in Figure 2.12(a). The plot of Figure 2.12(a) shows that Tyvek® has a greater slope than Propore™, which indicates that it is more air permeable than Propore™. The y-intercept of Figure 2.12(a) gives the vapour diffusion resistance of the material at a zero pressure gradient. This value is the same as the values shown in Figure 2.8 at a mean humidity of 50% RH.

The values of slope shown in Figure 2.12(b) are used in the calculation of the Darcy flow resistance. A material with a greater slope indicates less resistance to air flow

through the membrane since for a given pressure difference there is more air flow through the specimen. The air permeability of the Tyvek® and Propore™ membranes are given in Table 2.3 along with some other common materials included for comparison.

Table 2.3. Summary of the Darcy air flow resistance.

	Darcy air permeability resistance (1/nm)
Silk	0.04
Cotton	0.14
Thin Paper	0.18
ePTFE	4
Tyvek	27
Heavy Paper	61
Propore	111

Table 2.3 shows that Propore™ has approximately four times greater resistance to air flow than Tyvek®. It may be expected that a greater resistance to air flow will be accompanied by a greater vapour diffusion resistance; however, the pores of the Propore™ are oriented such that the vapour diffusion resistance is lower than that of Tyvek®. This increased air flow resistance of Propore™ makes it a better candidate for the RAEE system since any air leakage will be significantly less than with Tyvek® for the same pressure difference. Since the pressure of the liquid side should always be higher than the air side in the RAEE, this situation will likely never happen, although it is an added failsafe for the Propore™ membrane in this unlikely situation.

2.5.3 Modified test method

It is apparent from the literature that the results of vapour diffusion resistance are sensitive to test method (McCullough et al., 2003). The results of the DMPC are chosen since it is the method best suited to thin membranes and membranes with advective

mass transfer, but the fact remains that the results of the DMPC are for boundary conditions of air on both sides of a membrane. The RAEE system has boundary conditions of liquid on one side of the membrane and air on the other. It was shown by McCullough et al. (2003) that the difference in boundary conditions of the cup test resulted in a difference of 10 times in the mass flux through the specimen. To see if this dependence also exists in the DMPC, a set of tests are performed with the upper air stream replaced with liquid water providing a relative humidity of 100%. The test setup is identical to Figure 2.5 except that the test cell is modified and the top flow control is removed. A photo of the modified test cell is shown in Figure 2.13

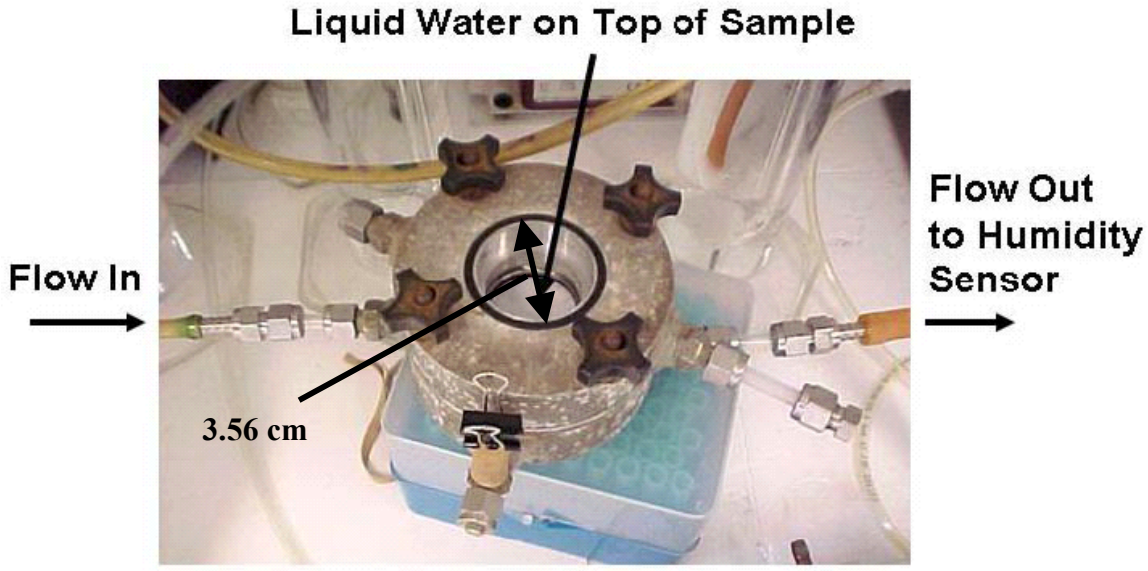

Figure 2.13. Modified liquid/vapour diffusion cell.

The results of the modified test method are summarized in Figure 2.14 where the water vapour diffusion resistance is shown as a function of mean humidity. Note that limited data points are available for the modified test method since the top humidity is always 100% RH and as the gradient becomes smaller the uncertainty becomes highly significant.

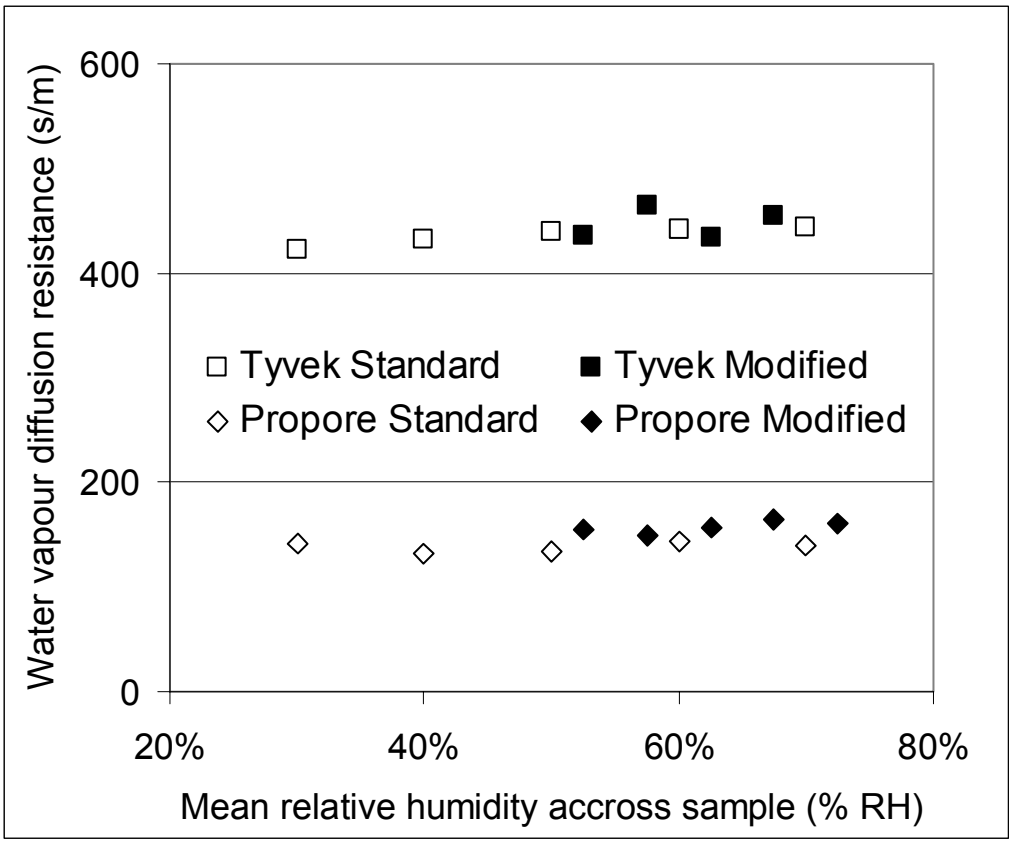

Figure 2.14. Vapour diffusion resistance as a function of the mean humidity for the modified test apparatus.

The standard values of Figure 2.14 are corrected for the boundary layer resistance as previously discussed. The modified values are corrected by half of the boundary layer resistance in the standard test due to the stagnant water layer on one side of the specimen. The results of the modified test agree very well with the standard DMPC test and this confirms that the use of the standard test results are valid for the alternative boundary conditions of the RAEE exchanger.

2.6 Application

The impact of a membrane's vapour diffusion resistance is best quantified by the effect on the overall effectiveness of the RAEE system. To investigate the performance of the membranes on the system, the mathematical/numerical model of Fan (2005) is

used. The model consists of a computer program written in the C++ language. The user inputs the supply and exhaust inlet conditions, the type of salt to be used and the physical dimensions of the exchanger cores. The program then solves the mass and energy balance equations with the known inlet conditions to iteratively compute the outlet conditions and effectiveness of the RAEE system at steady state. A more detailed description of the model including the energy balance, and effectiveness equations used can be found in Appendix C.

The model of Fan et al. (2006) uses a permeability constant, k_m, that is defined based on the humidity ratio from the following equation,

$$\dot{m}'' = k_m \frac{\Delta W}{\Delta z} \qquad [2.4]$$

where ΔW is the humidity ratio difference [$g_{\text{water vapour}}/kg_{\text{dry air}}$], and k_m is the vapour permeability [kg/(m s)].

A conversion of the following form is used to obtain the value of vapour diffusion resistance in the units of the DMPC tests from the vapour permeability of Fan's model (2005).

$$R_m = \frac{\Delta z \cdot M_w \cdot P_{atm}}{k_m \cdot R \cdot T \cdot 0.6219} \qquad [2.5]$$

To investigate the effects of changing R_m, the program of Fan (2005) is run several times at a set of standard conditions with only the vapour diffusion resistance changed between program runs. The standard condition is summarizes in Table 2.4. The inlet conditions are ARI 1060 (2001) summer conditions and the dimensions are for the second prototype exchanger. The operating conditions of the loop are chosen to

maximize effectiveness based on the work of Fan et al. (2006) (i.e. Mr=1 and Cr*=2.8). The parameters used in the model of Fan et al. (2006) are described in Appendix C.

Table 2.4. Summary of operating conditions for sensitivity study of vapour diffusion resistance in numerical model of Fan (2005).

Supply inlet temperature	308 K	ANSI/ARI Standard 1060 (2001) Summer conditions
Supply inlet humidity ratio	17.5 g/kg	ANSI/ARI Standard 1060 (2001) Summer conditions
Exhaust inlet temperature	297 K	ANSI/ARI Standard 1060 (2001) Summer conditions
Exhaust inlet humidity ratio	9.5 g/kg	ANSI/ARI Standard 1060 (2001) Summer conditions
Air flow rate	3.3 L/s (7 CFM)	
Face velocity (Air)	0.22 m/s (43 FPM)	
Salt solution in loop	$MgCl_2$	
Exchanger dimensions	0.3 x 0.6 x 0.1 m	Dimensions of second prototype
Air side channel spacing	5 mm	
Liquid side channel spacing	0.6 mm	
Membrane thickness	0.2 mm	Propore™ thickness
Membrane thermal conductivity	0.334 W/m K	PP conductivity
Capacitance ratio Cr*	2.8	
Mass flow ratio Mr	1	
Number of heat transfer units NTU	12.5	
Number of mass transfer units NTUm	0.05 – 12.9	Varies with membrane vapour diffusion resistance

Using the standard conditions, the total effectiveness of the RAEE system as a function of the changing vapour diffusion resistance is shown in Figure 2.15. Note that the vapour diffusion resistance is plotted on a log scale.

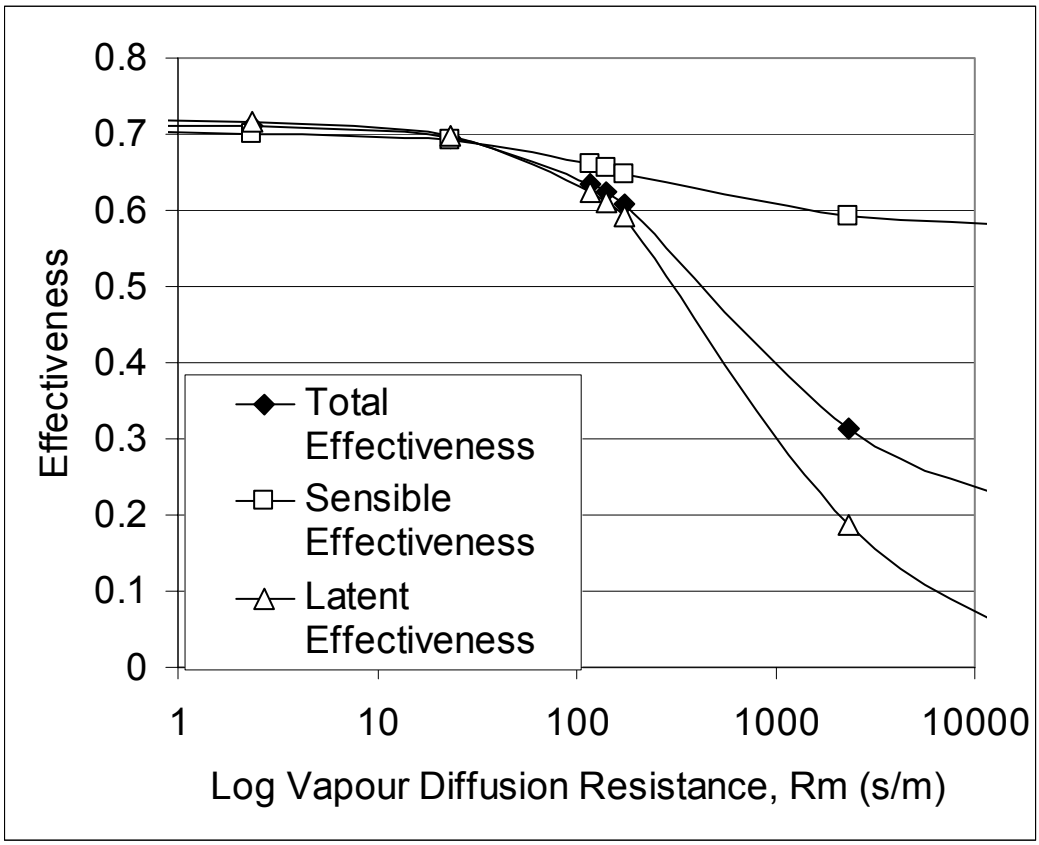

Figure 2.15. The maximum overall RAEE effectiveness as a function of the vapour diffusion resistance calculated from the numerical model of Fan et al. (2006) using $MgCl_2$ salt solution as the coupling fluid.

The sensitivity of the maximum overall effectiveness of the RAEE system as a function of the vapour diffusion resistance can be seen for vapour diffusion resistance values greater than 20 s/m. The data point at a vapour diffusion resistance of 140 s/m represents the simulation of the second prototype exchanger made with the Propore™ membrane. The data points above and below the point at 140 s/m represent the uncertainty bounds on the total effectiveness based on the uncertainty of the measured vapour diffusion resistance from Section 2.4. It is concluded that at the ARI summer operating condition shown in Table 2.4, the maximum overall effectiveness of an exchanger using the Propore™ membrane will be 62.4 ± 1.3% where the uncertainty is

due to the uncertainty in the membrane vapour diffusion resistance measurement. This value is well above the required 50% effectiveness for compliance with ASHRAE 90.1 (2004). The Tyvek® membrane simulation (not shown) results in a maximum overall effectiveness of 52%. Although, this is still in compliance with ASHRAE 90.1 (2004), it would not likely be acceptable for commercial manufacturing of the RAEE.

The second prototype exchanger was tested over the summer of 2006 by Erb (2006). The air flows tested by Erb ranged from 7 to 12 L/s (15 to 23 CFM) which corresponds to a face velocity of 0.4 to 0.6 m/s (75 to 115 FPM). These face velocities and flow rates are higher than the simulated conditions of Table 2.4; however, the most important dimensionless parameters; NTU, Cr*, and total effectiveness are directly comparable. Figure 2.16 shows a comparison of the total effectiveness of the RAEE system predicted by Fan (2005) to the testing of the second prototype by Erb (2006).

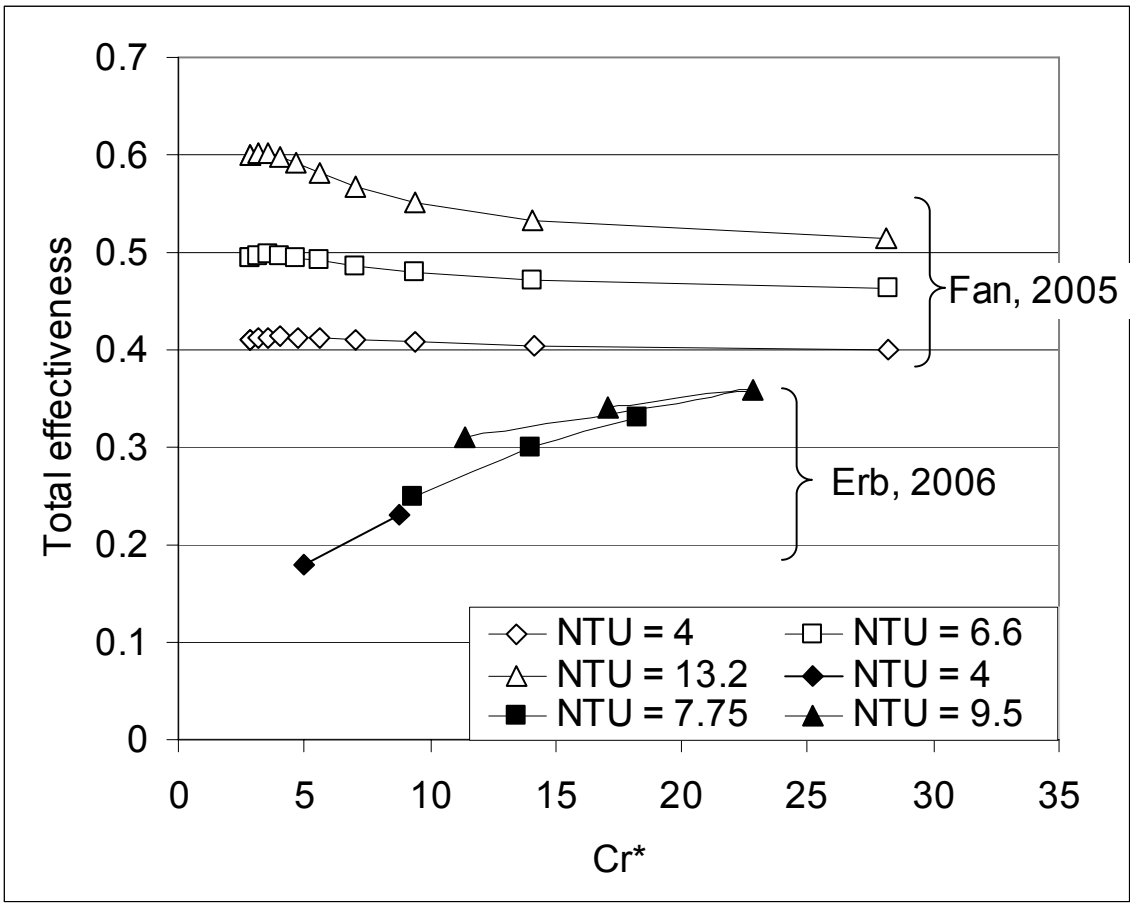

Figure 2.16. Comparison of Fan's numerical simulation (2005) to the testing of the second prototype by Erb (2006) using $MgCl_2$ as the coupling fluid.

The effectiveness predictions of Fan (2005) are consistently greater than the second prototype test results of Erb (2006). The effectiveness values of Erb (2006), and Fan (2005), increase with NTU. This increase is expected since a higher NTU corresponds to a higher heat transfer rate. The effectiveness predictions of Fan (2005) show a peak in the total effectiveness at Cr* = 3; however, a peak is not seen in the test results of Erb (2006). The values of effectiveness predicted by Fan (2005) reach a constant value with Cr* greater than 20, while the effectiveness values of Erb (2006) continue to increase with Cr*. The differences between the effectiveness values of Fan (2005) and Erb (2006) at the lower Cr* values are explained in part by uniformity of the liquid flow

distribution through the prototype exchanger. In the prototype testing, the flow of the liquid desiccant was increased to take measurements at an increased Cr* value. It was observed that as the flow rate of the salt solution was increased there was less salt solution remaining in the liquid reservoir. This reduction in the reservoir with increasing flow rate indicated that there was more fluid being held in the exchanger at the higher Cr* values, and therefore the exchanger was not likely completely full of fluid at the lower Cr* values. With a lack of fluid in the exchanger, heat and mass transfer is significantly diminished which results in the low effectiveness values of the second prototype testing at the low Cr* values. If higher Cr* values were tested it is likely that the results of Erb (2006) would reach the same steady value as Fan's model (2005) which assumes perfect flow distribution at all Cr* values. If each exchanger outlet flow were restricted so that each exchanger were completely filled with liquid, the test results might agree with Fan's model over the entire ranger of flow rate ratio Cr*.

2.7 Conclusions

Based on the measurements performed by Gibson and presented in this chapter, it can be concluded that the Propore™ membrane is better suited for use in the RAEE exchanger than the Tyvek® membrane. The Propore™ membrane has a vapour diffusion resistance that is approximately 50% lower than the Tyvek® membrane and an air flow resistance that is four times greater than the Tyvek® membrane. Both membranes are not sensitive to the mean humidity across the sample and show consistent vapour diffusion results, within the uncertainty bounds, with varying flow rates, and flow orientation and boundary conditions.

The application of the Propore™ membrane in the second prototype is explored numerically using the numerical model developed by Fan (2005). Results show that

variations in the material and the uncertainty of the measurement have a small effect on the total effectiveness of the RAEE system. The predicted maximum overall effectiveness using the defined ARI summer test conditions is 62.4 ± 1.4 %. This value is in compliance with ASHRAE standard 90.1 (2004) which requires an energy exchanger to have a total effectiveness of at least 50%.

The testing of the second prototype exchanger yielded a maximum total effectiveness of 36%. This low value is thought to be effected by the poor flow distribution through the prototype exchanger during testing and needs to be addressed in future testing of prototypes.

CHAPTER 3
LIQUID PENETRATION MEASUREMENTS

The water vapour permeability of the membrane governs the effectiveness of the RAEE system; however, the membrane is ineffective if liquid is allowed to pass through its microstructure. All membranes have a pressure at which the liquid will be forced through; this pressure is known as the liquid penetration pressure. In general, as a microporous material is made thinner, the vapour diffusion resistance will decrease and the liquid penetration pressure will also decrease. A balance of these properties is required to obtain optimum performance. The liquid penetration pressure should be as high as practical but at the very least must be greater than the operating system pressure of the RAEE.

Liquid penetration depends on the microstructure of the membrane and the pressure of the fluid on the membrane. Similar to the water vapour permeability, there are a number of standard tests to determine the liquid penetration resistance of a membrane. For this thesis a special test apparatus was designed, constructed and used for all tests.

3.1 Test methods

There are currently a number of different standards for testing of liquid penetration resistance of materials. The methods are all very similar in that they apply a liquid pressure to one side of a clamped specimen which is observed for leakage. The primary difference between the methods is the method of applying pressure to the specimen. AATCC test method 127 (2003) uses a column of water to apply the pressure to the specimen. This standard is commonly quoted by manufacturers of textiles and some

membranes. Although it is easy to perform, the main drawback of this test method is that the applied pressure is limited to the height of the water column. The Japanese standard JIS L 1092 (1998) uses a mechanical means of increasing the pressure via a piston and hand crank, while ASTM F 903 (2004) uses a source of compressed air to apply pressure and ASTM D 779 (2003) or the "boat test" applies pressure using a fixed standing water column and the time to penetration is measured. In all cases, the dry side of the specimen must be observed for drops of liquid and the test is terminated when the third drop of liquid is seen. A schematic of AATCC test method 127 (2003) and ASTM F 903 (2003) is shown in Figure 3.1

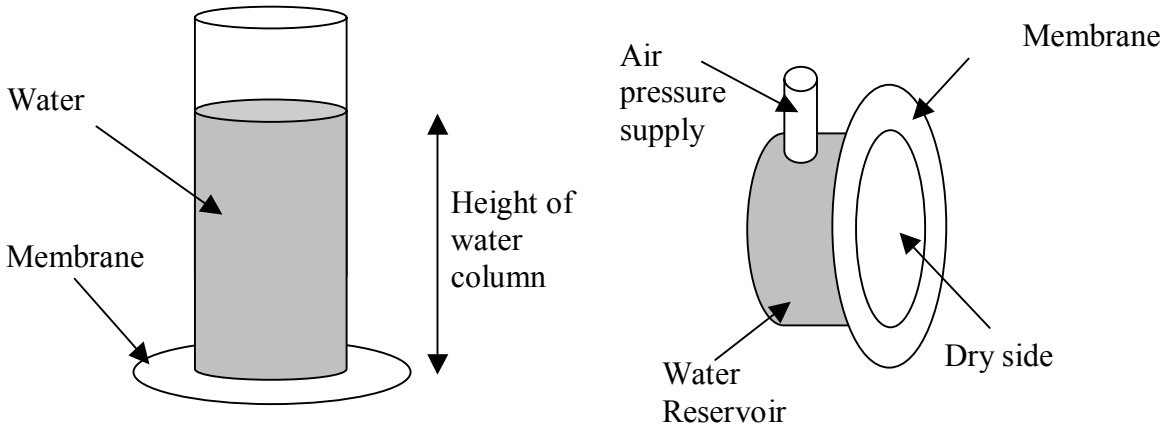

Figure 3.1. Schematic of liquid penetration measurements (a) AATCC test method 127 (2003) and (b) ASTM F 903 (2003).

The rate of pressure application varies between the standards as well. In AATCC test method 127 (2003) the pressure is increased at a constant rate of 6000 Pa/min by increasing the height of the column of water above the sample. In ASTM F 903 (2004) a given pressure is applied for a given amount of time and membranes either pass or fail the test. In ASTM D 779 (2003) a given pressure is applied and the time required for liquid penetration is measured. In JIS L 1092 (1998) provisions are made for low and

high liquid penetration resistance materials. In the high pressure test, the pressure is increased in steps of 0.5 kg/cm^2 per minute (49000 Pa/min) and the membrane is checked at each interval for liquid penetration.

The ASTM tests are qualitative since the results are only meaningful when compared to other membrane materials. The results of JIS and AATCC give values of liquid penetration pressure which are directly comparable to pressures within the RAEE system and are therefore more useful. In this thesis, the AATCC test method 127 (2003) is used due to its simpler procedure and apparatus; however, due to the high liquid penetration pressure of Propore™ a modified test apparatus is used. The JIS L 1092 (1998) test method is also desirable and has the ability to test materials with higher liquid penetration pressure. However, the apparatus is not readily available and is more complicated than that of AATCC test method 127 (2003) and therefore the JIS L 1092 (1998) standard test method is not pursued.

3.2 Test apparatus

Figure 3.2 shows a schematic of the system and Figure 3.3 shows a photo of the system as it is set up in the laboratory.

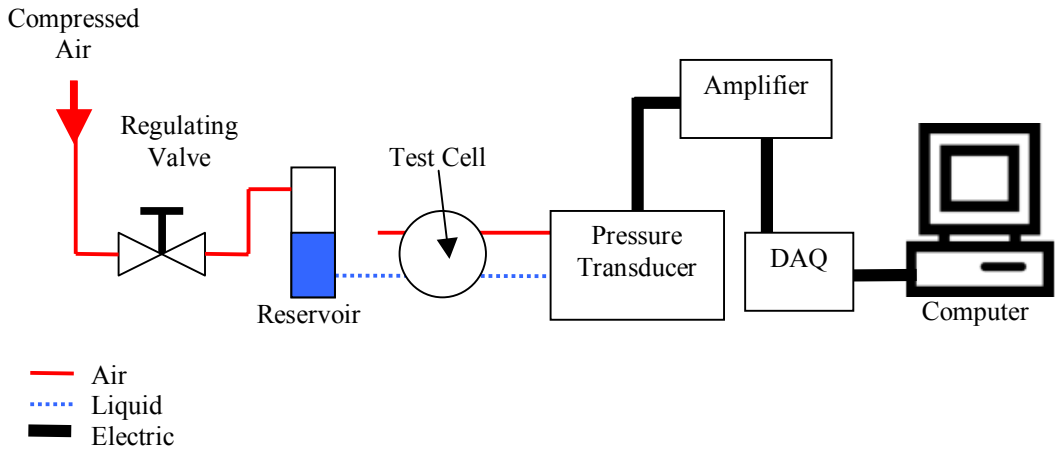

Figure 3.2. Schematic of the liquid penetration pressure apparatus.

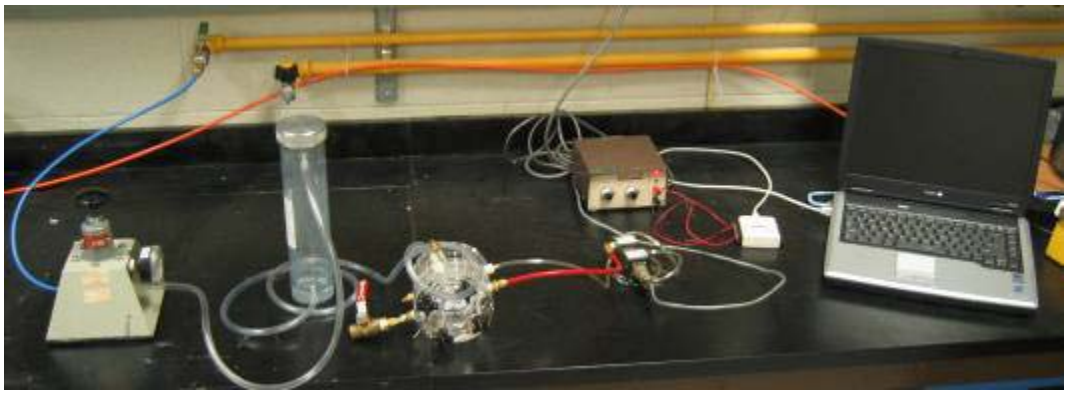

Figure 3.3. Picture of liquid penetration pressure apparatus showing the components listed in Figure 3.2.

The modified AATCC test method 127 (2003) apparatus and test cell is constructed according to the specifications of ASTM F 903 (2004). This method uses compressed air to pressurize the test water. Compressed air allows more flexibility in the range of test pressures and is easier to control than a column of water. As a result the test apparatus is capable of performing the ASTM F 903 (2004) standard test and a modified AATCC test method 127 (2003). The test method of ASTM F 903 (2004) is specified for protective clothing and is designed to give a pass fail result for material with short

exposure to liquids. Consequently AATCC test method 127 (2003) results are the only results presented in Section 3.3.

The size of the test specimen area is not stated in AATCC test method 127 (2003) although some commercially available apparatus use an area of 100 cm^2. The area of the modified apparatus uses the value of 25.8 cm^2 which is the area used in ASTM F 903 (2004).

Compressed air, obtained from the building supply, is used to pressurize the water reservoir shown in Figure 3.2 and Figure 3.3. The building supply air enters at approximately 690 kPa (100 psi). The air passes through a regulating valve that can be changed depending on the membrane being tested. This regulating valve serves as the control method for the applied pressure during a test. The air is then connected to a cylindrical reservoir of distilled water. The reservoir is a convenient means of filling the test cell with liquid and also ensures that no air will enter the test cell with deflection of the membrane being tested. The air side of the membrane is open to atmospheric pressure as shown in Figure 3.4(b). Both sides of the test cell are connected to a differential pressure transducer calibrated from 0 to 276 kPa. The transducer signal is amplified and the voltages are read by a National Instruments USB-6009 14 bit data acquisition system coupled with a personal computer using LabVIEW software to control the data acquisition system.

Figure 3.4 (a) and (b) are close up photos of the test cell. In Figure 3.4 (a) the cell is disassembled while in Figure 3.4 (b) the cell is assembled as it is during a test.

Figure 3.4. Liquid penetration test cell (a) disassembled and (b) as assembled during testing.

Each half of the cell has three threaded openings. Each half has an output to the pressure transducer, an opening in the top for the fluid to enter and an opening to drain the chamber by means of a ball valve. In Figure 3.4 (a) and (b) the liquid side has all three openings in use while the air side has only the transducer line in use; the other two openings on the air side are open to the atmosphere. The following results are for a pressurizing fluid of distilled water and all tests are done at laboratory temperatures.

3.3 Results

The results of the modified AATCC test method 127 (2003) are given in Table 3.1 and compared with the data of Butt (2005) and the manufacturers' data. The data of Butt (2005) and the manufacturer are obtained using AATCC test method 127 (2003). In the paper by Butt (2005), the Tyvek® tested was not the Japanese Tyvek® but the HomeWrap® version. An equivalent value is obtained by applying Darcy's equation ([A.19]) to the flow of liquid through the membrane. Since the velocity is approaching zero as the liquid is initially penetrating the membrane, the left hand side in set to zero. Darcy's equation is then written for the measured HomeWrap® membrane and for the Japanese Tyvek® membrane. Since the membrane is made of the same material the

Darcy permeability (k_D) is equal and since both membranes are tested using distilled water at the same temperature the water viscosities are equal. Cancelling out the common terms leaves the relation,

$$\frac{p_{p_1}}{\Delta z_1} = \frac{p_{p_2}}{\Delta z_2} \qquad [3.1]$$

where p_{p_1} [Pa] and p_{p_2} [Pa] are the liquid penetration pressures and Δz_1 [m] and Δz_2 [m] are the membrane thicknesses.

Note that the pressure difference is measured relative to atmospheric pressure so the Δp of equation [A.19] becomes the liquid penetration pressure. In general, the calculated liquid penetration pressure of a material is proportional to the thickness and can be predicted for any thickness if the liquid penetration pressure is known at any one thickness.

Table 3.1. Summary of liquid penetration results.

	Measured (kPa)	Butt, T.K.,(2005) Corrected (kPa)	Manufacturer (kPa)
Tyvek®	17.8	18.3	15.4
Propore™	>276	n/a	>345

The measured values of liquid penetration pressure for Tyvek® agree well with the available published data. The measured Tyvek® value is an average of 10 measurements consisting of samples oriented in both directions. The measured value of penetration resistance for Propore™ is given as greater than 276 due to the fact that there was no penetration of liquid at the maximum readable pressure of the pressure transducer. This occurred only in the case of the membrane being oriented with the non-woven PP layer away from the liquid source. In this configuration the non-woven layer

acted as a support for the weaker microporous PP layer. In the opposite configuration (with the microporous PP membrane away from the liquid) the membrane ruptured at a pressure of approximately 140 kPa. In either orientation, the liquid penetration pressure of the Propore™ membrane is an order of magnitude greater than the Tyvek®.

The liquid penetration pressure must be compared to the operating pressure of the system to draw conclusions about the usefulness of the membrane in the RAEE system. The operating pressure of the RAEE system is not fixed, nor has it been explicitly determined since the RAEE system is still in the prototype stage. Based on the dimensions of the current prototype, the pressure of the standing water is approximately 3 kPa. Assuming the exchangers of the RAEE system are separated by one floor (3 m), the additional pressure would be 30 kPa, giving a total pressure in the RAEE of 33 kPa not including additional system pressure. The values of liquid penetration pressure for Tyvek® are less than this total pressure but greater than the standing water only pressure. The Tyvek® membrane could only be used in specific cases where minimal pressure occurs. The pressure for the Propore™ membrane is nine times greater than the required pressure at 3 metres and could be successfully implemented in this scenario. However, the total system pressure of 33 kPa is a low estimate and this value could potentially be much higher due to increased system pressure and any greater difference in the height of the exchangers.

3.3.1 Time dependence

Since the RAEE system will be under a pressure for extended periods of time the effects of long term pressure application are investigated. Figure 3.5 shows the liquid penetration resistance as a function of time for the Tyvek® membrane. The data points

in Figure 3.5 are obtained by placing a fixed pressure on the membrane and checking the dry side of the specimen for penetration twice a day.

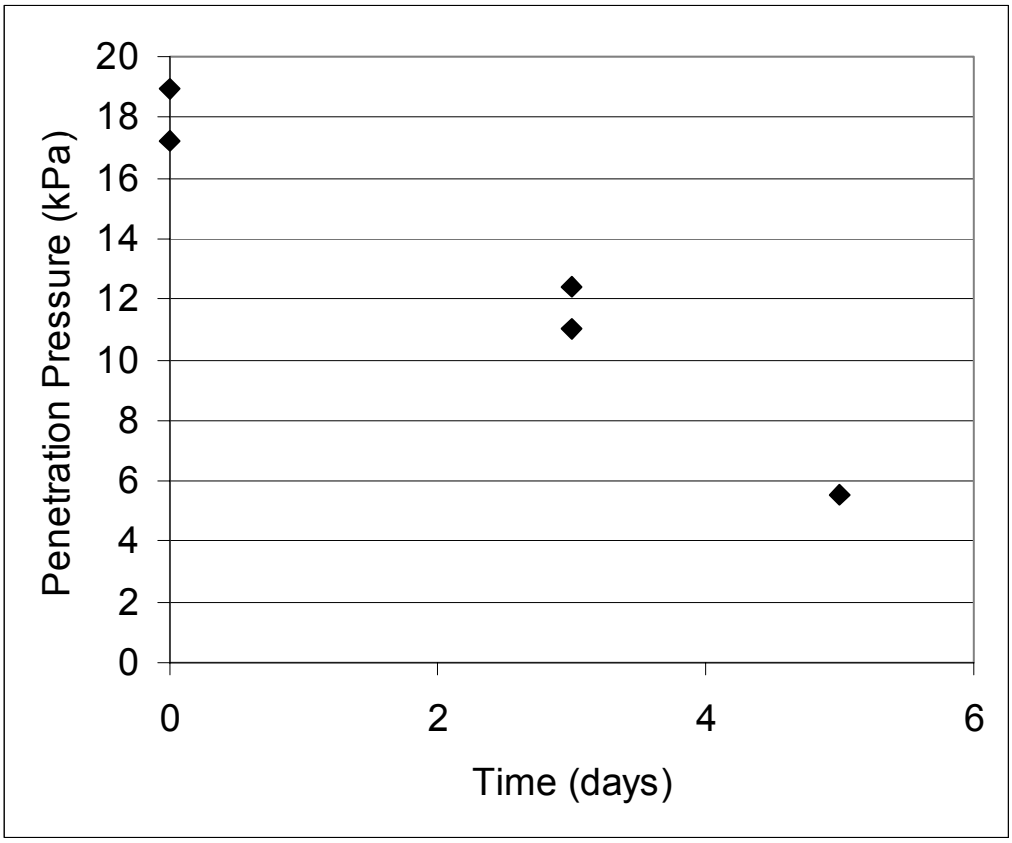

Figure 3.5. Liquid penetration pressure as a function of time for Japanese Tyvek®.

It can be seen that when left over several days, the membrane will allow water to pass at a much lower pressure than if the pressure is gradually increased during a shorter test. AATCC test method 127 (2003) states that the pressure is to be applied at a rate of 60 mbar/min (0.87 psi/min). For this standard rate, the results are as shown at time 0 in Figure 3.5. The results of Figure 3.5 indicate that there is possibly some time dependent deformation of the microstructure or creep occurring in the membrane as it is subjected to a constant load over a period of time. The Propore™ membrane did not allow any liquid penetration even when tested at 100 kPa for 5 days.

3.3.2 Effect of repeated tests

After a modified AATCC test method 127 (2003) penetration test is completed, there is some deformation visible in the Tyvek® membrane. To determine if this deformation will affect the liquid penetration pressure of the membrane, a series of consecutive tests are performed on the same membrane sample. These tests are performed at the standard rate of 60 mbar/min (0.87 psi/min). After each test, the membrane is removed from the apparatus and allowed to dry in front of a fan for at least 2 hours before re-testing. Figure 3.6 shows the results for two different samples of the Tyvek® HomeWrap® material (Not Japanese Tyvek®). Note that the values are greater than for the Japanese Tyvek® due to the increased thickness, however the trend is the same.

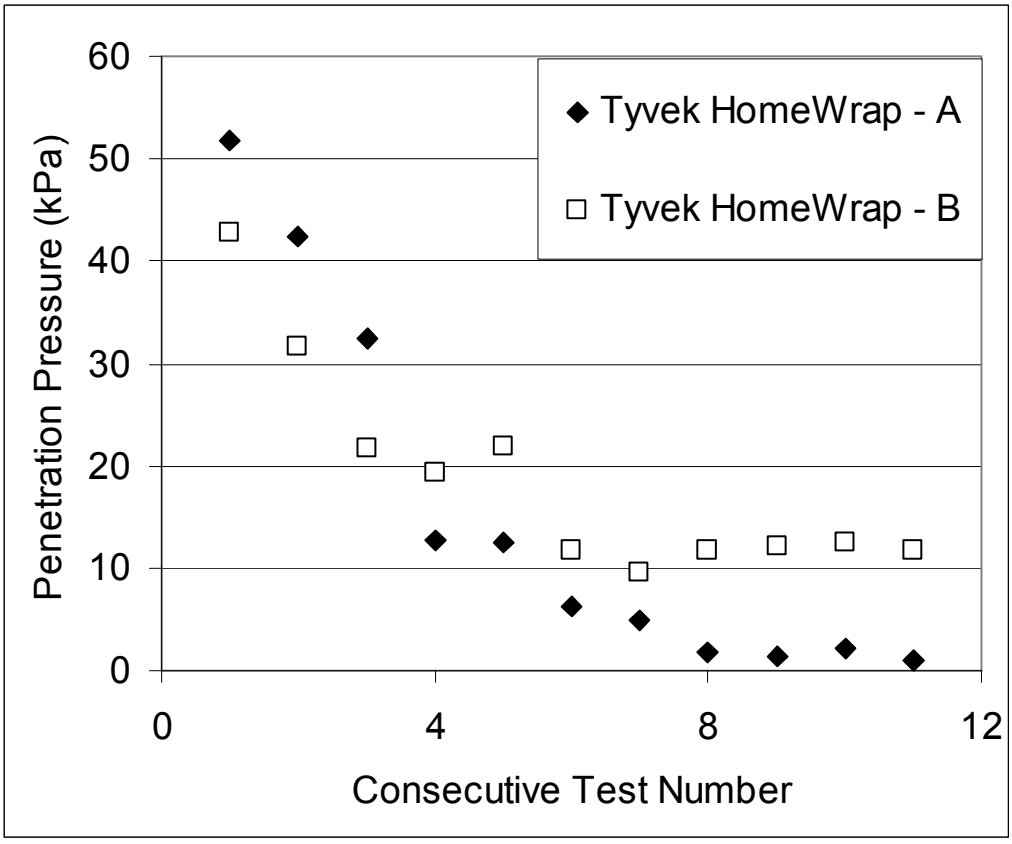

Figure 3.6. Liquid penetration pressure of Tyvek® HomeWrap® over a series of consecutive tests.

Figure 3.6 shows that as a specimen is consecutively tested the liquid penetration pressure decreases until it reaches a constant value. It is speculated that the stretching of the pores in the membrane as water passes through is plastic and that the membrane's capacity to resist the penetration of water is subsequently diminished. The current standards make no provision for testing specimens multiple times. This behaviour is of interest for the RAEE system since any liquid penetration could actually decrease the liquid penetration resistance of the membrane in the exchanger.

To further investigate the effect of the deformation of the membrane a series of tests are completed using the same sample once again, but placing a fine screen in the apparatus for support. Figure 3.7 is obtained.

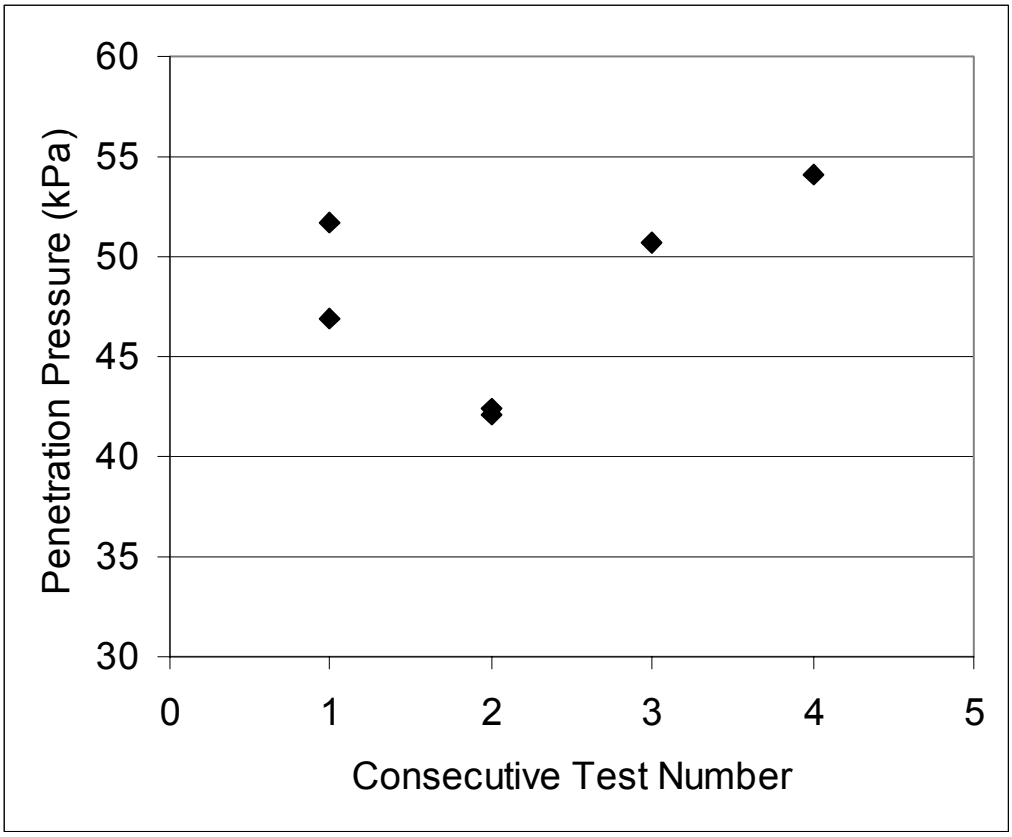

Figure 3.7. Liquid penetration pressure of Tyvek® CommercialWrap® for consecutive tests performed with a supporting screen.

Figure 3.7 shows that with the screen in place there is no decline in the liquid penetration pressure as observed in Figure 3.6. Thus using a screen can eliminate the problems of deforming the membrane during testing. The fine screen introduces a bias into the results; however, since the droplets cannot be seen immediately as in the case with no screen.

3.4 Conclusions

The measured pressure at which liquid water penetrates or passes through Tyvek® agrees well with the published data. The penetration resistance of the Tyvek® membrane is close to the design pressure of the RAEE system and could easily be exceeded during a pump failure or in a tall building. In addition, the liquid penetration pressure has been shown to decrease with an increased time of exposure.

The Propore™ material has a very high liquid penetration pressure relative to Tyvek® and is more likely to rupture before liquid passes through in the current test setup. In terms of liquid penetration pressure the Propore™ membrane is far superior to the Tyvek® and is the preferred membrane for the proposed RAEE exchanger.

CHAPTER 4
ELASTIC PROPERTY MEASUREMENTS

The design of a plate-type exchanger requires knowledge of the elastic properties of the membranes to ensure that the membrane's deflections will not significantly alter the flow of air or liquid. This is especially important for an energy exchanger made of vapour permeable membranes such as is the case for the RAEE. The RAEE system will have a positive pressure in the liquid channels and the deflection of the membrane into the air channel must be limited. This is accomplished by placing a screen over the membrane to give it support. The size of the screen squares must be as large as possible so that heat and moisture transfer area is not significantly reduced. The objective of this chapter is to determine the screen size to be used in the RAEE.

Fan (2005) has shown that an airflow channel size of 3mm gives good effectiveness results. The second prototype exchanger is constructed with 5mm airflow channels and therefore a design value of 1 mm is chosen as the maximum allowable deflection of the screen supported membrane into the air side channel. This limits the airflow channel to the desired 3mm and guarantees that the airflow will not be unduly restricted. It is important to note that deflection of the screen itself must also be considered in the final design. In this thesis the deflection of the screen is not considered and is left for future work. A schematic of the flow channels of the RAEE exchanger is shown in Figure 4.1

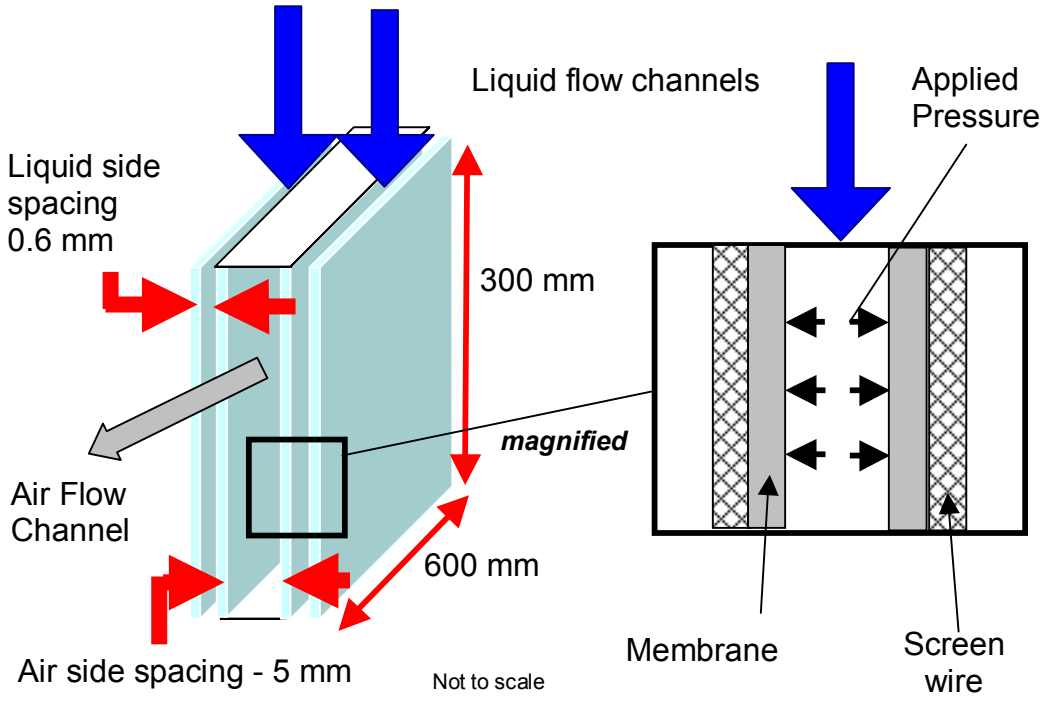

Figure 4.1. Schematic of the flow channels in the RAEE exchanger with a magnified cross section view.

The material properties required to predict the membrane's deflection are the elastic modulus (E) and the Poisson's ratio (ν) (Small and Nix, 1992). Since these properties are not available for the Propore™ and Tyvek® membranes, they need to be measured. The elastic modulus is traditionally determined using a tension test; however, an alternative method known as the bulge test is also used to determine the elastic modulus of thin membranes. To determine the best suited test method for the pressurized flow channel with screen support the effects of pre-stress, orientation, strain rate, and relative humidity are examined. Five test methods that are compared in this study include two ASTM tensile test methods and three analysis methods which use a bulge test.

Further bulge tests using different geometry are performed to experimentally confirm the accuracy of the obtained elastic modulus. This modulus is then used to predict

deflections of the pressurized membrane with a screen support. Finally, the size of screen that gives the maximum allowable deflection of 1 mm is chosen

4.1 Poisson's ratio test method and result

The definition of the Poisson's ratio for an elastic material subject to a uni-axial load is given by,

$$\nu = -\frac{\varepsilon_t}{\varepsilon_a} \qquad [4.1]$$

where ν is the Poisson's ratio, ε_t is the transverse strain measured in the thickness of a membrane and ε_a is the axial strain measured in the load direction.

Poisson's ratio is measured experimentally for both membranes by placing the membranes in uni-axial tension using a creep frame and measuring the corresponding strains. The axial strain is measured using a digital calliper accurate to 0.05mm and the transverse strain is measured using a micrometer accurate to 1μm. The measurement of the specimen' thickness reported at each increment of axial strain comprised the average of ten thickness measurements at two separate locations on the specimen. One sample of Propore™ is measured and two samples of Tyvek® are measured. Figure 4.2 shows a plot of transverse strain versus axial strain. The slope of this plot gives the Poisson's ratio of the material.

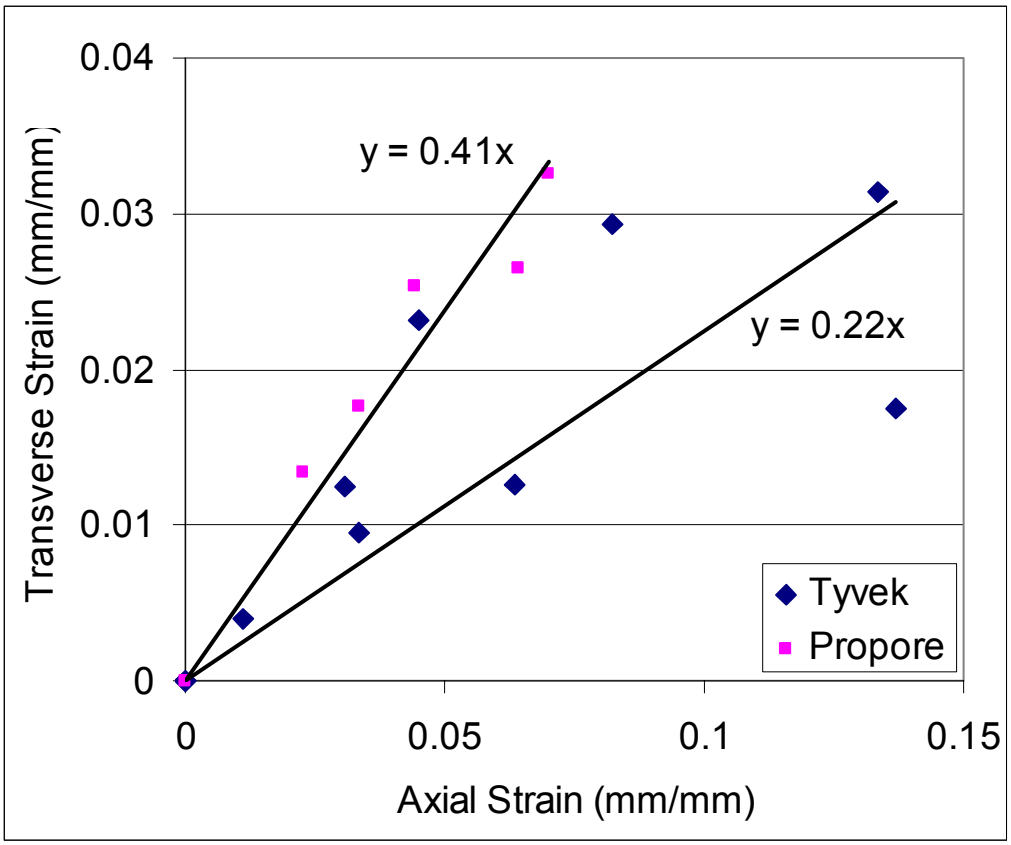

Figure 4.2. Transverse versus axial strain plot used to determine Poisson's ratio of both Tyvek® and Propore™ membranes.

The large scatter in the Tyvek® data is due to the fibrous nature of the material. The fibres of the Tyvek® individually shift and strain as the axial load is increased making it difficult to measure the same section of the material each time. The value of Poisson's ratio for Tyvek® is taken as 0.22. This value is a bulk value since it does not represent the Poisson's ratio of a HDPE fibre but of the random distribution of fibres. The value of Poisson's ratio for Propore™ is 0.41. This value is also a bulk value since Propore™ is made of two bonded layers. In the case of Propore™, each layer is continuous and homogeneous and therefore there is less scatter in the measurements. The manufacturer of both Propore™ and Tyvek® were unable to provide Poisson's ratio values to compare to the experimental results of Figure 4.2. A search of the CES3 database (2006)

gives values of Poisson's ratio for HDPE and PP in the range of 0.41-0.43. The value for Propore™ fits into this range while the value for Tyvek® is much lower, which is likely due to the fibrous nature of the material. The 95% uncertainty limit of the Poisson's ratio measurement for Propore™ is estimated to be 35% and the 95% uncertainty limit in the Tyvek® measurement is estimated to be 90%. While these uncertainties are very high, the membrane deflection is not sensitive to Poisson's ratio as shown by equation [4.13] where the deflection is proportional to the cubed root of (1-ν). In addition, the calculated results using these measured values show good agreement with the measured pressure deflection data in Section 4.5.2.

4.2 Elastic modulus test methods

The elastic modulus is commonly determined by calculating the slope of the elongation curve from stress-strain data obtained during a tension test. In the case where the material is nonlinear, a secant modulus can be used by taking the slope of the line from the origin to a prescribed level of strain. In this thesis, two test standards are used to determine the elastic modulus of the membranes: ASTM D 4595 (2001) and ASTM D 882 (2002); both use the secant method. As well, a bulge test using a circular perimeter supported membrane exposed to various test pressures is performed and analyzed using three different methods of analysis (Paviot et al. 1995., Small et al. 1993, Small and Nix 1992, Vlassak and Nix 1992, and Xiang et al. 2005). The first analysis method is the secant method which is the same as the secant method outlined in ASTM D 4595 (2001). The second analysis method is a linear curve fit method which assumes a linear elastic material and spherical deflection geometry. The third method is the energy

minimization method which is based on the minimization of strain energy as presented by Small and Nix (1992).

4.2.1 Tensile test

The ASTM D 882 (2002) test method is designed for thin plastic sheeting. Both membrane materials under consideration are polymers and, on a microscopic scale, they have a non-uniform structure. ASTM D 882 (2002) calls for a specimen width no greater than 25.4 mm (1.0 in.), and a preferred gauge length of 250 mm (10 in.) but not less than 100mm (4 in.). The tests in this thesis are performed with a 203.2 mm (8 in.) gauge length. The specified strain rate for this standard is 0.1 mm/mm/min when determining the elastic modulus of materials. For properties other than the elastic modulus, the specified strain rate is dependent on the percent elongation at the break point. For materials that are at less than 20% elongation at break, such as Tyvek®, a strain rate of 0.1 mm/mm/min is specified in the standard. For materials that have a 20 – 100% elongation at break, such as Propore™, the strain rate of 0.5 mm/mm/min is specified in the standard.

The ASTM D 4595 (2001) test method is used for geotextiles. Geotextiles are used in geological applications such as mining and they are permeable to liquids. Textiles are defined as materials manufactured from linear fibres. Both Tyvek® and Propore™ can be classified as textiles. Usually, the need for elastic properties of textiles is not as great as for geotextiles which are often used for structural applications. This standard is applicable since Tyvek®, Propore™ and geotextiles are the same in that their application is a membrane under uniform pressure. ASTM D 4595 (2001) calls for a specimen width of 200 mm (8 in.) and a gauge length of 100 mm (4 in.). Compared to ASTM D 882 (2002) which has a specimen width of 25.4 mm (1.0 in.) this increase in

specimen width helps to minimize the edge effects of the specimen. The specified strain rate for this standard is 0.1 mm/mm/min in all cases.

Both standards call for a relative humidity of 50 ± 5%. The majority of the tests were done during winter months at a relative humidity of 20 ± 5% which is typical of building occupied spaces in cold winter climates. Since these materials are not very hygroscopic, this change in test humidity is not considered to be significant. The effect of humidity is further investigated in Section 4.4.4.

4.2.1.1 Tension test facility

The tension tests are performed using a constant rate of extension test in a calibrated Instron 1122 tension testing machine. The ASTM D 882 (2002) tests are performed using pneumatic jaws with a clamping pressure of 1 MPa. Custom jaws were machined to accommodate the 200 mm (8 in.) specimen width used in the ASTM D4595 (2001) tests. Both types of jaws were pre-tested to ensure no test sample slippage during each test. This is accomplished by placing a visual mark on the specimens and ensuring that there is no movement relative to the jaw assembly during testing. The strain measurements are obtained from the strip chart recorder and are based on the total movement of the crosshead. Therefore the strain of the jaw assembly increases the measured strain but the strain of the frame and other components has been accounted for in the calibration of the Instron. It is assumed that the strain of the jaw assembly will be minimal compared to the strain of the specimen; however, it should be noted that the measured valued of the elastic modulus represents the lower limit of the elastic modulus since additional strain is potentially introduced due to the strain in the jaw assembly.

4.2.1.2 Tension test analysis

Load extension plots are obtained using a strip chart recorder and Figure 4.3(a) shows typical stress strain curves for the two materials tested in this thesis. The majority of tests are performed using the normal direction of the specimen. The normal direction is defined as perpendicular to the roll direction as received from the manufacturer. The effects of other orientations are discussed further in Section 4.4.2.

(a) (b)

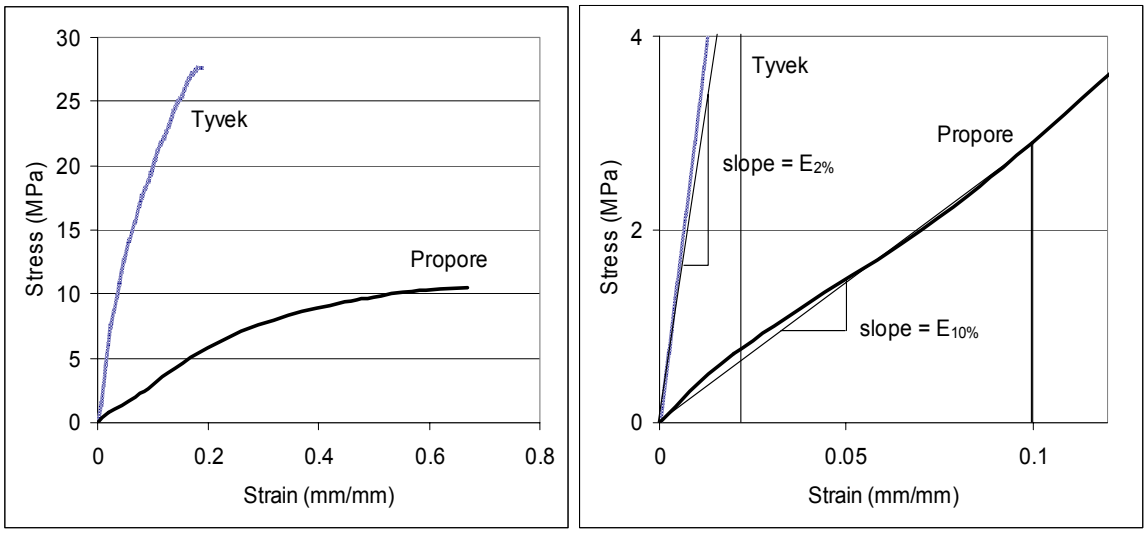

Figure 4.3. (a) Tensile tests results (ASTM D 882) of Tyvek® and Propore™ in the normal direction over the entire testing range and, (b) magnified view of the linear region showing the method of calculating the 10% and 2% secant moduli ($E_{10\%}$ and $E_{2\%}$).

It can be seen that these materials do not have a well defined linear elastic region except over small ranges of strain. The magnified region of Figure 4.3 shows stress below 5 MPa which is the region of interest since it is within the operating pressure of the RAEE system and where both membranes can be approximated as linear elastic. For consistent comparisons a secant modulus is used to calculate the elastic modulus from all tensile tests. The secant modulus is determined by calculating the slope of the line

from the origin to a designated strain as shown in Figure 4.3(b). For the Propore™ membrane a secant modulus at a strain of 10% ($E_{10\%}$) is used, as outlined in ASTM D 4595 (2001). For the Tyvek® membrane a 2% secant modulus ($E_{2\%}$) is used since it has a relatively low percent elongation compared to Propore™.

4.2.2 Bulge test

Bulge tests have been used since the 1950's to determine the mechanical properties of thin film materials (Small et al., 1993). Generally, the bulge test is simpler to perform than a tension test and is only used in the elastic region. The bulge test is only used for thin membranes and has no associated ASTM test standard designation.

The bulge test requires the clamping of the perimeter edges of a thin test specimen membrane with a circular shape and applying a uniform pressure on the exposed surface. A measurement of the deflection at the center of the membrane enables the experimenter to determine the deflection as a function of pressure. This deflection is then used to determine the membrane stress-strain properties.

4.2.2.1 Bulge test facility

In this test facility a source of compressed air is regulated through a pressure regulating valve. This air enters a liquid reservoir filled with the pressurizing fluid. The fluid enters the test cell where it applies a pressure on the clamped membrane. The pressure in the liquid side of the cell is measured using a pressure transducer calibrated from 0 to 138 kPa (0-20 psig). The displacement of the membrane is measured using a linear variable displacement transducer (LVDT). The pressure and LVDT transducer signals are read using a National Instruments USB-6009 14 bit data acquisition system coupled with a personal computer using LabVIEW software to control the data acquisition system. Figure 3.4 shows the test cell used for the bulge test, which is the

same test cell used for the liquid penetration pressure tests of Chapter 3. The test cell consists of a circular opening measuring 57mm in diameter. The test membrane is clamped horizontally between the two halves of the test cell and the deflection is measured by the vertical displacement of an armature assembly that rests on the horizontal membrane. Figure 4.4(a) shows a schematic of the test facility while Figure 4.4(b) shows a two dimensional schematic of a membrane deflected subject to a uniform pressure

(a) Test facility schematic

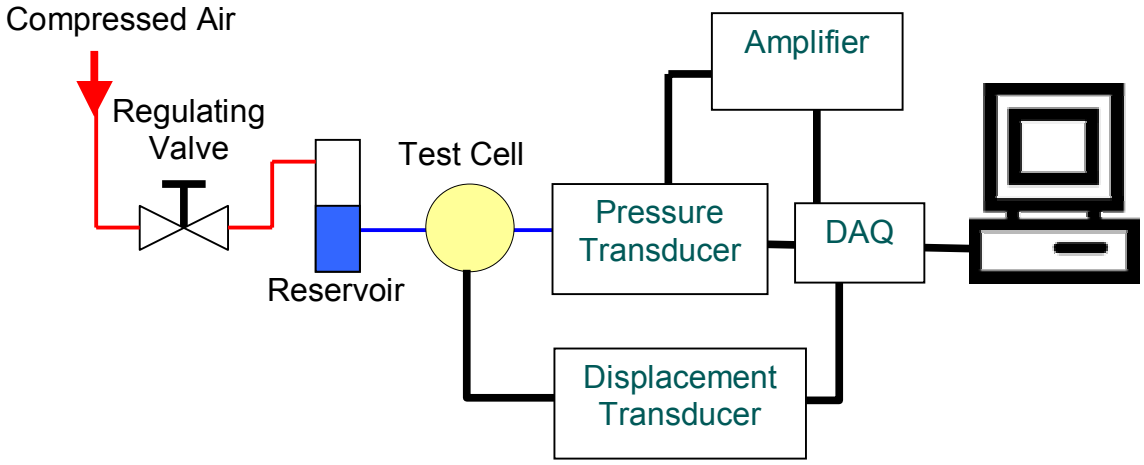

(b) Test cell membrane

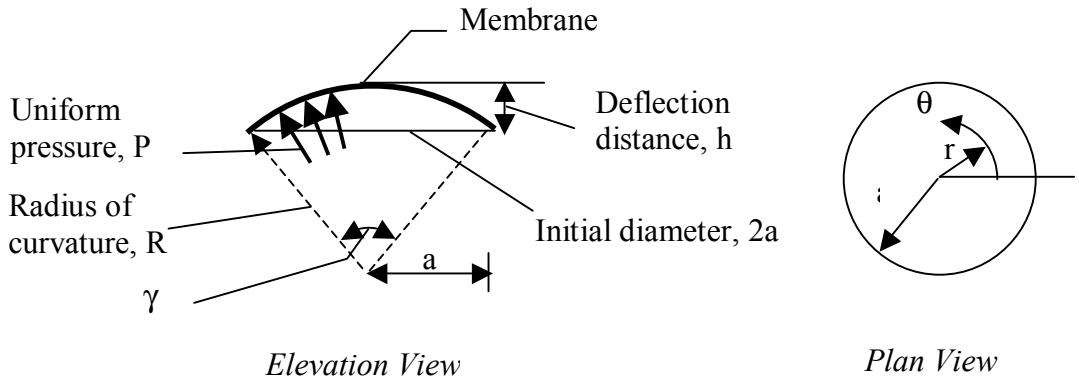

Figure 4.4. Schematic of (a) the bulge test facility and (b) the test cell membrane showing the various geometric characteristics.

This setup is a simplified version of that used by other authors (Paviot et al., 1995, Small et al., 1993, Small and Nix 1992, Vlassak and Nix 1992, and Xiang et al., 2005), the only difference being that it uses a different sensor to measure the membrane displacement. Since deflections of the Tyvek® and Propore™ are relatively large, an LVDT is used to measure this deflection. Water is used to pressurize the membranes since the materials of interest are permeable to air but not permeable to water, unless the liquid penetration resistance is exceeded.

4.2.2.2 Analysis of bulge test results

Assuming that the shape of the membrane deflection is spherical and the membrane is in the elastic region, the tensile stress component in the θ – r plane is given by,

$$\sigma_{\gamma} = \frac{pR}{2t} \qquad [4.2]$$

where p is the applied pressure [Pa], R is the radius of curvature [m], and t is the thickness of the membrane [m] (Small et al., 1993).

When the membrane deflection is small and symmetrical, the radial component of stress in the membrane is assumed to be independent of the radius, r, and the angular position, θ, in the deflected membrane. The stress component normal to the local plane of the spherically shaped membrane in the radial, R, direction is equal to –p at the inner surface where the liquid pressure is p and 0 at the outer surface where the air pressure is atmospheric.

The component of strain normal to the θ line of the membrane caused by the tensile stress in equation [4.2] is calculated by determining the change in the arc length for the

membrane under a pressure change compared to the initial arc length. This γ component of strain is given as,

$$\varepsilon_{\gamma} = \frac{s - s_o}{s_o} = \frac{s - 2a}{2a} \qquad [4.3]$$

where s is the arc length [m], and s_o is the initial arc [m] (or diameter 2a).

The circular arc length through the center of the membrane can be determined from the definition,

$$s = \gamma \cdot R \qquad [4.4]$$

where R is the radius of curvature [m] given by,

$$R = \frac{a^2 + h^2}{2h} \qquad [4.5]$$

and γ is the arc angle given by,

$$\gamma = 2 \cdot \arcsin\left(\frac{(2a)}{2R}\right) \qquad [4.6]$$

Assuming that the deflection, h, is much smaller than the test membrane diameter, 2a, equations [4.5] and [4.6] can be simplified. Substituting the simplified results into equations [4.2] and [4.3] the resulting stress and strain equations are written in terms of the membrane deflection, h, for the applied pressure, p, and are given by (Small et al. 1993),

$$\sigma_{\gamma} = \frac{pa^2}{4ht} \qquad [4.7]$$

and

$$\varepsilon_{\gamma} = \frac{2h^2}{3a^2} \qquad [4.8]$$

Equations [4.7] and [4.8] are useful because all parameters on the right hand side are easily measured which allows us to calculate the stress (σ_{γ}) and strain (ε_{γ}) in a deflected membrane.

Often some stress exists in a test membrane prior to the application of pressure i.e. pre-stress. For the case of a pre-stress in the membrane of magnitude σ_o, a corresponding strain ε_o is added to [4.8] as given in [4.9] to give the total strain as,

$$\varepsilon_T = \varepsilon_{\gamma} + \varepsilon_0 = \frac{2h^2}{3a^2} + \frac{\sigma_o}{Y} \qquad [4.9]$$

where Y is the biaxial modulus [MPa] given by,

$$Y = \frac{E}{(1-\nu)} \qquad [4.10]$$

The additional term of equation [4.9] is applicable to either a pre-stress or a pre-strain which are related by Hooke's law (equation [4.11]). The biaxial modulus Y is used because the stress is in the plane of the material or in a biaxial configuration, therefore the effects of Poisson's ratio must be taken into account.

Equations [4.7] and [4.8] can be combined with the definition of the elastic modulus for the case of a linear elastic material with uni-axial loading given by,

$$E = \frac{\sigma}{\varepsilon} \qquad [4.11]$$

to give a relationship between pressure and deflection, again using a biaxial modulus in place of the elastic modulus,

$$p = \frac{4Yt}{a^2} h \left[\frac{2}{3a^2} h^2 + \frac{\sigma_o}{Y} \right] \qquad [4.12]$$

where h is the total deflection of the membrane [m], including any initial deflection.

Equation [4.12] is specific to circular membranes, a general form of the equation is given by Xiang et al. (2005), and can be used to apply the bulge test to other geometries,

$$p = c_1 \frac{Et}{(1-\nu)a^4} h^3 + c_2 \frac{\sigma_o t}{a^2} h \qquad [4.13]$$

or in the dimensionless form,

$$\frac{p}{E} = c_1 \frac{\left(t/a\right)\left(h/a\right)^3}{(1-\nu)} + c_2 \left(\frac{\sigma_o}{E}\right)\left(\frac{t}{a}\right)\left(\frac{h}{a}\right) \qquad [4.14]$$

where for circular membranes c_1 and c_2 are implied by equations [4.12] and [4.13] to be $c_1 = 8/3$ and $c_2 = 4$.

For square membranes c_1 is a weak function of Poisson's ratio which is approximated by,

$$c_1(\nu) = 0.800 + 0.062\nu \qquad [4.15]$$

and c_2 is a constant equal to 3.393 (Xiang et al., 2005).

Xiang et al. (2005) noted that the bulge test of a square membrane has an identical dimensionless functional form as [4.14], which can be written as a function of dimensionless parameters,

$$\xi = \beta\left(c_1 \cdot \eta^3 + 3.393 \cdot \alpha \cdot \eta\right) \qquad [4.16]$$

where c_1 is 1.043 for Tyvek®, 1.375 for Propore™, $\xi = p/E$, $\beta = t/a$, $\eta = h/a$, and $\alpha = \sigma_o/E$

The bulge test data is analyzed using three different methods; the secant method, the linear curve fit method, and the energy minimization method. Each method makes different assumptions about the geometry of the deflection and the linearity of the material. These methods are outlined below.

The secant method of analysis assumes spherical deflection of the membrane, that there is no pre-stress in the membrane and makes allowances for material nonlinearity by using the secant method described in Section 4.2.1.2. Since elastic behaviour is not assumed, equation [4.11] does not strictly apply. The stress and strain are calculated using equations [4.7] and [4.8]. From these results the stress strain curve is plotted and retains any nonlinear features. The secant modulus is then graphically obtained from the slope of the line from the origin to a specific strain as in the tension test analysis.

The linear curve fit analysis method assumes spherical deflection geometry, a linear elastic material, and no pre-stress in the membrane. A curve fit of the pressure-deflection curve is developed. Simplifying equation [4.13] the curve is of the form,

$$p = K_1 h^3 \qquad [4.17]$$

where the elastic modulus value is then calculated by rearranging the constants from the first term of equation [4.13] and solving for E,

$$E = \frac{3K_1(1-\nu)a^4}{8t} \qquad [4.18]$$

The energy minimization method involves a curve fit to equation [4.19] where equation [4.19] is the solution to the minimization of the strain energy in the membrane as presented by Small et al. (1993). The solution involves solving the partial differential equation for strain energy subject to minimum energy and an assumed parabolic shape function for the deflection of the membrane and the assumption of a linear elastic material. The resulting equation is,

$$p = \frac{E(7-\nu)t}{3(1-\nu)a^4}h^3 \qquad [4.19]$$

Equation [4.19] is of a similar form to equation [4.12], only without the pre-stress term and with a different dependence on the Poisson's ratio due to the different assumed shape of deflection. The elastic modulus is then determined by fitting the data to a curve with the same form as equation [4.17], only with a new curve fit constant, K_2, and solving for the elastic modulus using the constants in equation [4.19] given as,

$$E = K_2 \frac{3(1-\nu)a^4}{(7-\nu)t} \qquad [4.20]$$

4.3 Uncertainty

The uncertainty of the elastic modulus is calculated using the techniques outlined in ANSI/ASME 19.1 (1998). The bias in the measurement instrumentation (i.e. the data acquisition system, dimensions, and strip chart data) is found to be less than 1% in all cases. The repeatability of any given test at a 95% confidence interval is found to be between 3% and 50% with an average of 15%. The uncertainty in the measurement instrumentation is therefore neglected because repeatability in the test data is due to

sample variation and small changes in the testing procedure. The uncertainty of the elastic modulus measurement is,

$$U_E = \delta_E \cdot t_s \qquad [4.21]$$

where U_E is the uncertainty in E, t_s is the two tailed student t value for a 95% confidence interval and δ_E is the sample standard deviation of the elastic modulus measurements.

The uncertainty of the average is given by,

$$U_{\bar{E}} = \frac{U_E}{\sqrt{N}} \qquad [4.22]$$

where N is the number of measurements taken.

The repeatability in the Tyvek® measurements are much lower than in Propore™, which is expected due to the random fibre distribution of Tyvek®. The uncertainty in all measurements could be reduced by increasing the number of measurements. Unless otherwise noted, 5 measurements are taken in each test.

4.4 Results

Before the construction of the second RAEE exchanger prototype a group of vapour permeable and water impermeable membranes were tension tested. This testing was performed before a pre-screening of the membranes had occurred and the Tyvek® and Propore™ membranes were chosen as the best candidates for the RAEE. The following figure is obtained using the ASTM D 882 (2002) test standard with a strain rate of 0.1 mm/mm/min. The results of Figure 4.5 are given in Newton's per unit width for a given thickness since the thickness of some of the materials is difficult to measure accurately.

The typical thickness of Tyvek® is 150 μm and the typical thickness of Propore™ is 200 μm.

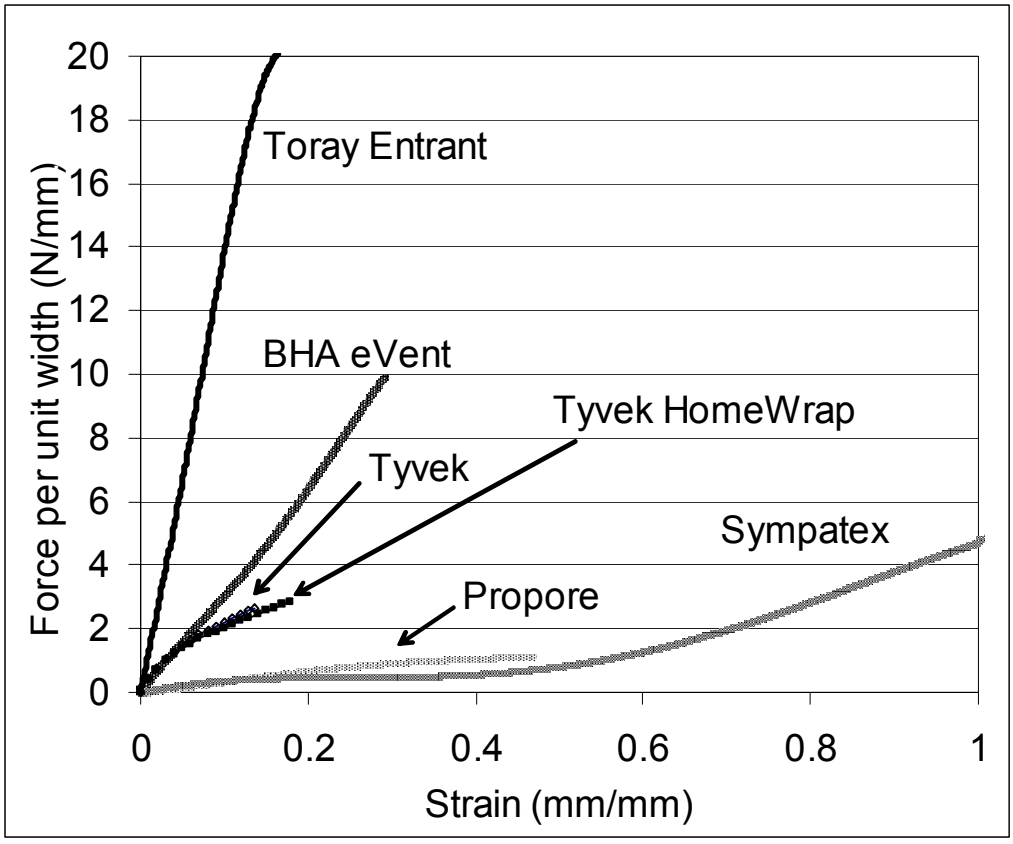

Figure 4.5. ASTM D 882 (2002) tensile test results for several membranes.

The Tyvek® and Propore™ membranes have relatively low ultimate tensile strength (UTS). The Toray Entrant™ is made of a coated woven nylon fabric and thus has the strength of the woven nylon fabric; similarly the BHA eVent® is a laminate of a nylon fabric and an ePTFE membrane and thus has the strength of the nylon fabric. The Tyvek® and Tyvek® HomeWrap® have nearly identical tension curves although it can be seen that the Tyvek® HomeWrap® has a slightly higher UTS, which is expected since it is a thicker material. The Sympatex® laminate shows material nonlinearity, caused by the Sympatex® membrane which is laminated to a non-woven nylon fabric.

Since the RAEE system will be operating at relatively low pressures and will have a support screen, the choice of any membrane can be accommodated. However, a membrane with greater stiffness requires less support and will therefore have a greater heat and mass transfer area.

For the remainder of this chapter only the Tyvek® and Propore™ membranes are considered since they are the only membranes that currently meet the cost requirements of the RAEE.

4.4.1 Comparison of methods

Figure 4.6 shows a comparison of the two tensile test methods and the three bulge test analysis methods. Each value is the average of 5 tests with a strain rate of 0.1 mm/mm/min and the uncertainty bars are calculated using the uncertainty of the average (equation [4.22]). The tension tests are performed in the normal direction and the bulge test of Propore™ is performed with the microporous PP membrane facing the liquid. The non-woven PP layer must be oriented opposite to the applied pressure to ensure that the membrane does not rupture under the applied pressure.

(a) (b)

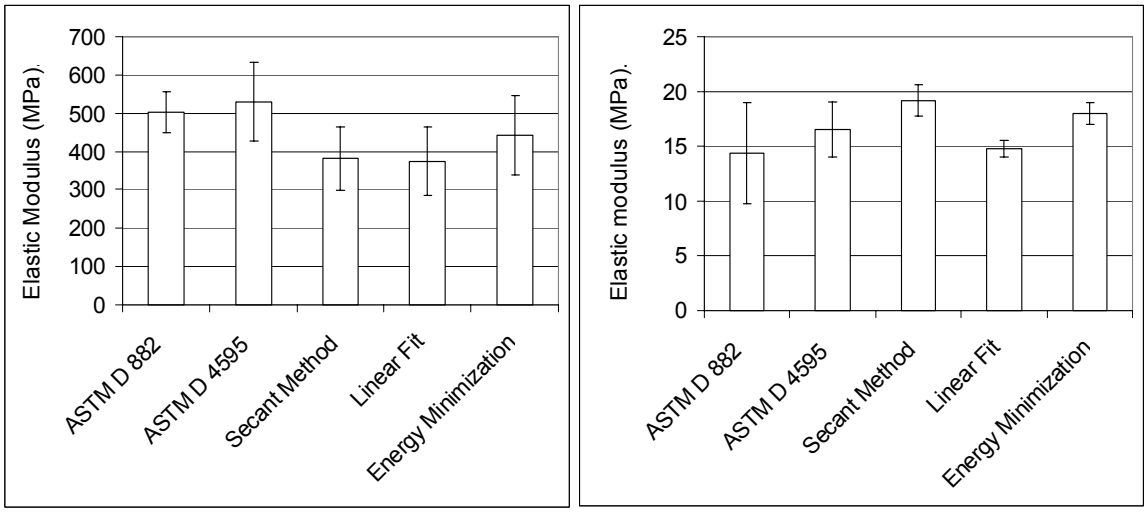

Figure 4.6. Comparison of the test methods and bulge test analysis methods for (a) Tyvek® and (b) Propore™.

For Tyvek®, the three bulge test analysis methods agree with each other within the bounds of uncertainty. For Propore™, the uncertainties of the three bulge test methods do not agree within the uncertainty of the measurements. The linear fit method assumes a linear elastic relationship between stress and strain which corresponds to a cubic relationship of pressure and deflection as the form of equation [4.17]. The constant K_1 from equation [4.17] cannot be well fitted to a curve that follows a non-linear stress strain relationship and from Figure 4.3(a) it can be seen that Propore™ demonstrates more non-linear behaviour than Tyvek®. This non-linear material behaviour is the reason for the difference in the calculated elastic modulus for the linear curve fit method.

Propore™ allows more strain than Tyvek® at the same stress level, or a larger deflection for a given pressure. Both the secant method and the linear fit method assume spherical deflection geometry; however, as the pressure is increased the assumption of

spherical deflection breaks down as the membrane takes on a parabolic shape during a test. The energy minimization method uses a parabolic membrane shape function to approximate the membrane which better captures the deflection shape over a range of pressures. This difference in shape assumption accounts for the differences in the elastic modulus for the energy minimization method.

In the secant method, for Propore™, the spherical deflection assumption breaks down; however, the secant method accounts for the non-linear material behaviour. Although both the secant method and the energy minimization method agree well with each other, the secant method is simpler to compute and provides an easier comparison to the standard tensile tests which are already analyzed using the secant method. In the following sections, the secant method will be used when comparing data.

The two ASTM tensile tests in Figure 4.6 show very good agreement within the uncertainty bounds for Tyvek®, while the bulge test results for Tyvek® show slightly lower values than the tensile tests. The difference in the results is due to the differences in the test methods, specifically, the difference in the boundary conditions. Both test methods can introduce errors due to the effect of membrane clamping. The tension tests have an axial loading condition with two clamped boundaries and two free boundaries while the bulge test has a biaxial loading condition and is clamped on all boundaries. This difference in boundary conditions changes the distribution of the stress within the membrane since unconstrained boundaries are more easily strained.

The results from Propore™ show that the tensile test methods agree well with each other within the repeatability of the measurements. The secant and energy minimization analysis method for the bulge test are slightly higher than the tension tests which is due

to the biaxial stress condition. This effect of the membrane orientation is further investigated in Section 4.4.2.

4.4.2 Effect of orientation

To investigate the effects of membrane orientation, ASTM D 882 (2002) tensile tests are performed with three different membrane orientations and the data are compared to the secant method results from the bulge test (Figure 4.7). The normal direction is defined as perpendicular to the roll direction. The cross direction is taken 90 degrees to the normal direction and the bias direction is taken 45 degrees to the normal. It should be noted that only 3 samples were tested in the bias and cross directions.

(a) (b)

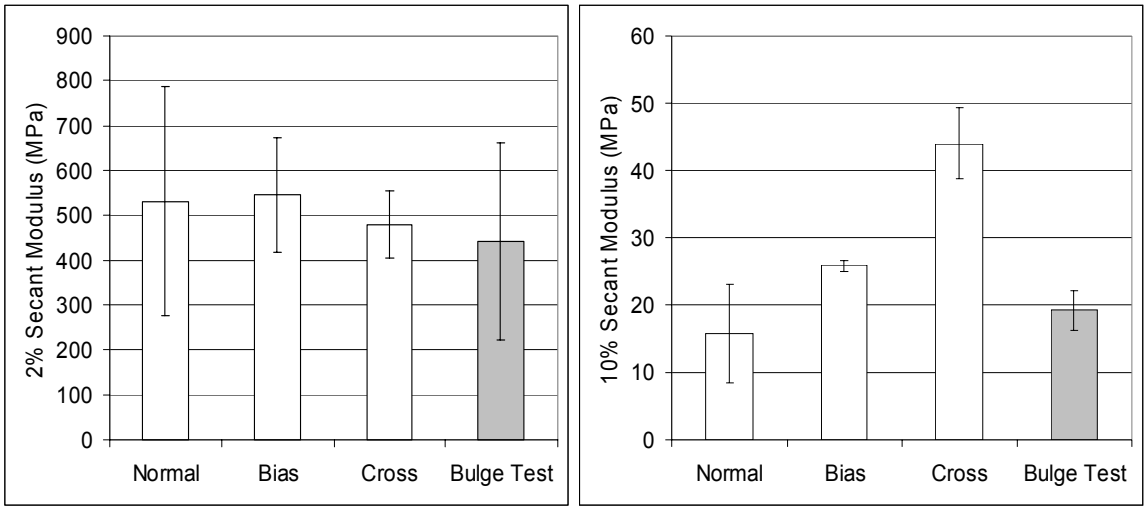

Figure 4.7. Comparison of average elastic modulus for three membrane orientations with ASTM D 882 tensile tests and the bulge test (a) Tyvek® and (b) Propore™.

For Tyvek®, the elastic modulus in the normal and bias directions agrees well with the normal tension test data and the bulge test data. This isotropic behaviour is expected due to the random orientation of the fibres in the membrane.

The Propore™ measurement shows significant differences between the three membrane orientations. The structure of the non-woven layer in Propore™ is not uniform and therefore the elastic modulus is expected to be anisotropic. For Propore™, the elastic modulus obtained in the cross direction is 160% greater than the elastic modulus obtained in the normal direction. The elastic modulus in the bias direction is 50% greater than the elastic modulus obtained in the normal direction. The bulge test elastic modulus is much closer to the elastic modulus obtained from the normal direction which indicates that when Propore™ is loaded in a biaxial fashion it gains little benefit from the increased strength in the cross direction. The bulge test result provides an effective modulus for the situation of a membrane under pressure and so it appears to be the best test for the proposed application of a pressurized flow channel in a plate type energy exchanger.

It is also interesting to note that for Propore™, 25% of the tests performed in the normal direction failed at the bond of the two materials. This is highly undesirable and is considered to be a manufacturing defect. In the bulge test, Propore™ is oriented with the non-woven PP fabric on the low pressure side of the test cell and there were no failures of the membrane. Placement of the membrane with the non-woven PP fabric on the high pressure side does result in delamination of the membrane from the support fabric.

4.4.3 Effect of strain rate

Both ASTM D 822 (2002) and ASTM D 4595 (2001) recommend a strain rate of 0.1 mm/mm/min for determining the elastic modulus. The effect of the strain rate on the modulus is of interest since the end use of the membrane could involve rapid pressure changes as well as slowly changing pressures.

Figure 4.8 shows the effect of strain rate on the secant modulus for both materials. The values of Figure 4.8 (a) and (b) are for the bulge test analyzed using the secant method, while the values of (c) and (d) are for both the ASTM D 882 (2002) and ASTM D 4595 (2001) tensile tests.

(a) Bulge test (Tyvek®) (b) Bulge test (Propore™)

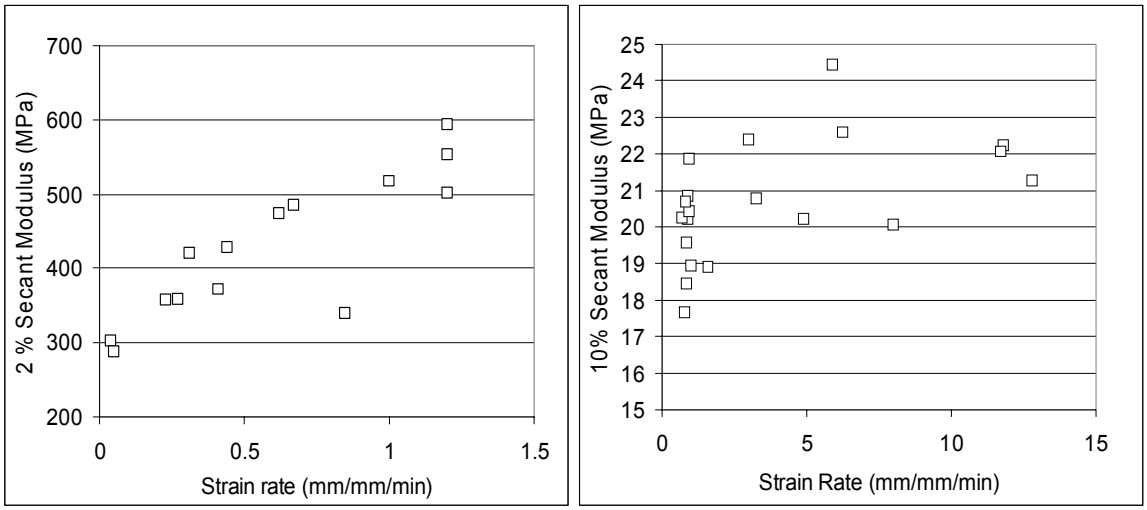

(c) Tension test (Tyvek®) (d) Tension test (Propore™)

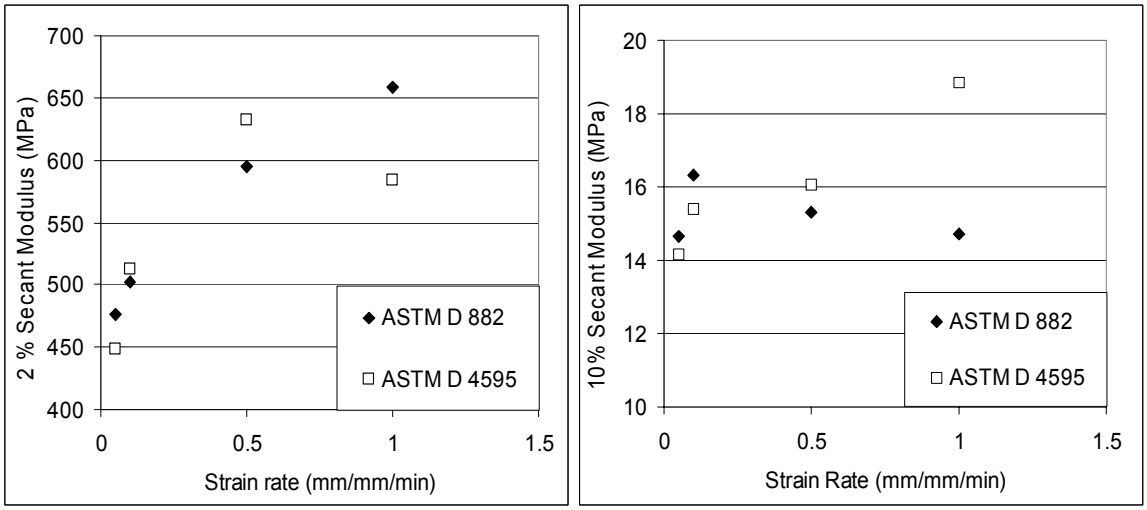

Figure 4.8. Secant elastic modulus versus strain rate for (a) bulge test - Tyvek® (b) bulge test - Propore™ (c) Tension tests – Tyvek® and (d) Tension tests - Propore™.

It can be seen that in both the bulge test and the standard tensile tests, the stiffness of Tyvek® increases as the strain rate increases. This increase in stiffness is caused by the fact that the individual fibres do not have time to realign themselves at greater strain rates. At low strain rates, the fibres have time to realign in the most favourable equilibrium state and therefore the membrane will have a larger deflection (strain) for a given load. This phenomenon is observed during the ASTM tension testing where at low strain rates visible creases begin to form in the Tyvek® membrane load direction and are accompanied by audible snapping of the individual fibres before total failure. At high strain rates the creases formed much quicker and the sound of individual fibres breaking is evident only a moment before total failure.

For Propore™ there is relatively little change with strain rate (note that the strain rate scale is 10 times larger in Figure 4.8(b) than in Figure 4.8(a)). The microporous PP membrane is non fibrous and therefore is not subject to changes in orientation like the non-woven PP fabric or Tyvek®. The difference between Tyvek® and the non-woven PP fabric is the fact that the non-woven fabric has uniform fibre structure unlike the random structure of Tyvek®. This uniform structure does not allow the same rearrangement of the fibres as Tyvek®. The non-woven PP fabric carries the majority of the load and some rearrangement of the fibres within the fabric accounts for the slight increase in the modulus with increasing strain rate that is seen in Figure 4.8. The results presented exclude those samples that became delaminated during testing. Bulge test results using the other analysis methods show similar trends and are not presented.

4.4.4 Effects of relative humidity

The effects of relative humidity on the elastic modulus are investigated by tension testing samples that have been pre-conditioned at different humidities and by bulge

testing samples using salt solutions at different humidities as the pressurizing fluid. Two salt solutions representing two humidities, other than the 100% RH distilled water, are used as the pressurizing fluid in the bulge test. Magnesium chloride is used for a 48% RH test and magnesium nitrate solution is used for a 65% RH test. These relative humidity values in Figure 4.9 are an average of measurements taken before and after the test using a Vaisala humidity sensor.

The relative humidity is also investigated using the ASTM D 882 (2002) tensile test by testing specimens that are preconditioned in a specific humidity environment for 24 hours. A 22% RH environment is obtained using a saturated potassium acetate solution and an 88% RH environment is obtained using a saturated potassium chloride solution. All tests are performed within 20 seconds from the removal of the specimen from the controlled environment. Figure 4.9 shows the comparison of the different humidity conditions for both the bulge tests and the tensile test.

(a) Bulge test (Tyvek®) (b) Bulge test (Propore™)

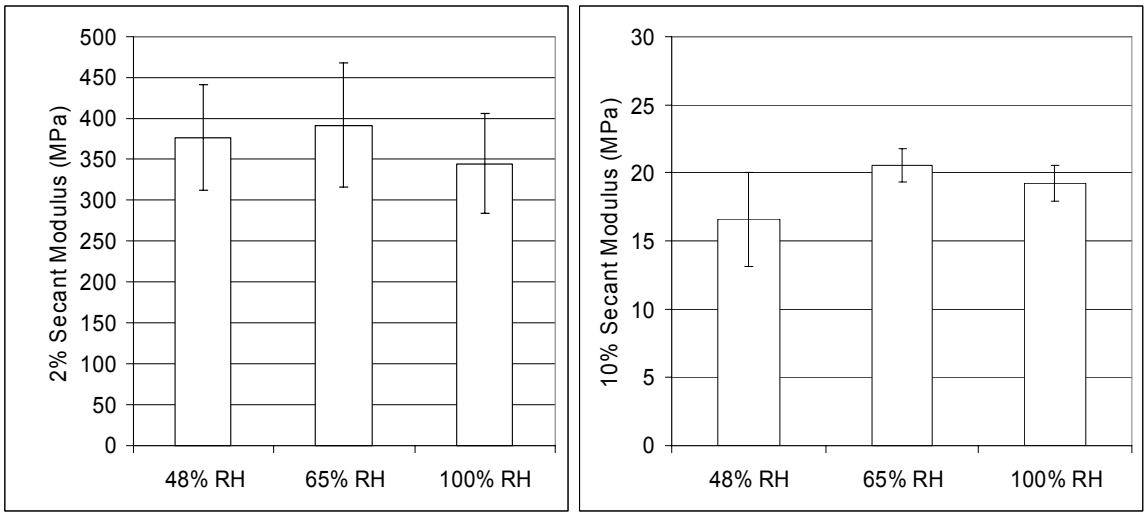

(c) Tension test (Tyvek®) (d) Tension test (Propore™)

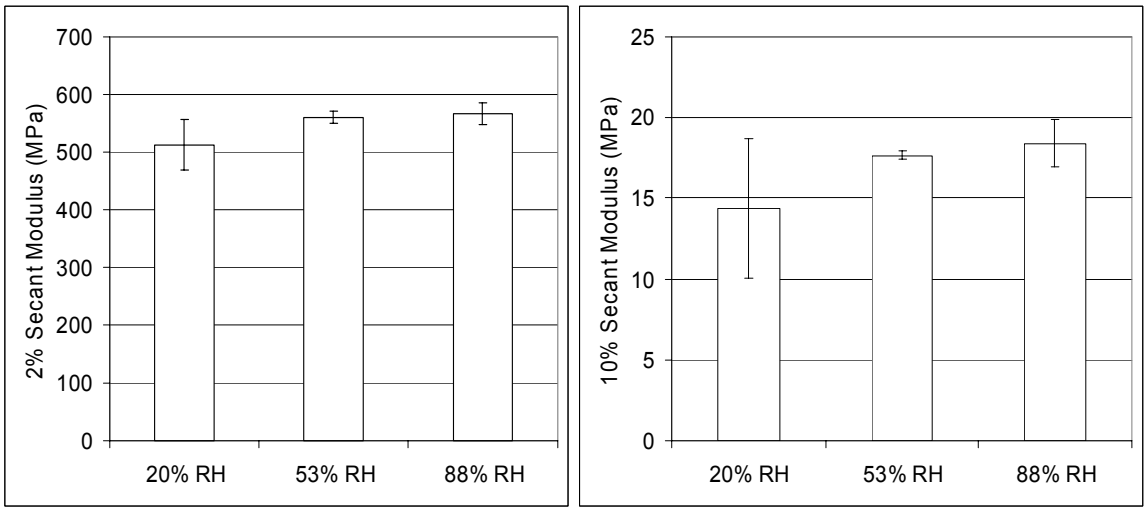

Figure 4.9. Comparison of humidity effects on secant modulus for (a) bulge test - Tyvek® (b) bulge test - Propore™ (c) ASTM D 882 – Tyvek® and (d) ASTM D 882 – Propore™.

For both the bulge test and the tension testes, the elastic modulus values obtained at the different humidities agree with each other within the bounds of uncertainty and therefore the effects of humidity appear to be negligible. The tensile test results for Tyvek® show a slight increasing trend with increasing humidity, however in the tensile

tests performed to determine the effects of humidity only two samples at each humidity level are tested. This low amount of sampling results in low uncertainty because the two measurements are very close to each other. It has been shown in previous sections that an uncertainty of approximately 15% is more realistic. The negligible effect of humidity on the modulus is expected due to the fact that both materials are low surface energy hydrophobic membranes. Previous measurements of sorption isotherms (Larson, 2005) have indicated that Tyvek® adsorbs little water vapour and therefore the effects of adsorbed water vapour are expected to be negligible.

Changes of temperature will likely affect the elastic modulus results, particularly at negative temperatures where the glass transition point of the materials may be reached. Any temperature dependence is left for future work.

4.5 Application to the RAEE exchanger

The purpose of determining the elastic modulus is to determine the required screen size to keep the deflection of the membrane and screen assembly into the air stream to a minimum of 1 mm. The results of Section 4.4 are based on a circular membrane, which has a simplified analysis due to the spherical or parabolic shape of deflection. Commercially available screens typically have square openings. The deflection of a square membrane can be calculated using equation [4.13] and associated empirical constants for square geometry. Good agreement of a measured square membrane to the predicted results of equation [4.13] verifies that the constant parameters, i.e. elastic modulus and Poisson's ratio, used in the equation are accurate. This allows the deflection of the membrane in different sizes of squares (screen openings) to be determined with confidence.

Finally, the measurement of a membranes deflection within a non-rigid screen support is compared to the predicted value of equation [4.13] with a correction for the movement of the screen itself. Good agreement in this case shows that the deflection of a membrane in an actual screen can be predicted with confidence and that the empirical constants are not limited to predicting the deflection of a membrane in a fixed boundary condition square geometry, but can be applied to the situation of a pressurized membrane supported by a square screen. Figure 4.10 shows a schematic of the square bulge test and the circular bulge test geometry, as well as a typical square screen.

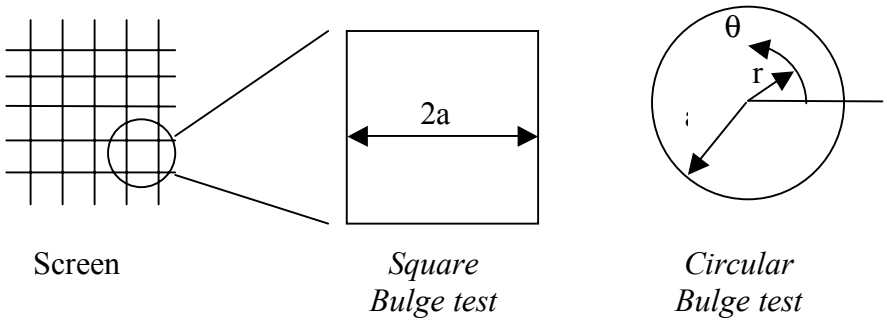

Figure 4.10. Schematic of a screen showing the square bulge test geometry compared to the circular bulge test geometry.

The most suitable values of the elastic moduli for the design of the energy exchanger are the values obtained from the secant method analysis of the bulge test. For Tyvek® the design value of the elastic modulus is 300 ± 45 MPa which corresponds to the results from the lowest strain rate. This value is chosen as a conservative estimate. For Propore™ the design value of the elastic modulus is 20 ± 3 MPa which is also an average of the lowest strain rate values. The data presented in the application section are all for square shaped deflections.

4.5.1 Effect of pre-stress

The data in Section 4.4 are presented and analyzed assuming that there is no pre-stress in the membranes. The membranes are freely placed in the bulge apparatus and the tightening of the clamping system is assumed to impart minimal pre-stress in the membranes being tested. To investigate the effects of pre-stress and slack, a series of tests are performed in which the membrane is left slack before testing and a series in which the membrane is pulled tight before the apparatus is clamped down. Figure 4.11 shows the measured results of a pre-stressed membrane, a slack membrane and the theoretical result given by equation [4.13] for no pre-stress and for a pre-stress of 200 kPa. The value of pre-stress used in the theoretical calculation is obtained by curve fitting the measured data to equation [4.13] and using the known properties to calculate σ_o.

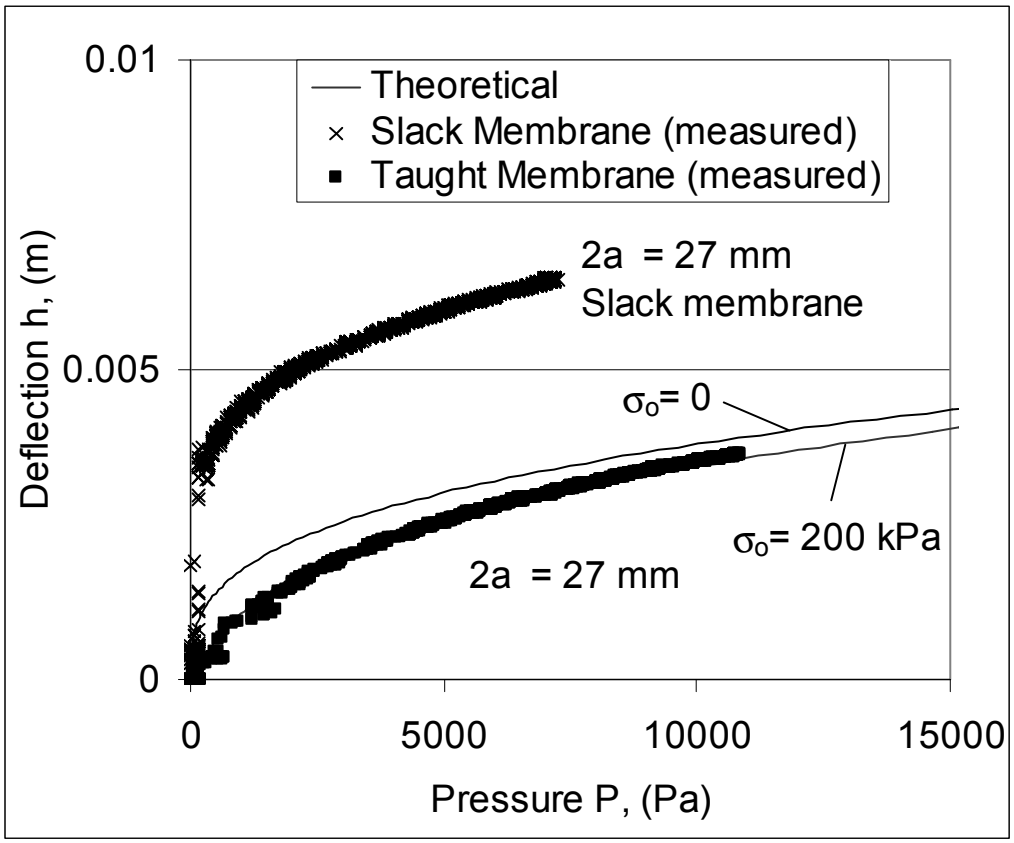

Figure 4.11. Comparison of the pressure deflection curves of pre-stressed and slack membranes for Propore™.

Good agreement is seen between the measured pre-stressed membrane and the total predicted deflection with a pre-stress of 200 kPa. The slack membrane has an initially large jump in the deflection at very low pressure due to the taking up of the slack. The curve after the initial slack region is very similar to the predicted curve with no pre-stress, although it has a slightly different shape which is due to the lack of the pre-stress component in the deflection.

The effects of slack are eliminated when analyzing a pressure deflection curve to obtain the elastic modulus. This effect is eliminated by shifting the 0 deflection point to the point on the curve where the pressure begins to increase. In the proposed application the total deflection is ultimately of interest and the effects of slack are crucial. It can be

seen from Figure 4.11 that eliminating the slack is crucial to limiting the total deflection of the membrane for a given pressure. It can also be seen that increasing the pre-stress component will shift the curve to the right and result in less deflection for a given pressure. This information can be used to determine the level of pre-stress required to maintain a deflection at a given pressure.

4.5.2 Verification of elastic modulus

The use of a pressurized membrane flow channel supported by a screen is very similar to the square bulge test geometry. The deflection pressure relationship of Equation [4.13] can be applied to square membranes with the appropriate constants and material properties.

To obtain data for a square membrane deflection, a modified test cell with a square opening is designed. The elastic modulus and Poisson's ratio that are determined from the circular bulge test are used in the square bulge test. Agreement between the theoretical and measured square bulge test thus serves as a verification of the elastic modulus determined in the circular bulge test.

Figure 4.12 shows the average measured pressure deflection curve compared to the solution given by equation [4.13]. The measured values are represented by a fourth order polynomial curve fit through the averaged data of 5 tests. The value of pre-stress used in the theoretical calculation is the average pre-stress value obtained from a curve fit of the measured data to equation [4.13]. The elastic moduli used are the design values obtained from the circular bulge test.

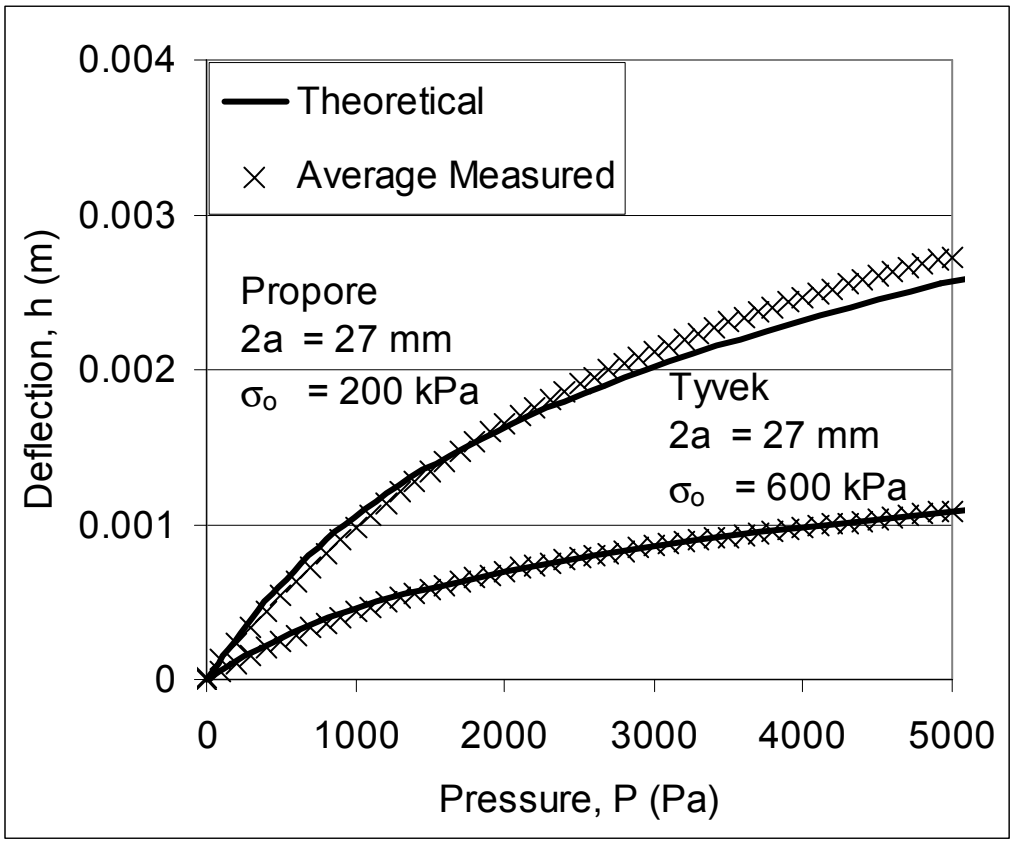

Figure 4.12. Comparison of pressure deflection curves for the case of a square membrane bulge test, for Tyvek® and Propore™.

The agreement is very good between the measured values and the calculated values. There is more notable difference in Propore™ which showed more nonlinear material behaviour in the traditional tension test. This non-linear behaviour causes deviation from the cubic pressure deflection of a linear material. The repeatability of the deflection measurements for both materials is found to be 0.4 mm. This repeatability includes the effects of different samples and the test method and attributes to the deviation of the measured and theoretical lines in Figure 4.12.

4.5.3 Determining the size of the RAEE support screen

Two commercially available screens of different opening sizes are considered for the RAEE support screen. The difference between the membrane supported by a screen

measurement and the square bulge test is the boundary conditions. In the case of the membrane supported by a screen, the boundaries are not completely clamped down but are free to interact with the material in the adjacent screen squares. It is important to verify the assumption that the membrane with screen support boundary acts like the fixed square bulge test boundaries. This verification allows the results of equation [4.13] to be used with confidence to predict the deflection heights for other screen dimensions. Two screens are used to verify that the equation could be applied to screens of other dimensions. The screen spacings are $2a = 5.8\text{mm}$ and $2a = 12.7\text{mm}$ (the dimension 2a is defined in Figure 4.10).

Figure 4.13 contains plots of measured deflection for Tyvek® and Propore™ membranes within a screen. The total measured deflection is the directly measured deflection of the membrane in the center of a square section in the screen. The screen measured deflection is the average of four measurements of the screen itself surrounding the square section of the membrane measurement. It can be seen that the deflection of the screen itself must be taken into account when considering the deflection of the membrane alone. The corrected measured deflection is the total deflection of the membrane and screen minus the deflection of the screen. The theoretical deflection is the result of equation [4.13] with a pre-stress value obtained from a curve fit of the corrected data to equation [4.13].

(a) Propore™ – 5.8mm screen

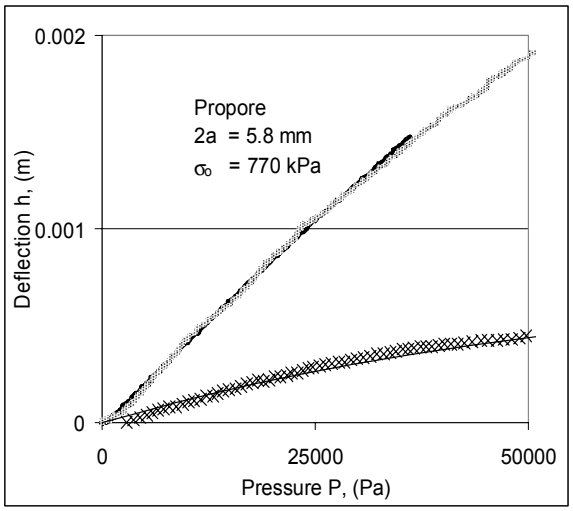

(b) Propore™ – 12.7mm screen

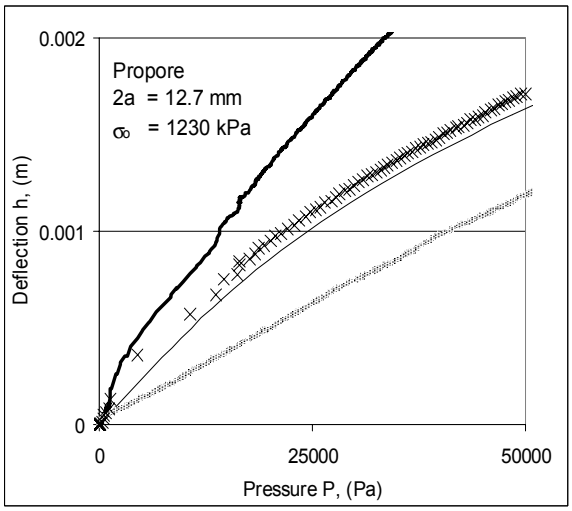

(c) Tyvek® – 5.8mm screen

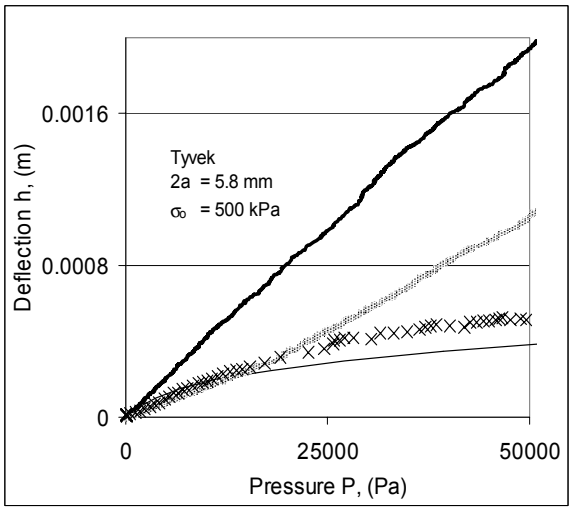

(d) Tyvek® – 12.7mm screen

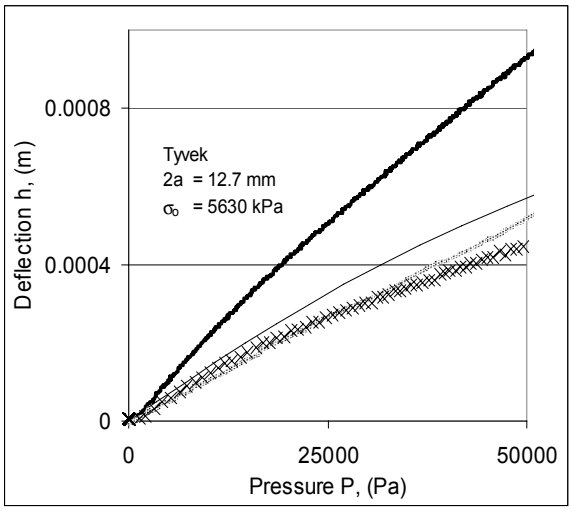

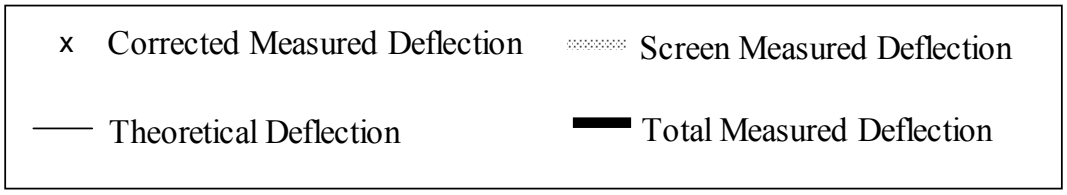

Figure 4.13. Pressure deflection of a square membrane within a screen for (a) Propore™ – 5.8 mm screen (b) Propore™ – 12.7 mm screen (c) Tyvek® – 5.7 mm screen (d) Tyvek®- 12.7 mm screen.

It can be seen that there are small differences between the corrected measured deflection and the theoretical values. In the case of the 5.8mm screen, the deflection of the screen is a significant portion of the total deflection. This results in larger uncertainty of the corrected membrane deflection. Another source of error is that the square in which the deflection is measured is not always at the center of the bulge test apparatus. This is compensated for by averaging the measurements of the screen on the 4 sides of the square in which the membrane is being measured. Figure 4.13 also shows only one measurement per screen and therefore there is a significant uncertainty due to the repeatability of the measurement. The repeatability of the bulge test measurements is found to be 0.4 mm in Section 4.5.2 and the same magnitude of repeatability is assumed for this test. Considering this uncertainty all corrected measured values of Figure 4.13 agree with the theoretical results within the uncertainty bounds of the measurements. The fact that there is good agreement between the corrected measurement and theoretical curves show that the theoretical equations can be applied to the case of membrane deflection within a screen which has a different boundary condition than the traditional fixed membrane of the bulge test. From Figure 4.13(b) it can be seen that the design deflection limit of 1 mm is reached at a pressure of approximately 20 kPa. Since this is greater than the minimum operating pressure of the RAEE system (3 kPa), the 12.7 mm screen will provide adequate support when a pre-stress of 1230 kPa is applied.

The results of Figure 4.12 and Figure 4.13 can be combined and shown in the dimensionless groups of equation [4.16]. The dimensionless pressure deflection curves for both materials are summarized in Figure 4.14

(a) (b)

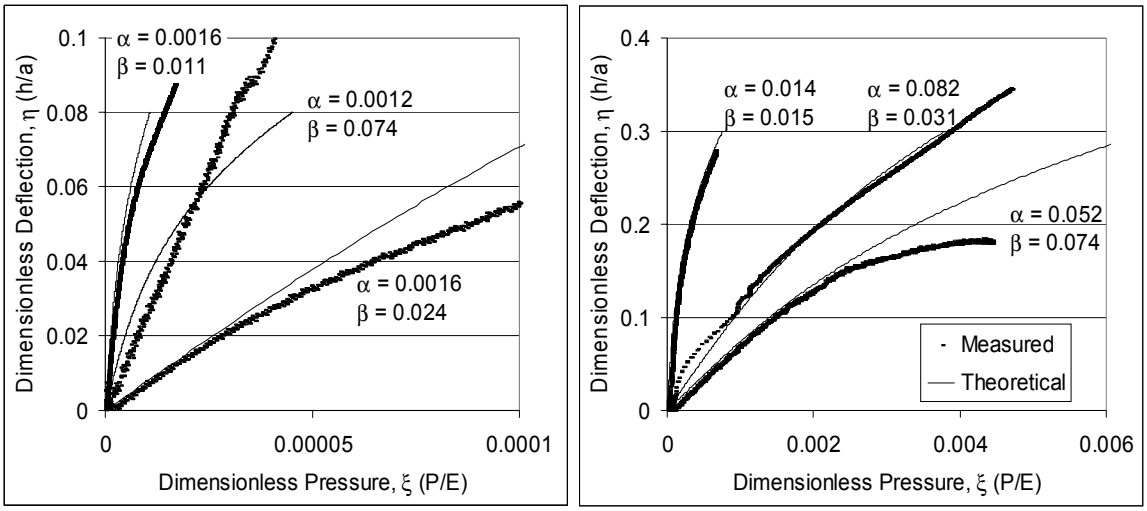

Figure 4.14. Dimensionless pressure deflection curves for (a) Tyvek® and (b) Propore™.

In the case of Propore™, the agreement between the measured and theoretical curves is very good. The agreement is especially good at the higher values of α where the measurements are more accurate due to the larger sized square size, and the use of an average of 5 measurements. The deviation between the measured and theoretical curves of the $\alpha = 0.052$ case for Propore™ can be explained by the break down of the theoretical equation as the deflection (h) approaches the size of the square screen opening (2a) at larger pressure. As h approaches a, the assumption of spherical deflection no longer holds. A similar situation can be seen in the results of Tyvek® for the $\alpha = 0.0016$ case. In general, the agreement between he measured and theoretical values are better for Propore™ than for Tyvek®. This is due to the fact that the uncertainty in the Tyvek® tends to be larger due to the relative size of the deflection versus the repeatability of the measurement of 0.4 mm.

4.6 Conclusions

Comparisons of three different test methods for determining the elastic modulus of two thin membranes are presented in this chapter. Tyvek® has a random structure and its orientation does not affect its elastic modulus; however, the elastic modulus of Propore™ is heavily dependent on the orientation. The elastic modulus of Tyvek® is more sensitive to strain rate than Propore™ due to its fibrous structure. Relative humidity is found to have little or no effect on the mechanical properties of both membrane materials due to their hydrophobic properties.

The bulge test analysis methods show greater differences in the calculated elastic modulus for Propore™ than for Tyvek®. This is due to the fact that Propore™ is more elastic than Tyvek® and is more likely to challenge the assumptions of deflection geometry and material linearity. The bulge test analyzed using the secant method is concluded to provide the most effective and easily obtainable elastic modulus for use in the proposed pressurized flow channel with screen support of the RAEE system.

The elastic moduli obtained from the circular deflection bulge test are verified by comparing the theoretical results calculated using the elastic modulus obtained from the circular bulge test to the measured results of a square bulge test. The agreement is found to be very good and a test of the deflection of the membrane supported by a screen verified that the theoretical equation could also be used to determine the deflections in the case of the proposed pressurized flow channel with screen support. It is found that a commercially available 12.7 mm (0.5 in.) screen will provide less than 1 mm of membrane deflection into the air side of the exchanger at the minimum operating pressure of 3 kPa. A dimensionless representation of the deflection is presented and agrees well with the theoretical solution.

CHAPTER 5
SHORT WAVELENGTH UV DEGRADATION MEASUREMENTS

The increase in poor indoor air quality (IAQ) has prompted investigation into techniques of controlling both microbial growth (e.g. SARS, TB, influenza) in buildings as well as reducing harmful volatile organic compounds (VOC's) (e.g., Formaldehyde, Toluene, Carbon dioxide). Both microbes and VOC's have associated health risks ranging from mild coughs and irritation to cancer (Chen et al., 2005). Traditionally, an acceptable limit of microbes and VOC's in an indoor space can be maintained by filtration and ventilation. In situations where IAQ is of increased importance, such as hospitals, and clean rooms, etc. there are other systems that have been established to maintain lower concentration levels. Some examples include: sorption filtration, ionization, ozone reduction, and UV light irradiation (Chen et al., 2005). All of these technologies have advantages and disadvantages and can be used in conjunction with an RAEE system. The use of UV light is the only method studied in this thesis since it is the only technology that may degrade the membranes in the RAEE system. The use of sorption filtration, ionization and ozone producing products are assumed to have no effect on the RAEE membranes.

UV light has been used in laboratory settings since the 1960's to sterilize equipment and is well established in many markets; however, it is relatively new to the HVAC market (VanOsdell et al., 2002). Several in-situ studies have been performed in recent years. Levetin et al. (2001) studied the effect of UV light in a 4 story office building in Tulsa, Oklahoma where UV emitters were placed adjacent to the cooling coils of the air

handling units (AHU) of 2 floors and not in the other two. The UV emitters were left on continuously from May to September and significant decreases in several microbes (e.g. 70% decrease in Aspergillus, and a 92% decrease in Cladosporium) were observed. Menzies et al. (2003) performed a similar study in an office building in Montreal, Quebec. In the study of Menzies et al. (2003) a significant decrease in microbes (e.g. 25% decrease in Aspergillus, and a 88% decrease in Cladosporium) was also found and surveys of building workers indicated that 25% fewer people reported health issues with the UV emitters on. Both authors conclude that the use of UV light helps destroy microbes, although Levetin et al. (2001) also concluded that more research needs to be done.

Due to the membrane separation of the supply and exhaust streams in the RAEE, it has the ability to provide very low to no leakage between the supply and exhaust air streams, and thus has excellent potential to be used in situations where energy recovery is required and IAQ is important. The RAEE system may have even greater potential for IAQ applications when combined with a UV irradiation system. While it is known that UV light causes degradation of polyethylene (Tyvek®) and polypropylenes (Propore™), (CES3 database, 2006) the level of degradation at from a commercially available UV emitter with peak output at a 254 nm wavelength with varying intensities and exposure times is of interest.

The UV light spectrum includes the wavelengths from 10 to 400 nm with the range from 200 to 400 nm known as near UV. Near UV can be further divided into UVA or long wave UV (320-400), UVB or medium wave UV (290-320), and UVC or short wave UV (200-290 nm) (Diffey, 2002). The peak wavelength for the destruction of

microbial DNA is at 265 nm (Nagy, 1964) which corresponds to short wave or UVC irradiation and thus the most efficient UV emitter is one at or near this peak wavelength. To construct a UV bulb that will emit the desired wavelength of 265 nm an arc is passed through low pressure mercury vapour. The resulting radiation spectrum includes a peak at 253.7 nm. Although this is not the peak wavelength desired for microbial destruction, it is very close and is still very effective (Nagy, 1964).

UVC light can be used to directly eliminate microbes but it has no direct effect on airborne VOC's. VOC's can be targeted, however, by using a UVC emitter in conjunction with a semi conducting surface such as Titanium dioxide. The energy of the UVC light creates hydroxyl radicals on the surface of the semi-conductor which then oxidize adsorbed VOC's. The use of UVC in this fashion is known as photo catalytic oxidation UV or UV-PCO.

Both UV-PCO and UVC have potential uses in conjunction with the RAEE depending on the type of contaminate to be eliminated. It is important that microbial growth on the membrane be minimal and, depending on the application, VOC's may also be of concern. If either UVC or UV-PCO is used to remove contaminates in the RAEE system, then the membranes will be exposed to the UVC light and the effects of this exposure are of interest. It is expected that some degradation will occur in the membranes under consideration. However, if the degradation can be minimized by increasing the distance between the UVC emitter and the membranes so that the effects of the UV exposure are minimal, then the benefit of the UV may be worth the possible loss in structural performance or scheduled replacement costs. It should be noted that in

this chapter any reference to UV light is a reference to the UVC light emitted from a mercury bulb, unless stated otherwise.

5.1 Test methods

At present there are no known standards for exposing materials to UVC light, but several papers outlining the effects of UV degradation have been published. Authors such as, Shyichuk et al. (2005), Kelly et al., (1997), and Kaczmarek et al., (2005) have published results on the degradation of materials due to UVC light exposure, but few details of the exposure and experimental facility are given. In general, the samples are uniformly exposed and a measurement of the intensity is made and reported. Since there is no standard technique for the exposure of materials to UVC light, a unique apparatus is designed and tested

5.2 Apparatus

An ultra violet exposure compartment (UVEC) is designed to simulate exposure of the membranes to short wave UV irradiation in an AHU or duct. The UVEC is designed to give the maximum exposure to the specimens over a uniform area. The following figure shows a schematic of the UVEC facility.

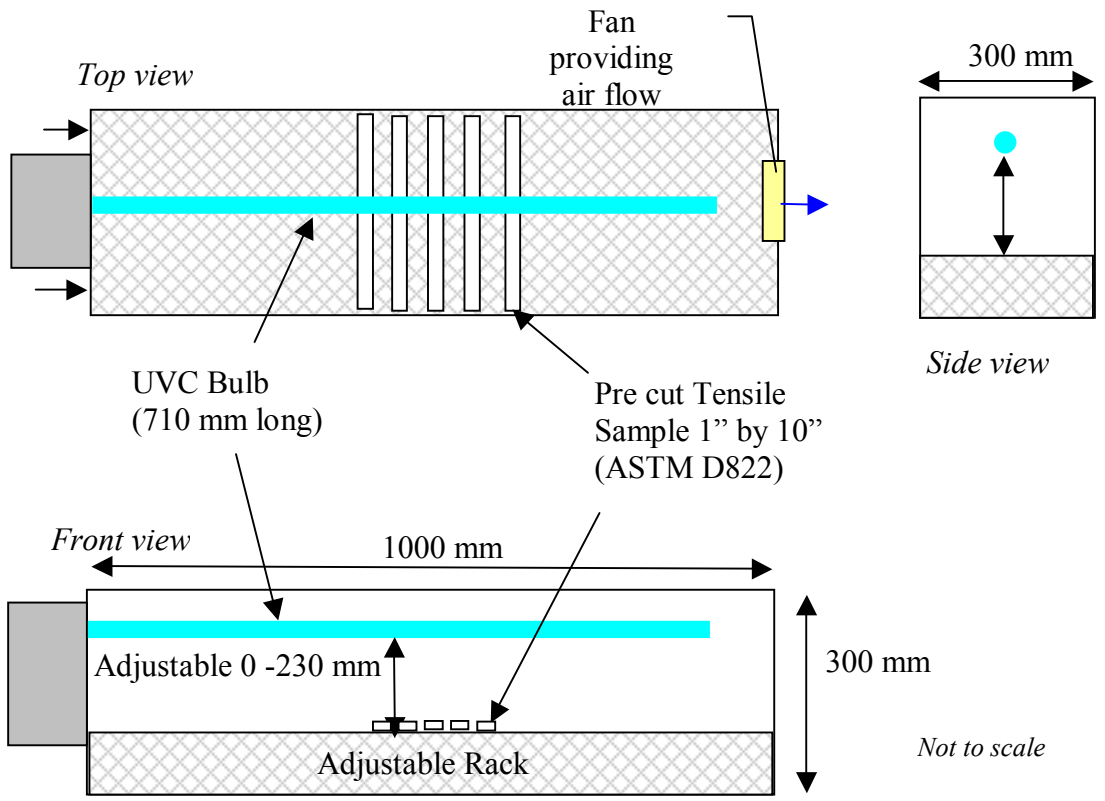

Figure 5.1. Schematic of the UV exposure facility (UVEC).

The UVEC is made from 20 gauge galvanized steel which is typical of an AHU construction. The UV lamp used was obtained from Altru-V Inc. and has the commercial name V-Strike. The lamp has a power input of 16W and is a low intensity, low pressure mercury lamp. The lowest intensity bulb was chosen to represent the lower limit of commercially available UVC emitters. The lamp is mounted in the UVEC so that the distance between the bulb and the galvanized steel sample tray can be adjusted from 0 to 230 mm (0 to 9 in). The samples are masked so that only 645 mm^2 (1 in^2) at the center of the specimen is exposed. This masking ensures that the exposed portion receives a uniform dose of UV and provides a clear distinction between the exposed and unexposed regions.

5.2.1 Air flow and heat transfer

A fan is installed in the UVEC along with ventilation holes as shown in Figure 5.1. The fan provides a flow rate of 35 L/s (75 CFM) which corresponds to an airflow Reynolds number in the UVEC of 7500. The Reynolds number is defined as,

$$\mathrm{Re} = \frac{\rho V D_h}{\mu} \qquad [5.1]$$

where D_h is the hydraulic diameter of the UVEC cross section [m], V is the velocity of the airflow [m/s], and ρ is the density of the air [kg/m^3].

The fan is chosen to ensure turbulent flow conditions and good mixing occurring within the UVEC. This is important because oxidation of the polymers is a primary reaction, and therefore a constant supply of oxygen must be available at all times. The face velocity over the samples is 0.5 m/s (100 FPM) on average. Higher face velocities provide more convective cooling of the bulb, resulting in a decrease in bulb intensity (although increasing the face velocity can increase the intensity of the bulb at high temperatures). In general, the performance of the lamp will decrease with decreasing temperature and increasing face velocity. This is due to the fact that the colder temperature affects the vapour pressure of the mercury in the bulb, and any decrease in vapour pressure results in less intensity at the desired wavelength of 254 nm.

The fan also provides cooling of the UVEC and maintains a constant temperature. A basic energy balance on the surface of the specimens shows that the fan provides adequate convective cooling to balance the radiation heat transfer from the UV bulb, which has a surface temperature of 47^{o}C when in operation. This convective cooling maintains the samples at the surrounding room conditions which is important because

the effect of temperature on the membranes in not considered in this thesis. The energy balance is confirmed by measuring the surface temperature of the specimens in the UVEC (Figure 5.1) and ensuring that it is the same as the surrounding conditions which are maintained at 23^{o}C. VanOsdell et al. (2002) concluded that humidity has little effect on the output of UV lamps and previous studies (Larson, 2005) have shown that the materials being considered are not hygroscopic, therefore humidity is not controlled.

5.2.2 Intensity field measurements

Measurements of the UV intensity are taken using a UVP Inc. photovoltaic UV meter. The meter is calibrated for low pressure mercury lamps with a peak response at the 254 nm wavelength. The UV irradiation is measured to ensure that all samples are receiving the same amount of irradiation and to ensure that there is no significant drop in the bulbs irradiance over time. Figure 5.2 shows the irradiance field within the UVEC at the plane of the bulb at the beginning of testing. Table 5.1 shows a summary of the intensity values ($\mu W/cm^2$) at commonly used distances from the UV bulb.

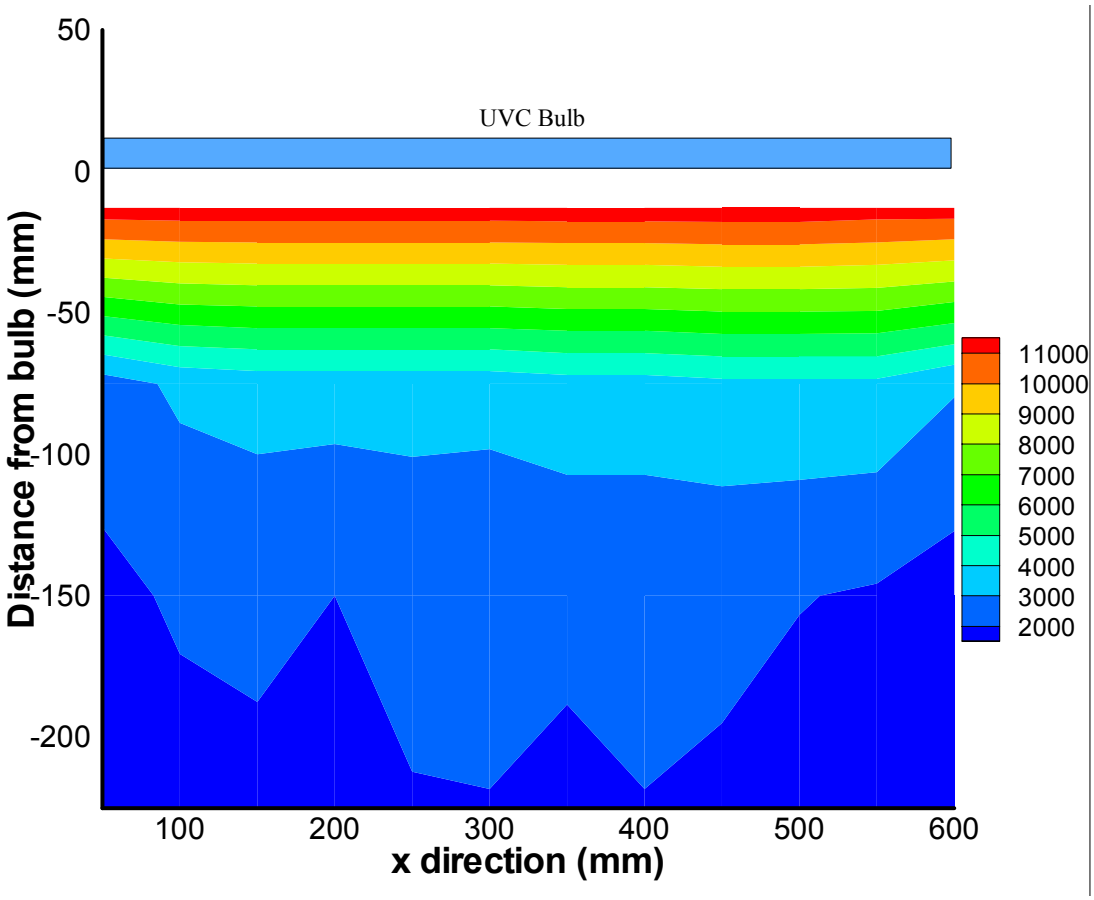

Figure 5.2. UV intensity contours within the UVEC measured prior to testing.

Table 5.1. Summary of the intensity values at various distances along the center of the UVEC.

Distance from bulb, mm (in.)	Measured Intensity, $\mu W/cm^2$
25 (1)	11,400
75 (3)	4,000
150 (6)	2,100

It can be seen that the intensity drops off rapidly with increased distance from the bulb. The relationship is known to be proportional to the inverse square of distance although this is not exactly the case in the UVEC due to the highly reflective surfaces. The UV contours are also measured at the conclusion of the testing and there is no significant change in the bulb's intensity.

5.3 Analysis

Tyvek® and Propore™ are both initially placed at a distance of 25 mm (1 inch) from the bulb. Samples exposed 24 hours per day and are left for 1, 2, and 3 week time periods. Based on the measured intensity at the samples position and the time of exposure the dose is calculated using,

$$D_{UVC} = t_{exp} \cdot E_{bulb} \qquad [5.2]$$

where D_{UVC} is the dose of the UVC [kWs/m^2], t_{exp} is the exposure time [s] and E_{bulb} is the intensity of the bulb [kW/m^2].

Samples are also exposed to the UV at 75mm (3 in) and 150 mm (6 in) distances for exposure times of up to 10 weeks. The effects of UV are also quantified using Raman spectroscopy analysis and atomic force microscope images.

5.4 Comparison to the solar spectrum

The total dose of energy received by the specimens can be compared to the dose that a specimen would receive from the sun. This reference to the solar spectrum is solely for the purpose of providing a sense of magnitude of the UV dose administered to the membrane sample. The dose of the UV emitter is known, and the intensity of the sun can be calculated. Setting the dose of the UV emitter equal to the solar dose the equivalent time of solar exposure is calculated. Rearranging equation [5.2] to give the equivalent solar exposure gives,

$$t_{solar} = \frac{D_{UVC}}{E_{atm,254}} \qquad [5.3]$$

where $E_{atm,254}$ is the emissive power at a wavelength of 254 nm [W/m^2].

The solar intensity at the earth's surface has a lower wavelength limit of 280 nm (Incropera, 2002). Therefore, at the earth's surface, there can be no equivalent comparison of the UVC dose and the solar dose. The reason for this limit is the scattering and absorption of the radiation at these low wavelengths in the upper atmosphere. The intensity spectrum from the sun at the upper atmosphere is well modelled by a black body irradiating at 5800K. This model includes the wavelength of the UVC emitter used in the experiments, and hence a comparison of the UVC energy of the bulb to the solar blackbody is useful. The total solar emission of a blackbody at 5800K is given by the Stefan-Boltzmann law,

$$E_b = \sigma_{sb} T^4 \qquad [5.4]$$

where E_b is the emissive power of a blackbody [W/m^2], T is the blackbody temperature [K] and σ_{sb} is the Stefan-Boltzmann constant [$W/(m^2\ K^4)$]. The total amount of emissive power that hits a surface perpendicular to the sun at the earth's outer atmosphere is determined by the inverse square law, and is given by,

$$E_{b,atm} = E_{b,sun} \frac{4\pi b^2}{4\pi B^2} \qquad [5.5]$$

where $E_{b,atm}$ is the energy received at the top of earth's atmosphere [W/m^2], $E_{b,sun}$ is the emission of the sun as a black body [W/m^2], b is the diameter of the sun [km], and B is the mean distance from the earths atmosphere to the sun [km].

The total emissive power at the upper atmosphere $E_{b,atm}$, includes the energy at all wavelengths. To make a comparison to the energy in a band from 250 nm to 258 nm the

emissive power must be multiplied by the fraction of energy in this wavelength band. The fraction of energy occurring in a given band of radiation, $F_{\lambda_1 \to \lambda_2}$, is given by,

$$F_{\lambda_1 \to \lambda_2} = F_{0 \to \lambda_2} - F_{0 \to \lambda_1} \qquad [5.6]$$

where the integrated fractions $F_{0 \to \lambda}$, are tabulated in the textbook of Incropera (2002).

From the tabulated values, the fraction of energy between 250nm and 258nm for a blackbody at 5800K is 0.002767. The irradiation from the sun at the earth's upper atmosphere in the desired wavelength band, $E_{atm,250 \to 258}$, is then given by,

$$E_{atm,250 \to 258} = E_{b,atm} \cdot 0.0028 = 3.8 \, {}^{W}\!/_{m^2} \qquad [5.7]$$

Substituting the value of $E_{atm,250 \to 258}$ into equation [5.3], the equivalent solar time is calculated for each UVC exposure time. The results are summarized in Table 5.2.

Alternatively, the emissive power can be calculated based on the average solar power measured at the outer edge of the atmosphere by NASA satellites. The mean value of this measured emissive power over the last 20 years is 1368 W/m^2. Multiplying this value by the same fraction (0.0028) as above, the emissive power can be calculated. The difference in the equivalent solar exposure time between the two techniques is less than 1%.

Table 5.2. Summary of the UVC dose and the equivalent solar exposure time.

UVC dose (kWs/cm^2)	Equivalent solar exposure time at outer atmoshphere (days)	Exposure time at 25 mm (1 in.) from bulb (days)	Exposure time at 150 mm (6 in.) from bulb (days)
4	108	4	20
7	205	7	35
14	411	14	70
21	617	21	105

The values of Table 5.2 serve as a comparison for the level of UV exposure from the sun at the outer atmosphere in the wavelength band of 250nm to 258nm. Recall that the equivalent solar exposure times are not valid at the earth's surface due to the absorption and scattering of electromagnetic radiation at these low wavelengths. The exposure times are quite large in comparison to the actual exposure times in the UVEC due to the higher intensity of the UVC bulb at 25 mm (1 in.) and 150 mm (6 in.). Based on the results presented in Table 5.2. the equivalent solar exposure times are equivalent to placing the bulb 1.07 m (42 in.) from the membrane in the UVEC.

5.5 Results

The degradation of the Propore™ and Tyvek® membrane with exposure to UVC are quantified using three different tests: a tension test, Raman spectroscopy and atomic force microscopy (AFM). The tensile tests are performed using ASTM D 882 (2002), where all reported values are the average of 5 samples, a strain rate of 0.1 mm/mm/min is used and tests are carried out in laboratory conditions. The Raman spectroscopy and AFM tests are performed by the Saskatchewan Structural Sciences Center (SSSC) at the University of Saskatchewan.

5.5.1 Tension tests

The tensile results are presented in terms of the ultimate tensile strength (UTS) which is the stress at the breaking point of the sample, and in terms of the percent elongation which is calculated from

$$\frac{e_f - e_o}{e_o} \times 100\% \qquad [5.8]$$

where e_f is the gauge length of the specimen after breaking [mm], and e_o is the gauge length of the specimen before the test [mm].

The UTS and the percent elongation are used to quantify the degradation of the Tyvek® and Propore™ membranes with UV exposure since they are more easily determined from the tensile tests than the secant modulus discussed in Chapter 4. This is especially true for the more deteriorated samples because the samples failed at low stresses with small strains.

In general, as the samples are exposed to the UV light they become discoloured and brittle. In the case of the Tyvek® membrane there is a visible change in the surface roughness and both the Tyvek® and the Propore™ membranes leave a powdery residue when touched after extended exposure. The physical effects on the membrane are further discussed in Section 5.5.3.

Figure 5.3 shows the decline in the percent elongation and the UTS of both Propore™ and Tyvek® as a function of the UVC dose. Each data point in Figure 5.3 is the average of five samples. The four data points from left to right correspond to an exposure time of 0, 1, 2, and 3 weeks with the samples located 1 inch from the UVC bulb.

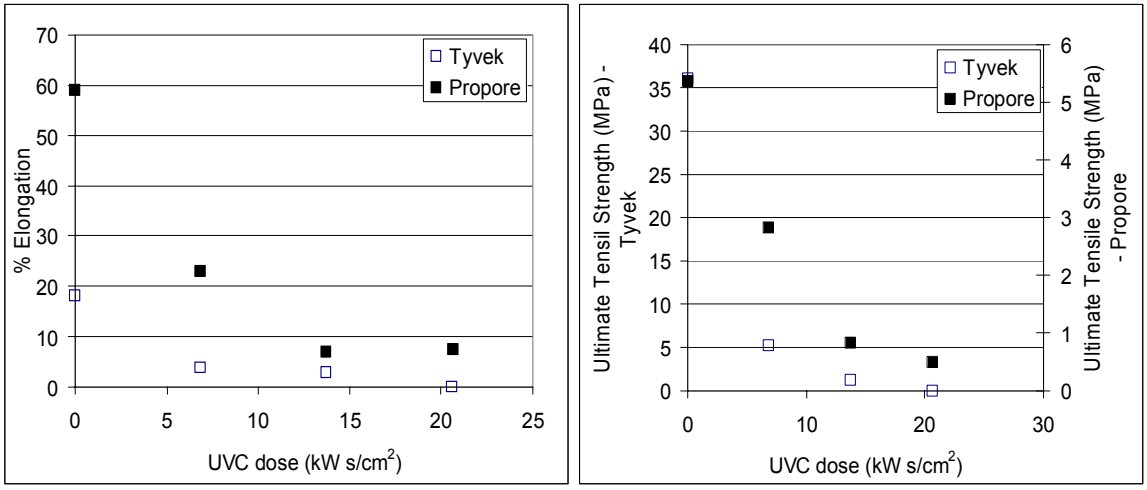

Figure 5.3.Decay of the (a) percent elongation and (b) UTS with UVC dose for both the Tyvek® and Propore™ membranes.

As expected from the literature, the mechanical properties of the membrane materials are significantly changed with exposure to the UVC irradiation. The percent elongation of the Propore™ drops by 87% with an exposure of just over 20 kWs/cm^2, while the percent elongation of Tyvek® drops by 100% at the same dose. The zero percent elongation and UTS measurements in Figure 5.3 occur when the specimen becomes so brittle that is cannot be handled without breaking and therefore tension testing is not possible. The UTS values show the same trend, with the Propore™ dropping 83% and the Tyvek® dropping 100%. These significant changes in the mechanical properties indicate that there has been a significant change in the polymers at the molecular level.

The results of Figure 5.3 seem to indicate that both Propore™ and Tyvek® are highly unsuited for UV exposure since the materials are rendered useless after three weeks of exposure. The dose of UV, however, comprises two components: the exposure time and the exposure intensity. The effects of these two components are individually considered for the Propore™ membrane only in Figure 5.4 and Figure 5.5.

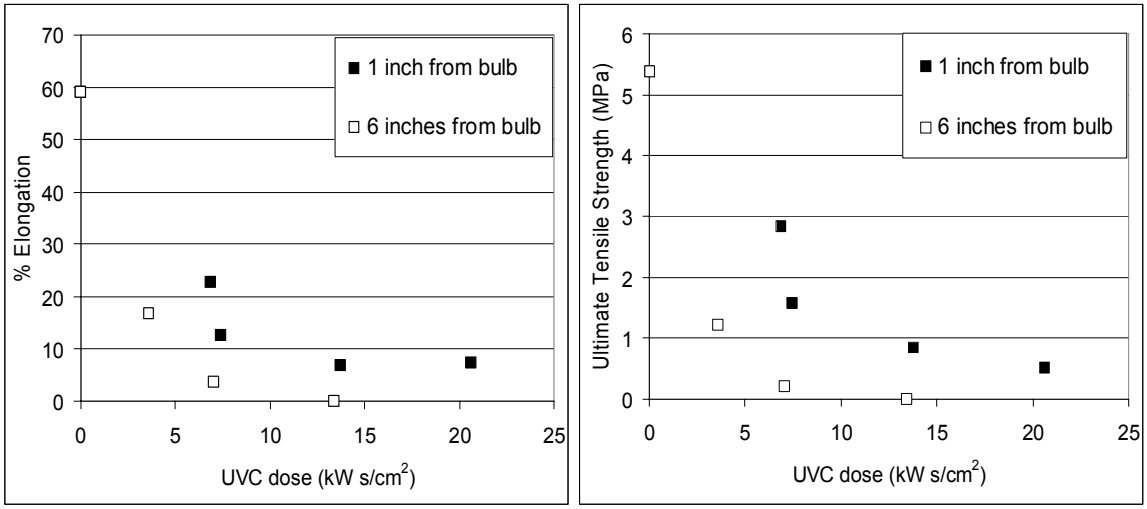

Figure 5.4. The percent Elongation and UTS of Propore™ for two difference exposure distances.

Figure 5.4 shows the decay of the percent elongation and the UTS as a function of the total UVC dose for exposure at two difference distances which correspond to two different bulb intensities (see Table 5.1). The plot for the 1 inch case is the same as in Figure 5.3, while the exposures at 6 inches have the same dosage but they are kept in the UVEC for a longer period of time. It can be seen that for a given dosage, the degradation of the properties is greater for the case of a 6 inch exposure distance which required more time. This indicates that of the two components of the dosage, the time is the dominant factor.

Figure 5.5 shows results of the percent elongation and UTS plotted versus exposure time for two different total UVC dosages.

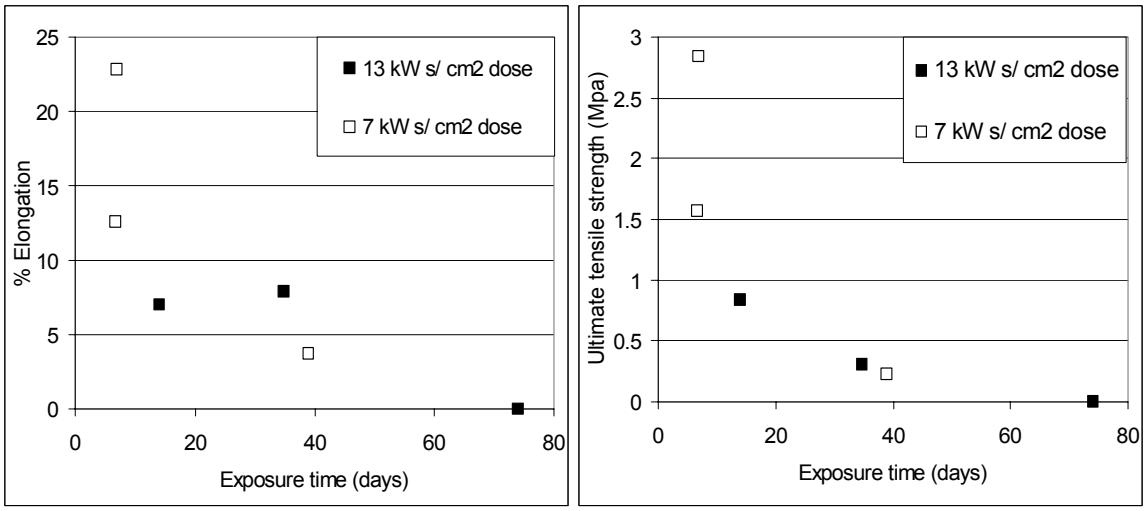

Figure 5.5. The percent elongation and UTS of Propore™ as a function of exposure time.

In this case the values appear to collapse onto a common decay curve of the given mechanical property versus time. This further enforces the conclusion that the materials mechanical properties are sensitive primarily to the time of exposure and not the intensity. While this appears to be the case in the range of times and intensities studied, it may not be true in all cases. An analysis of the theory on exposure time and intensity is left for future work.

5.5.2 Raman spectroscopy

Raman spectroscopy is a form of vibrational spectroscopy used to test materials, which uses the Raman effect to determine the types of molecular bonds in a molecule. When a photon traveling at a specific wavelength strikes the electron cloud of a molecule, an electron will be elevated to a higher energy state. The electron will then relax and release a corresponding photon. When the electron relaxes to the same energy state in which it started, the released photon will have the same wavelength as the original exciting photon. This process of excitation and relaxation at a common

wavelength is known as elastic or Rayleigh scattering of photons. Raman scattering, or inelastic scattering, occurs when the excited electron relaxes to an energy state other than the energy state in which it started. In this case, the photon released in the relaxation of the excited electron will have a different wavelength than the incoming photon wavelength. Raman scattering occurs in only 1 in 10^7 incident photons and the measurable shift in photon wavelength, or Raman shift is the basis of the Raman spectroscopy method (Kaiser Optical Systems, Inc., 2006). Figure 5.6 shows the difference between elastic Rayleigh scattering and inelastic Raman scattering.

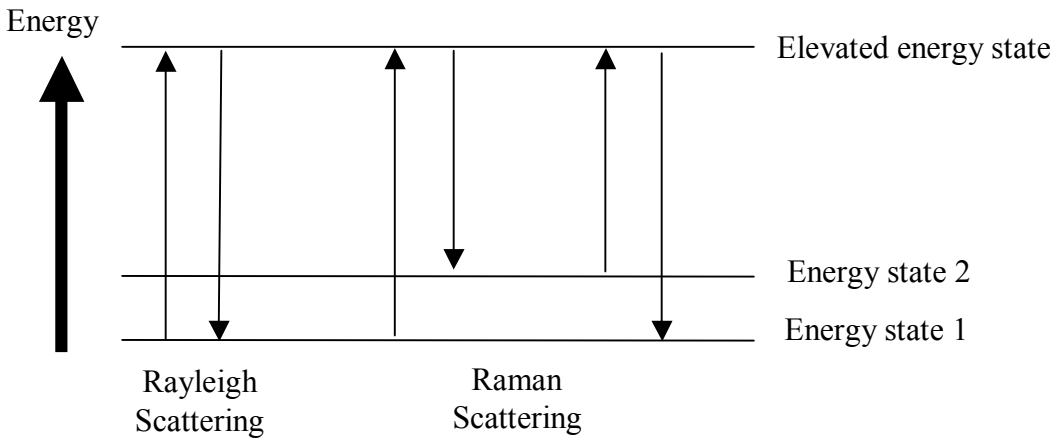

Figure 5.6. Schematic showing energy states and the difference between Rayleigh and Raman scattering.

The Raman spectroscopy results in this thesis are obtained from the Saskatchewan Structural Science Center (SSSC) at the University of Saskatchewan. The SSSC uses a Renishaw 2000 Raman microscope using an Argon laser operating at a wavelength of 514 nm. The photons scattered by the specimen are collected on a charge-coupled device CCD with the elastically scattered photons from the incident laser removed by an optical filter. The spectra obtained are the accumulation of 4 spectra scanned in a

1micron square. The intensity of the Raman scattered radiation is measured as a function of the Raman shift, where the Raman shift is the difference of the measured wavenumber and the incident wavenumber given by,

$$\text{Raman Shift} = \frac{1}{\lambda_{\text{measured}}} - \frac{1}{\lambda_{\text{incident}}} \qquad [5.9]$$

where λ_{measure} is the measured wavelength of the Raman scattered photons [nm], $\lambda_{\text{incident}}$ is the incident laser wavelength of 514 nm. The wavenumber is defined as the inverse of the wavelength.

Peaks of intensity in the Raman spectra correspond to vibration modes of specific molecular bonds. The study of these bonds and the peaks of the Raman spectra are beyond the scope of this thesis. However, it is known that the peak at a wavenumber of approximately 2100 cm^{-1} corresponds to CH bonds. Even without knowing what molecular bonds the individual peaks in the Raman spectra correspond to, the spectra are still useful because any change in the spectra from before the UV exposure and after the UV exposure is suggestive of a change at the molecular level. It should be noted that the units of intensity are arbitrary and that the curves in Figure 5.7 to Figure 5.9 are offset for clarity. UV exposed samples in this section are left in the UVEC for 3 weeks at 25mm (1in.) from the bulb which corresponds to a total dose of 21 kWs/m^2.

(a) Propore™

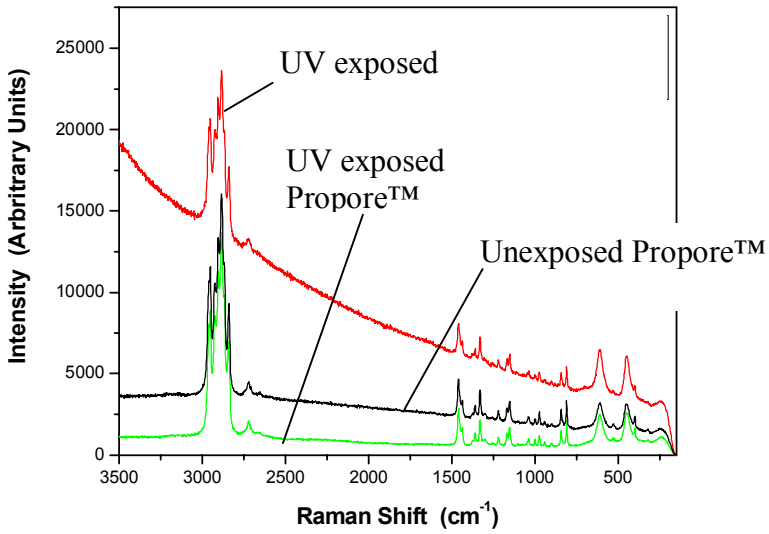

(b) Tyvek®

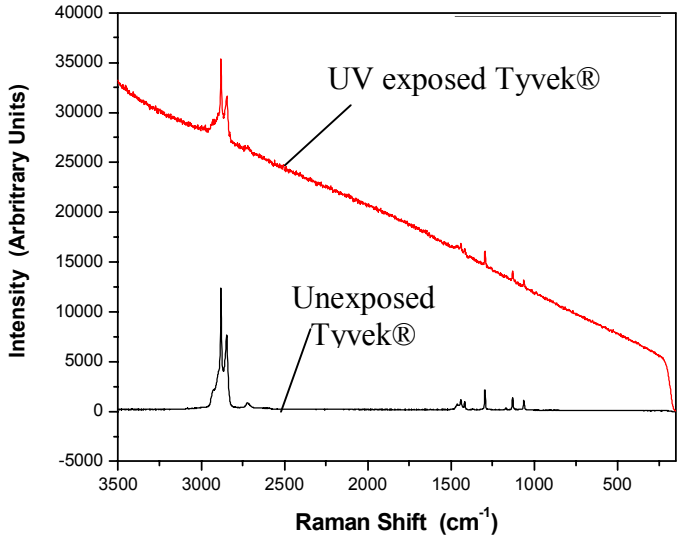

Figure 5.7. The Raman shift spectra of UV exposed and unexposed membranes for (a) Propore™ and (b) Tyvek®.

The most notable difference between the exposed and unexposed samples for both Tyvek® and Propore™ is the large negative slope of the spectra, this is known as a sloping baseline. A sloping base line occurs when a material has fluorescence. Fluorescence is an optical phenomenon that occurs when an incident photon triggers the

release of a photon with a longer wavelength (caused by the Raman effect). It is the fluorescence lifetime that causes the sloping baseline, where the fluorescence lifetime is the length of time that an electron remains at an excited state. This delay of the excited electron causes a delay in the release of a photon and the subsequent build up of photons, or the increase in intensity of Figure 5.7 as the test progresses. The fact that the spectra are not sloped before the exposure indicates that the UV exposure has increased the fluorescence in both materials.

Figure 5.7(a) also shows the Raman shift spectrum for the underside of the exposed sample. The fact that the underside of the exposed sample is unchanged from the unexposed sample, indicates that the molecular altering UV effects do not penetrate through the thickness of the sample.

The fluorescent lifetime that causes the sloping base line observed in Figure 5.7(a) and (b) can be corrected for by taking a reading of the Ramam shift after the sample area has been exposed to the incident laser for an extended period of time. Figure 5.8 shows the Raman shift spectrum for Propore™ after being exposed to the laser for three different amounts of time.

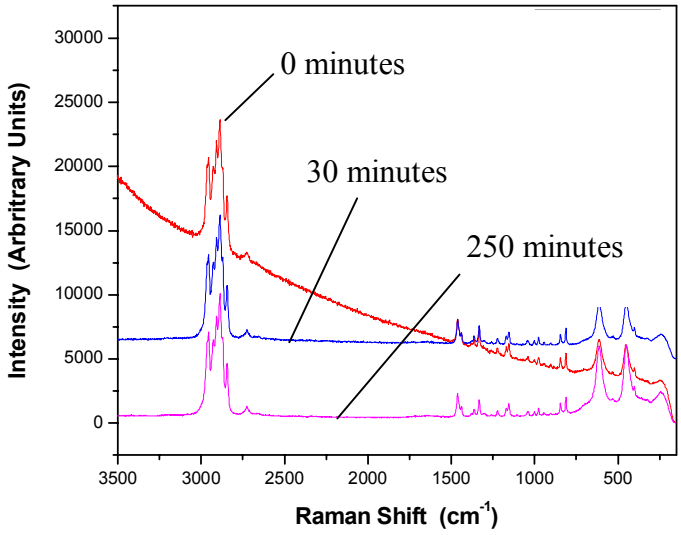

Figure 5.8. Raman shift at different pre-test exposure times.

It can be seen that as the pre-test exposure time is increased the sloping baseline is eliminated from the Raman shift spectrum. The fluorescence is eliminated because the sample becomes photobleached after the extended exposure time. There is no difference between the spectrum obtained at 30 and 250 minutes therefore the time to photobleach the sample is less than 30 minutes.

The corrected results of Figure 5.9 are exposed for 30 minutes to remove the effect of fluorescence. The corrected UV exposed spectra are shown with the unexposed spectra in Figure 5.9.

(a) Propore™

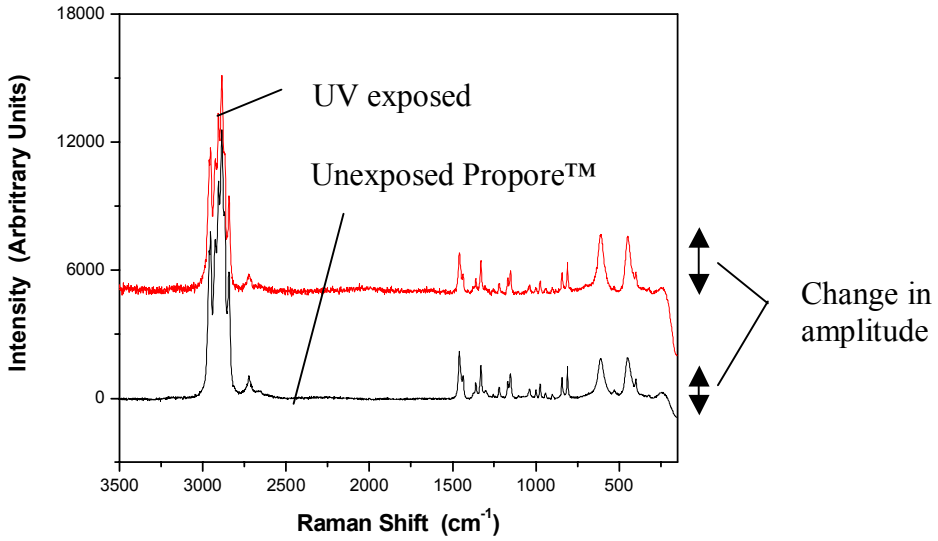

(b) Tyvek®

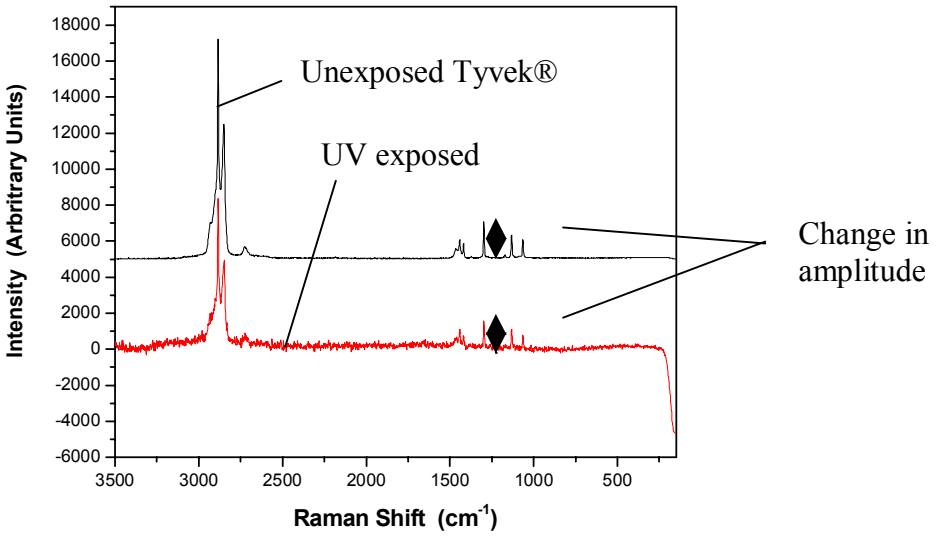

Figure 5.9. Corrected Raman shift for (a) Propore™ and (b) Tyvek®.

A notable change is seen in the Propore™ spectrum where the amplitude of two peaks is increased after the UV exposure. A similar change is seen in one of the peaks of the Tyvek® membrane. These changes are relatively small and indicate a change in a

specific unknown bond. There are no additional peaks or loss of peaks which would indicate a change in the type of bonds in the membrane.

The fact that the materials take on fluorescence with UV exposure and that a change in the amplitude of at least one peak is observed in both the Tyvek® and Propore™ membranes is conclusive that the UV exposure is altering the microstructure of the membranes.

5.5.3 Atomic force microscope

The atomic force microscope is a very high resolution scanning microscope. The AFM was first used in 1986 and is one of the leading techniques for measuring at the nano-scale. The operation for the AFM is based on the interacting forces of a sample and a fine tip connected to a cantilever beam. In the intermittent contact mode used in the tests of this section, the cantilever beam is oscillated near its resonant frequency (40-75 kHz) such that the tip of the cantilever makes contact with the sample with every cycle. The movement of the cantilever is measured using a laser and photodiode assembly (Figure 5.10). The amplitude of the oscillating movement of the cantilever tip changes as the tip interacts with the sample surface. An image is created using the difference between the measured amplitude of the tip and the known input amplitude of the tip (Pacific Nanotechnology, Inc., 2006). The image is created by scanning at a rate of 0.5-1 line per second at 512 pixels per line. Figure 5.10 shows a schematic of the AFM method.

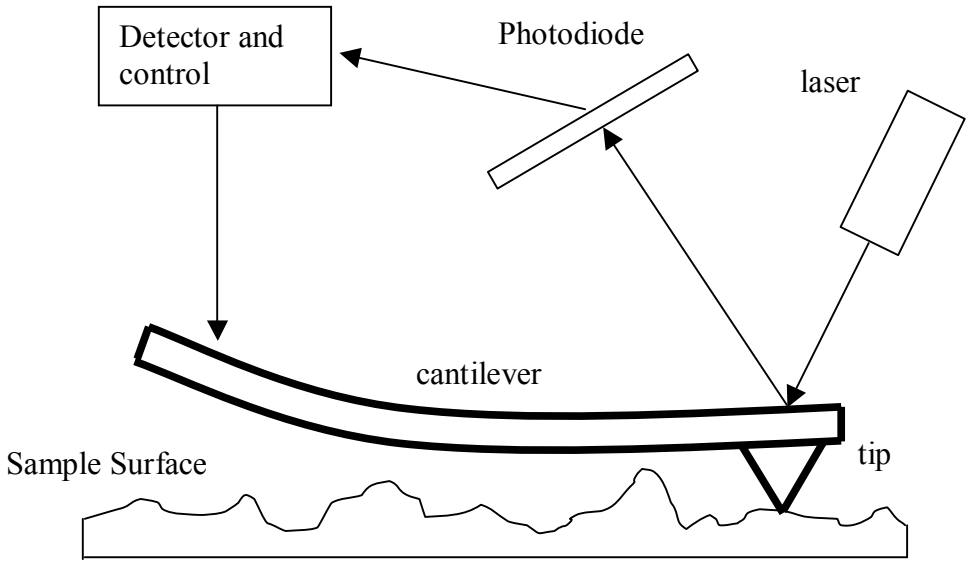

Figure 5.10. Schematic of Atomic force microscope technique.

The following images are taken using a PicoSPM AFM with a Veeco DPN-S cantilever with a force constant of 0.58 N/m. All images are taken by the Saskatchewan Structural Science Center at the University of Saskatchewan.

(a) Propore™ - unexposed (b) Propore™ - UVC exposed

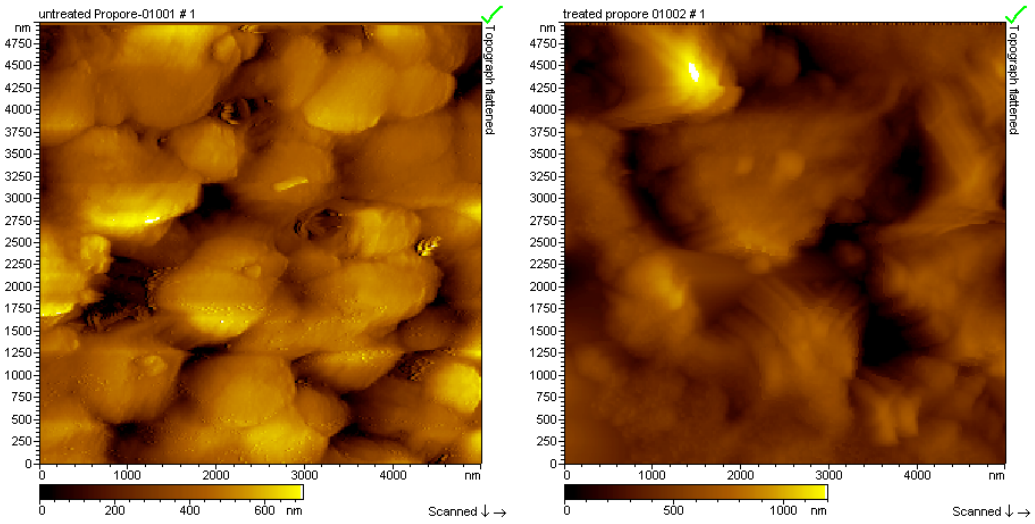

(c) Tyvek® – unexposed (d) Tyvek® – UVC exposed

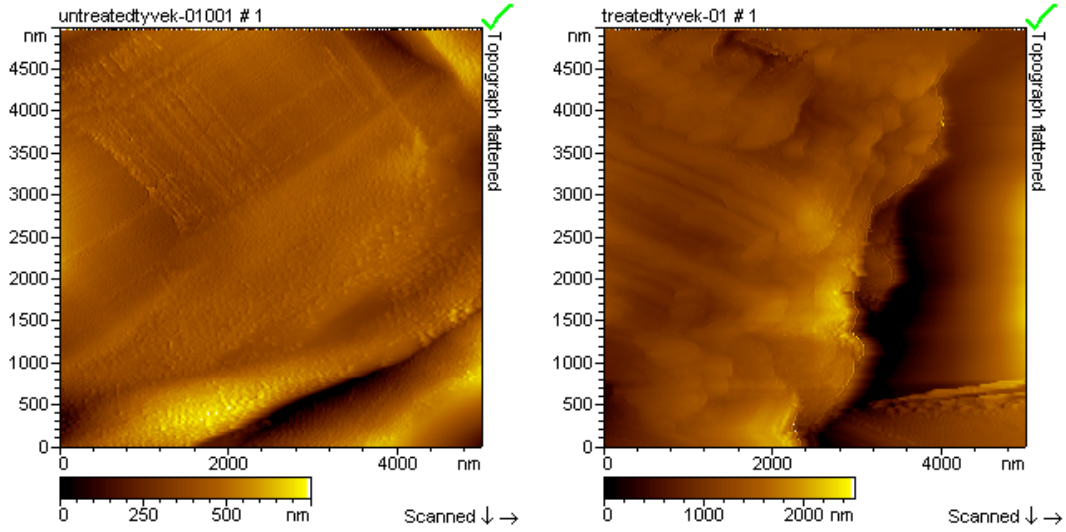

Figure 5.11. AFM images, 5 microns square of (a) Propore™ – unexposed, (b) Propore™ – UVC exposed (c) Tyvek® – unexposed and (d)Tyvek® – UVC exposed.

It can be seen that there are significant changes in the microstructure of the UVC exposed samples. The samples appear to have been “melted” by the UV light exposure, although this is not the case since the temperature is held constant throughout the test. The images show conclusive evidence that the samples are significantly changes by the

UVC exposure. The AFM also measures the surface roughness which is shown as light and dark shades in Figure 5.11. The exposed samples have a greater occurrence of contrasting dark and light spots which indicate a change in the surface roughness with UV exposure. The root mean square surface roughness values of each sample are summarized in Table 5.3

Table 5.3. Summary of surface roughness values from before and after UVC exposure.

	Unexposed RMS roughness (nm)	UVC exposed RMS roughness (nm)	Percent Increase (%)
Propore	124	194	56%
Tyvek	95	882	828%

It can be seen that the exposure to UVC greatly increased the surface roughness of both the Tyvek® and Propore™ samples. The roughness increase in the Tyvek® is large enough to be seen with the naked eye.

5.6 Application

Since the UTS approaches zero for both Propore™ and Tyvek® over time regardless of the distance between the material and the bulb, it is concluded that neither membrane should be used in conjunction with a UVC emitter. The degradation effects on the membrane have been quantified in terms of the UTS and percent elongation. In order to use this data in a design analysis, a design property is required. The effects of UV degradation cannot be correlated to liquid penetration pressure or vapour diffusion resistance however there is a relationship between the UTS and the secant modulus discussed in Chapter 4. With a known elastic modulus, the deflection equations used in Chapter 4 can be applied and the deflection of the membrane can be determined after UV exposure.

Figure 5.12 shows the correlation of the UTS with the secant modulus for the Propore™ membrane. Both values before and after the UV exposure are included.

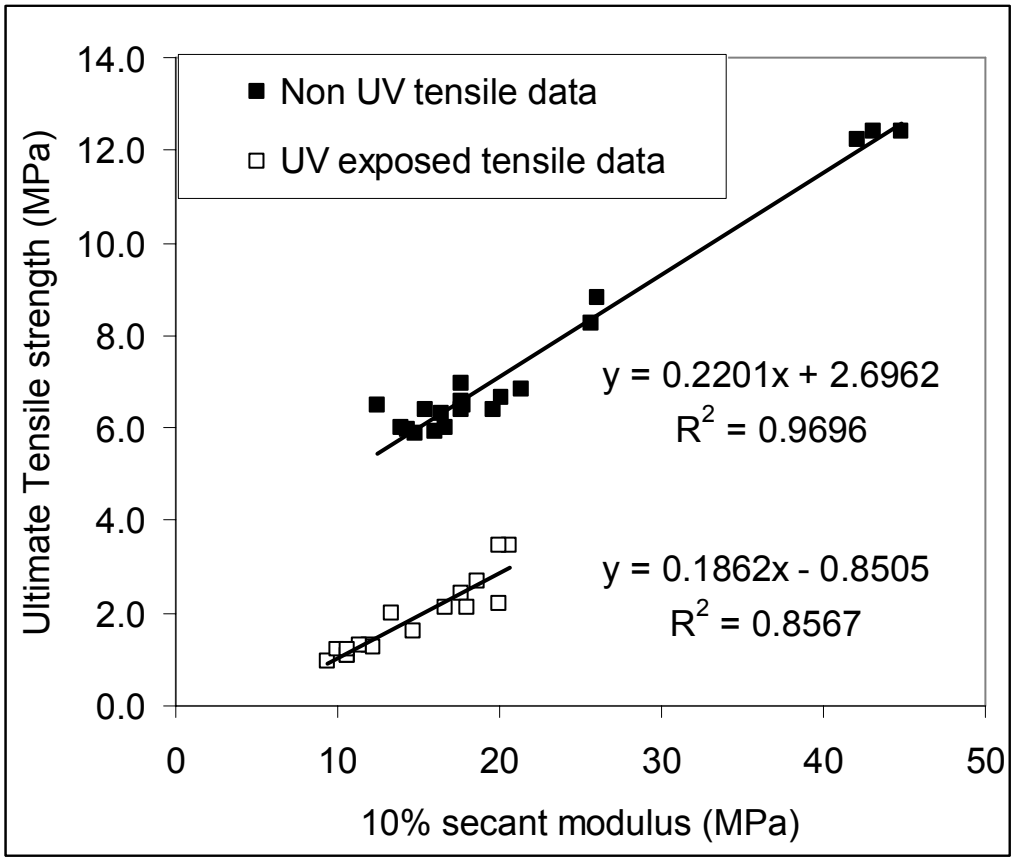

Figure 5.12. Correlation of UTS and secant elastic modulus for Propore™ for both UV exposed and non-UV exposed samples using ASTM D 882 (2002).

It can be seen that for the UV exposed specimens the correlation of UTS and secant modulus is different than the case of non exposed samples. The exposure embrittles the membrane and thus for a given modulus the UTS of the specimen will be significantly lower in a sample that has been exposed to UVC light.

The lower values of 10% secant modulus for the UV exposed case shown in Figure 5.12 are for an exposure time of 2 weeks at a distance of 25 mm (1 in.) from the bulb or a dose of 14 kWs/cm^2. At this UV dosage, the secant modulus has dropped by 65% from the design value of 20 MPa. From equation [4.12] it can be seen that a 65% drop in

elastic modulus corresponds to an increase in the deflection, for a given pressure, of 42%. The screen size could be altered to accommodate this change; however, since it is known that the material will fail over an extended UVC exposure time, the amount of reinforcement required to make the membranes usable in a UVC exposed RAEE is impractical.

5.7 Conclusions

The exposure of the Tyvek® and Propore™ membranes to UVC light resulted in catastrophic failure after weeks of exposure time. It was postulated that the degradation could be minimized when the UVC emitter is placed at a greater distance from a membrane. However, it is discovered that the exposure time is the dominant factor in the degradation and therefore even with the UVC emitter at a significant distance from a membrane there are detrimental effects to the membranes microstructure.

The effects of the UVC are characterized in terms of UTS and correlated to an elastic modulus value. It is found that the reduction in elastic modulus is highly significant for short exposure times. The exposure time is also compared to that of solar radiation at the outer atmosphere. It is found that the equivalent exposure time for the sun is much longer than the exposure time of the UVC bulb in the UVEC. The solar exposure is equivalent to exposing a sample to the UVC bulb in the UVEC at a distance of 1.07m (42 in.).

CHAPTER 6
SUMMARY, CONCLUSIONS AND FUTURE WORK

In this thesis several material properties of DuPont™ Tyvek® and 3M™ Propore™ membranes are examined. The membranes are examined for their use in a liquid to air energy exchanger core which is part of an air-to-air energy exchanger for a building ventilation system. The material properties that are examined in this thesis are determined based on the previous numerical work of Fan et al. (2006) and the building and testing of two prototype exchangers (Erb, 2006 and Hemmingson, 2005).

6.1 Summary of results

From the numerical model of Fan et al. (2006) it is determined that the overall effectiveness of the air-to-air exchanger is sensitive to the water vapour permeability of the membrane. Due to this sensitivity a standard test method that is similar to the RAEE application is chosen to test the vapour diffusion resistance of the Tyvek® and Propore™ membrane. Results are obtained from the U.S. Army Soldier Systems Center, and show that under ideal operating condition with an NTU of 12.5, Cr* of 2.8 and a mass flow rate ratio of 1 the maximum overall effectiveness of an exchanger using a Propore™ membrane is 62%. With the same conditions, the effectiveness of the exchanger using a Tyvek® membrane is found to be 52%. The uncertainties in the measured values of vapour diffusion resistance correspond to an uncertainty of ± 1.4% in the maximum overall effectiveness. Testing of the second prototype exchanger (Propore™ membrane) by Erb (2006) yielded a total effectiveness of 36% which is

much lower than predicted. This is likely due to the differences in the flow characteristics between the numerical model and the second prototype exchanger.

Due to the fact that some liquid penetrated through the membrane of the first prototype (Hemmingson, 2005), the liquid penetration pressure is measured using a modification of the standard AATCC test method 127 (2003). The liquid penetration pressure for Tyvek® is found to be 18 kPa which agrees well with the published data. However, when Tyvek® is exposed for long periods of time or with fluctuating pressure, it shows a decrease in liquid penetration pressure. Propore™ has a high liquid penetration pressure and therefore accurate data is unattainable using the modified method. The fact that an exact liquid penetration pressure value is not determined is inconsequential since Propore™ did not fail at the maximum applied pressure of 276 kPa, which is over 15 times greater than the liquid penetration pressure of Tyvek®. The liquid penetration pressure of Tyvek® is concluded to be too small for use in the RAEE system.

The elastic modulus of the Tyvek® and Propore™ membranes is investigated to ensure that the membrane in the RAEE does not deflect more than 1 mm into the air side of the exchanger with the system pressure and cause an air blockage. Two ASTM tensile tests and a bulge test are used to obtain the elastic modulus of the Tyvek® and Propore™ membranes. The effects of a number of parameters, including strain rate, specimen size, relative humidity, and pre-stress are all considered. A design value of 20 MPa is found for Propore™ and a value of 300 MPa is found for Tyvek®. These values are then used to predict the deflection of the membranes in a square screen that is used to support the membrane in the RAEE. Based on a minimal deflection of 1mm, a screen

size with a square opening dimension of 12.7 mm is determined to provide adequate support for the membrane while minimizing the obstruction of heat and mass transfer area. This screen is used in the construction of the second prototype exchanger core (Erb, 2006) and is successful in limiting the deflection of the membrane to 1 mm.

The UV degradation of the two membranes is quantified by comparison of the percent elongation at break and ultimate tensile stress from before and after UV exposure. It is found that both materials have adverse reactions to the UV light and that the exposure time is more dominant than the exposure intensity in the degradation of the mechanical properties of the materials. The Raman shift spectrum and atomic force microscope images are also investigated before and after exposure. Both the Raman and AFM show significant amount of change in the microstructure of the Tyvek® and Propore™ membranes with UV exposure. Both Tyvek® and Propore™ failed catastrophically after weeks of exposure to a moderate amount of UV. It is concluded that Tyvek® and Propore™ are unfit to be used in an RAEE exposed to UVC light.

6.2 Design conclusions

According to the numerical model of Fan et al. (2006), the Propore™ membrane will provide a maximum overall effectiveness of 62% at the ideal operating conditions. The Propore™ membrane tested in the second prototype exchanger only provided a 36% effectiveness.

The standard screen size of 12.7 mm (0.5 in.) provides less than 1mm deflection of the membrane into the air stream when a pressure of 20 kPa is applied to the liquid side of the RAEE system. This is confirmed through theoretical calculations and the testing of Erb (2006). The Tyvek® material has a liquid penetration pressure that is very close to the operating conditions of the system and is therefore not recommended for use in

the RAEE. The air permeability of the Tyvek® is four times greater than that of Propore™ and therefore the chance air contamination from the supply to the exhaust airstreams of the RAEE is greater for the Tyvek® membrane. Both materials are not suitable for use in UVC environments. Propore™ is the recommended membrane for use in the next RAEE exchanger core.

6.3 Future work

This thesis focuses primarily on the Tyvek® and Propore™ membranes since they are the least expensive options at this time and can therefore be readily implemented into a prototype RAEE. All work presented should be repeated for other membranes including, Toray Entrant™, Sympatex®, and especially ePTFE membranes and their laminates. Additional properties to be tested and further analysis include:

- To determine the dependence of the material properties examined in this thesis with temperature. Any significant variation may be important since the RAEE system may experience supply air temperatures from -40^{o}C to 40^{o}C.
- To determine the creep behaviour of any membrane to be used in the RAEE. Since the membrane will be under a constant pressure load, any increase in the membrane deflection with time may block the airflow in the air side of the RAEE.
- To determine the effects of the salt solutions on any membrane under consideration for the RAEE. The effects of the salt solutions used in the RAEE are known to be negligible on Tyvek® and Propore™; however, this may not be the case for other membranes considered for future prototypes of the RAEE.

- To explore the option of creating a new membrane with the required properties for use in an RAEE system, or to further develop existing membranes with properties of the RAEE in mind.

.

LIST OF REFERENCES

AATCC test method 127, 2003. Water resistance: Hydrostatic pressure test, *American Association of Textile Chemists and Colorists*, Research Triangle Park, North Carolina.

ANSI/ARI Standard 1060, 2001. Standard for Rating Air-to-Air Exchangers for Energy Recovery Ventilation Equipment, *Air-Conditioning & Refrigeration Institute*, Arlington, Virginia.

ANSI/ASME 19.1-1998. Test Uncertainty, *American Society of Mechanical Engineers*, New York, New York.

ASHRAE, 2001. ASHRAE Handbook-Fundamentals, *American Society of Heating, Refrigerating, and Air-Conditioning Engineers*, Atlanta, Georgia.

ASHRAE, 2004. ASHRAE Handbook-HVAC System and Equipment, *American Society of Heating, Refrigerating and Air Conditioning Engineers*, Atlanta, Georgia.

ASHRAE standard 90.1, 2004. Energy Standard for Buildings Except Low-Rise Residential, *American Society of Heating, Refrigerating, and Air-Conditioning Engineers*, Atlanta, Georgia.

ASTM F 903-03, 2004. Standard Test Method for Resistance of Materials Used in Protective Clothing to Penetration by Liquids, *ASTM International*, West Conshohocken, Pennsylvania.

ASTM D 779-03, 2003. Standard Test Method for Water Resistance of Paper, Paperboard, and Other Sheet Materials by the Dry Indicator Method, *ASTM International*, West Conshohocken, Pennsylvania.

ASTM D 4595-86, 2001. Standard Test Method for Tensile Properties of Geotextiles by the Wide-Width Strip Method, *ASTM International*, West Conshohocken, Pennsylvania.

ASTM D 882-02, 2002. Standard Test Method for Tensile Properties of Thin Plastic Sheeting, *ASTM International*, West Conshohocken, Pennsylvania.

ASTM E 96-00, 2000. Standard Test Method for Water Vapour Transmission of Materials, *ASTM International*, West Conshohocken, Pennsylvania.

ASTM F 1249-01, 2001. Standard Test Method for Water Vapour Transmission Rate Through Plastic Film and Sheeting Using a Modulated Infrared Sensor, *ASTM International*, West Conshohocken, Pennsylvania.

ASTM F 2298-03, 2003. Standard Test Method for Water Vapor Diffusion Resistance and Air Flow Resistance of Clothing Materials Using the Dynamic Moisture Permeation Cell, *ASTM*, Philadelphia.

Besant, R.W. and Simonson, C.J., 2003. Air-to-air exchangers, *ASHRAE Journal*, 45(4), 42-52.

Butt, T.K., 2005. Water Resistance and Vapor Permeance of Weather Resistive Barriers, *Journal of ASTM International*, 2 (10), 2-15.

CAN/CGSB-4.2 No. 49-99, 1999. Textile Test Methods: Resistance of Materials to Water Vapour Diffusion, *Canadian General Standards Board*, Ottawa.

CES3 database, 2006. Cambridge Engineering Selector, Software package.

Chen, W., Zhang, J.S., and Zhang, Z., 2005. Performance of Air Cleaners for Removing Multiple Volatile Organic Compounds in Indoor Air*, ASHRAE report OR-05-17-2.*

Diffey, B.L., 2002. Sources and measurement of ultraviolet radiation, *Methods,* 28, 4-13.

Dolhan, P.A., 1987. A Comparison of Apparatus Used to Measure Water Vapour Resistance, *Journal of Coated Fabrics*, 17, 96-109.

DuPont™, What is Tyvek®, Retrieved October 19, 2006, from: www.Tyvek®.com/whatisTyvek®.htm.

Erb, B., 2006. Designing and Testing a Run-Around Heat and Moisture Recovery System. Summer Work Report, Department of Mechanical Engineering, University of Saskatchewan, Saskatoon, Saskatchewan.

Fan, H., 2005. Modelling a Run-Around Heat And Moisture Recovery System*, M.Sc. Thesis,* Department of Mechanical Engineering, University of Saskatchewan, Saskatoon, Saskatchewan.

Fan, H., Simonson, C.J., Besant, R.W. and Shang, W., 2006. Performance of a Run-Around System for HVAC Heat and Moisture Transfer Applications Using Cross-Flow Plate Exchangers Coupled with Aqueous Lithium Bromide, *Int. J. HVAC&R Research*, 12 (2), 313-336.

Galbraith, G.H., Kelly, D.J., and McLean, R.C., 2003. Alternative methods for measuring moisture transfer coefficients of building materials, *Research in Building Physics: Proceeding from the 2nd annual conference on Building Physics*, Antwerp, Belgium, 249-254

Gibson, P.W., Kendrich, C., Rivin, D., Charmchi, M., and Sicuranza, L., 1995. An automated dynamic water vapour permeation test method. *Technical Report Natick/TR-95/032*, Natick, Massachusetts.

Gibson, P.W., Elsaiid, A.E., Kendrick, C.E., Rivin, D., and Charmchi, M., 1997. A test Method to Determine the Relative Humidity Dependence of the Air Permeability of Textile Materials, *Journal of Testing and Evaluation,* 25 (4), 416-423.

Gibson, P.W., 2000a. Effect of temperature on water vapour transport through polymer membrane laminates, *Journal of Polymer testing*, 19, (6), 673-691.

Gibson, P.W., 2000b. Water vapour transport properties of textiles, *Clemson University coated fabrics conference*, Clemson, SC, May 9-10.

Hemmingson, H., 2005. Preliminary Testing for Run Around Heat and Moisture Exchanger, *Summer Work Report*, Department of Mechanical Engineering, University of Saskatchewan, Saskatoon, Saskatchewan.

Incropera, F. P.and Dewitt, D. P., 2002. Fundamentals of Heat and Mass Transfer, 4th Edition, John Wiley & Sons Inc., New York.

ISO 15496, 2004. Textiles- measurement of water vapour permeability of textiles for the purpose of quality control, *International Standards Organization*, Geneva, Switzerland.

ISO 12572, 1997. Building Materials – Determination of water vapour transmission properties, *International Standards Organization*, Geneva.

JIS L 1092, 1998. Testing Methods for Water Resistance of Textiles, *Japanese Industrial Standards*, Tokyo, Japan.

Johnson, D.W., Yavuzturk, C., and Pruis, J., 2003. Analysis of heat and mass transfer phenomena in hollow fiber membranes used for evaporative cooling, *Journal of Membrane Science*, 227, 159-171.

Kaczmarek, H, Oldak, D., Malanowski, P., and Chaberska, H., 2005. Effect of short wavelength UV-irradiation on ageing of polypropylene/cellulose compositions, *Journal of Polymer Degradation and Stability*, 88, 189-198.

Kaiser Optical Systems, Inc. Retrieved: October 24, 2006 from: www.kosi.com/raman/resources/tutorial

Kelly, C.T., Tong, L., and White, J.R., 1997. Slow strain-rate testing of polymers with ultraviolet exposure, *Journal of Materials Science*, 32, 851-861.

Kumaran, M.K., 1998. Interlaboratory Comparison of the ASTM Standard Test Methods for Water Vapour Transmission of Materials (E 96-95*), Journal of Testing and Evaluation*, 26 (2), 83-88.

Larson, M.D., 2004. Membrane Selection for a Cross Flow Heat and Moisture Exchanger. NSERC/Venmar CRD Report No. 10, Department of Mechanical Engineering, University of Saskatchewan, Saskatoon, Saskatchewan.

Larson, M.D., 2005. Numerical Modelling of Heat and Mass Transfer Through a Tyvek® Membrane, M.E. 880.3 Term project, Department of Mechanical Engineering, University of Saskatchewan, Saskatoon, Saskatchewan.

Levetin, E., Shaughnessy, R., Rogers, C.A., and Scheir, R., 2001. Effectiveness of Germicidal UV radiation for reducing fungal contamination within Air-Handling Units, *Journal of Applied and Environmental Microbiology*, Aug, 3712-3715.

McCullough, E.A., Myoungsook, K., and Huensup, S., 2003. A comparison of standard methods for measuring water vapour permeability of fabrics, *Measurement science and technology*, 14, 1402-1408.

Menzies, D., Popo, Julia, Hanley, J.A., Rand, T., and Milton, D.K., 2003. Effect of ultraviolet germicidal lights installed in office ventilation systems on workers heath and wellbeing: double-blind multiple crossover trial, *The Lancet*, 362, 1785-1791.

Morillon, V., Debeaufort, F., Blond, G., and Voilley, A., 2000. Temperature influence on moisture transfer through synthetic films, *Journal of Membrane Science*, 168, 223-231.

Nagy, R., 1964. Application and Measurement of Ultraviolet Radiation, *American Industrial Hygiene Association Journal*, 25, 274-281.

Osczevski, R.J., 1996. Water Vapor Transfer Through a Hydrophilic Film at Subzero Temperatures, *Textile Research Journal*, 66 (1), 24-29.

Pacific Nanotechnology, Inc., Retrieved October 27, 2006, from: www.pacificnano.com/afm-tutorial

Paviot, V.M., Vlassak, J.J., and Nix, W.D., 1995. Measuring the mechanical properties of thin metal films by means of the bulge testing of micromachined windows, *Material Research Society Symposium Proceedings,* 356, 579-584.

Scovazzo, P., Burgos, J., Hoehn, A., and Todd, P., 1998. Hydrophilic membrane-based humidity control, *Journal of Membrane Science*, 149, 69-81.

Shyichuk, A.V., White, J.R., Craig, I.H., and Syrotynska, I.D., 2005. Comparison of UV-degradation depth-profiles in polyethylene, polypropylene and ethylene-propylene copolymer, *Journal of Polymer Degradation and Stability*, 88, 415-419.

Small, M.K., and Nix, W.D., 1992. Analysis of the accuracy of the bulge test in determining the mechanical properties of thin films*, Journal of Materials Research*, 7, 1553-1563.

Small, M.K., Vlassak, J.J., Powell, S.F., Daniels, B.J., and Nix, W.D., 1993. Accuracy and reliability of Bulge test experiments, *Material Research Society Symposium Proceedings*, 308, 159-164.

Svennberg, K., and Wadso, L, 2003. A modified cup-method for lightweight and highly permeable materials, *Research in Building Physics: Proceeding from the 2nd annual conference on Building Physics*, Antwerp, Belgium, 177-182.

Tye R.P.,1994. Relevant moisture Properties of Building Construction Materials, Chapter 3, Moisture Control in Buildings, Trechsel, H.R.Ed., *ASTM Manual Series*, MNL 18, 35-53.

VanOsdell, D, and Foarde, K, 2002. Defining the effectiveness of UV lamps installed in circulating air ductwork, *ARTI-21CR/610-40030-01*.

Venmar CES Inc., product descriptions, Retrieved October 26, 2006, from: www.venmarces.com

Vlassak, J.J., and Nix, W.D., 1992. A new bulge test technique for the determination of the Young's modulus and Poisson's ratio of thin films, *Journal of Materials Research*, 7, 3242-3248.

Xiang, Y., Chen, X., and Vlassak, J.J., 2005. Plane-strain bulge test for thin films, *Journal of Materials Research*, 20, 2360-2370.

Zhang, L.Z., and Jiang, Y., 1999. Heat and mass transfer in a membrane-based energy recovery ventilator, *Journal of Membrane Science*, 163, 29-38.

APPENDIX A
DMPC ANALYSIS

The following analysis of the DMPC results is obtained from the work of Gibson (1995, 1997, 2000, 2000a, and 2000b). The analysis of the water vapour diffusion resistance is based on Fick's law of diffusion. For one dimensional diffusion, assuming a linear concentration gradient through the sample the equation is written as,

$$\dot{m}'' = D_m \frac{\Delta C}{\Delta z} \qquad [A.10]$$

where $\dot{m}''$ is the mass flux of vapour through the specimen [kg/(m^2 s)], D_m is the diffusion coefficient of the membrane [m^2/s], ΔC is the concentration difference across the sample [kg/m^3], and Δz is the thickness of the material [m].

In the case of the DMPC where there is a flow along the specimen length, the flux can also be given by the change in concentration from the inlet and outlet of the sample cell on the same side of the specimen. This flux is used for the analysis of the DMPC and is given as,

$$\dot{m}'' = \frac{Q \cdot \delta C}{A} \qquad [A.11]$$

where Q is the volume flow rate in the test cell [cm^3/min], A is the test sample area [m^2], and δC is the change in concentration from the inlet to the exit of the respective side of the cell [kg/m^3].

The volume flow rate provided by the flow controller is referenced to 273.15 K. The actual volume flow rate, Q, is obtained from the indicated volume flow rate and a correction for the test temperature given by,

$$Q = Q_s\left(\frac{T}{T_s}\right) \qquad [A.12]$$

where Q_s is the indicated flow rate [cm^3/min], T is the temperature of the insulated chamber [K], and T_s is the reference temperature of 273.15 K.

It is convenient to work in terms of relative humidity instead of concentration since humidity sensors are used to measure the outgoing streams. The definition of relative humidity is given by,

$$\phi = \frac{p_v}{p_{v,sat}} = \frac{C_v}{C_{v,sat}} \qquad [A.13]$$

where ϕ is the relative humidity [%], p_v and C_v are the vapour pressure [Pa] and the vapour concentration [kg/m^3], respectively, and $p_{v,sat}$ and $C_{v,sat}$, are the saturation vapour pressure [Pa] and the saturation vapour concentration [kg/m^3] respectively.

An empirical equation is used to calculate the saturation vapour pressure which is a function of temperature. The equation is,

$$p_{v,sat} = 614.3\exp\left[17.06\left(\frac{T-273.15}{T-40.25}\right)\right] \qquad [A.14]$$

The value of saturation vapour concentration is then obtained from the saturation vapour pressure using the ideal gas law ,

$$C_{v,sat} = \frac{p_{v,sat}M_w}{RT} \qquad [A.15]$$

where M_w is the atomic mass of water [kg/kmole], and *R* is the universal gas constant [J/(kg kmole)].

Equation [A.11] is rewritten by replacing the concentration difference with the definition of humidity in equation [A.13] and substituting the parameters of equation [A.15] for the saturation concentration. The true flow rate in equation [A.11] is also replaced by equation [A.12] to give the result is terms of the indicated flow rate, the resulting equation is,

$$\dot{m}'' = \frac{\delta\phi \cdot Q_s \cdot p_{v,sat} \cdot M_w}{A \cdot R \cdot T_s} \qquad [A.16]$$

where $\delta\phi$ is the relative humidity difference [%] between the inlet and the outlet on one side of the test cell.

The mass flux through the sample will change based on the humidity gradient across the sample and the sample area. It is useful to compare membranes using a common vapour diffusion resistance defined as,

$$R_m = \left[\frac{\Delta\bar{C}}{\dot{m}''}\right] - R_{bl} \qquad [A.17]$$

where R_m is the vapour diffusion resistance of the membrane [s/m], R_{bl} is the associated boundary layer resistance [s/m], and $\Delta\bar{C}$ is the log mean concentration difference [kg/m^3] across the sample given by,

$$\Delta\bar{C} = \frac{\Delta C_a - \Delta C_b}{\ln\left(\Delta C_a / \Delta C_b\right)} \qquad [A.18]$$

where ΔC_a is the concentration difference [kg/m^3] at one end of the cell and ΔC_b is the concentration difference [kg/m^3] at the other end of the cell i.e. for parallel flow, ΔC_a

will be the difference of the inlet streams and ΔC_b will be the difference of the outlet streams. The log mean concentration difference is used because of the changing concentration gradient over the sample during the test. The effects of counter flow versus parallel flow on the results are further discussed in Section 2.5.1

The boundary layer resistance is known for given flow rates and was determined by Gibson et al. (1995). The boundary layer resistance was determined by measuring the total resistance of various layers of ePTFE membrane and determining the common resistance due to the boundary layer for a given flow condition. It has been determined that the resistance of the ePTFE film is approximately 6 to 8 s/m (Gibson et al., 1995), and the boundary layer resistance is approximately 140 s/m at the standard flow of 2000 cm^3/min. It is common practise to neglect the resistance of the ePTFE membrane and take the measurement of the ePTFE vapour diffusion resistance as a measurement of the boundary layer resistance.

It is very important to maintain zero pressure difference when performing a diffusion test so that there is negligible air flow through the sample. This same control is also used to maintain fixed pressure gradients across the sample during an advection test. The analysis presented above is valid for the case of a pressure gradient although there may be contributions to the mass flux through the sample from advective mass transfer. The relationship between resistance and pressure differential gives insight into the performance of the material under a pressure gradient. In addition to the analysis above, the air permeability of the material can be determined by applying Darcy's equation to the flow through the sample. Darcy's equation is given as,

$$V = -\frac{k_D}{\mu}\frac{\Delta p}{\Delta x} \qquad [A.19]$$

where V is the velocity of the flow [m/s], μ is the dynamic viscosity of the fluid [kg/(m s)], Δp is the pressure difference across the material [Pa] and k_D is the Darcy permeability of the material [m^2].

Rearranging equation [A.19] and replacing the velocity with volume flow rate divided by area, the following expression is obtained for the Darcy permeability,

$$k_D = \left(\frac{\mu \cdot \Delta x}{A}\right)\left(\frac{Q}{\Delta p}\right) \qquad [A.20]$$

where the first term consists of constant properties and the second term is equal to the slope of the flow rate versus pressure graph obtained in the convective test. The flow rate, Q, is measured at the exit of the bottom of the cell and includes the flow entering the cell and any additional flow (or loss) through the material. The initial flow entering the cell does not have to be subtracted from the flow through the sample nor does the measured flow rate need to be corrected for temperature using equation [A.12] since the slope of the flow rate versus pressure difference plot will be unchanged.

For convenience the Darcy permeability can also be represented by a Darcy air flow resistance given as,

$$R_D = \frac{\Delta z}{k_D} \qquad [A.21]$$

where R_D is the Darcy air flow resistance [1/m] and Δz is the membrane thickness [m].

APPENDIX B
UNCERTAINTY OF THE DMPC MEASUREMENTS

The uncertainty analysis of the DMPC is based on the uncertainty analysis method of ANSI/ASME 19.1 (1998). The following gives a brief introduction to the equations used to calculate the uncertainty in measured and calculated parameters.

The uncertainty of a calculated parameter, or result, is a function of the uncertainty of the dependent parameters. The general form of the uncertainty in a calculated parameter is,

$$U_r = \left[\sum_{i=1}^{n} \left(\frac{\partial r}{\partial \bar{x}_i} U_{\bar{x}i} \right)^2 \right]^{1/2} \qquad [B.1]$$

where U_r is the uncertainty in the calculated result at the 95% confidence interval, $U_{\bar{x}}$ is the uncertainty in the mean parameter $\bar{x}$ at the 95% confidence interval, $\partial r/\partial \bar{x}$ is the sensitivity coefficient of the result, r, to the mean parameter $\bar{x}$, i is a counter index, and n is the total number of parameters on which r is dependent.

To determine the uncertainty in a measured parameter the equation is of the general form,

$$U_{\bar{x}} = \left[B_{\bar{x}}^{\,2} + \left(tS_{\bar{x}} \right)^2 \right]^{1/2} \qquad [B.2]$$

where $B_{\bar{x}}$ is the bias in the measurement of parameter $\bar{x}$, $S_{\bar{x}}$ is the precision index of the mean for parameter x, and t is the student t value for the 95% confidence interval which is dependent on the number of measurements taken.

The results in Chapter 2 are given in terms of the vapour diffusion resistance which is given by,

$$R_s = \left[\frac{\Delta \bar{C}}{\dot{m}'' / A} \right] - R_{bl} \qquad [B.3]$$

where the mass flux is given by,

$$\dot{m}'' = \frac{\delta\phi \cdot Q_s \cdot p_s \cdot M_w}{A \cdot R \cdot T_s} \qquad [B.4]$$

and the log mean concentration difference is given by,

$$\Delta \bar{C} = \frac{\Delta C_a - \Delta C_b}{\ln\left(\Delta C_a / \Delta C_b \right)} \qquad [B.5]$$

First, consider the uncertainty in the mass flux which is given by the expanded equation [B.1], or,

$$U_{\dot{m}} = \left[\begin{array}{l} \left(\frac{\partial \dot{m}}{\partial \delta\phi} \cdot U_{\delta\phi} \right)^2 + \left(\frac{\partial \dot{m}}{\partial Q_s} \cdot U_{Q_s} \right)^2 + \left(\frac{\partial \dot{m}}{\partial p_s} \cdot U_{p_s} \right)^2 + \\ \left(\frac{\partial \dot{m}}{\partial M_w} \cdot U_{M_w} \right)^2 + \left(\frac{\partial \dot{m}}{\partial R} \cdot U_R \right)^2 + \left(\frac{\partial \dot{m}}{\partial T_s} \cdot U_{T_s} \right)^2 + \left(\frac{\partial \dot{m}}{\partial A} \cdot U_A \right)^2 \end{array} \right]^{1/2} \qquad [B.6]$$

where U_x is the uncertainty in a parameter x and $\partial \dot{m}'' / \partial x$ is the sensitivity coefficient of the mass flux to the parameter x.

Equation [B.6] can be simplified by the assumption that the following parameters have zero uncertainty or,

$$U_{M_w} = U_R = U_{T_s} = 0 \qquad [B.7]$$

The uncertainty of the indicated flow rate Q_s is 1.5% of the full scale measurement, or 30 cm^3/min, which is given by the manufacturer.

The uncertainty in the saturation pressure is a function of temperature and is given by,

$$U_{p_{v,sat}} = \frac{\partial p_{v,sat}}{\partial T} \cdot U_T \qquad [B.8]$$

where the uncertainty in the temperature is assumed to be 0.2°C.

The specimen area is defined by the clamping plate in the sample holder. The uncertainty in this area, U_A, is assumed to be 0.1%.

The change in the relative humidity on one side of the test cell is given by,

$$\delta\phi = \phi_{out} - \phi_{in} \qquad [B.9]$$

where ϕ_{out} is the humidity exiting the test cell and ϕ_{in} is the humidity at the entrance of the test cell. The uncertainty in the humidity difference is given by,

$$U_{\delta\phi} = \left[\left(\frac{\partial \delta\phi}{\partial \phi_{out}} \cdot U_{\phi_{out}} \right)^2 + \left(\frac{\partial \delta\phi}{\partial \phi_{in}} \cdot U_{\phi_{in}} \right)^2 \right]^{1/2} \qquad [B.10]$$

where the sensitivity coefficient are,

$$\frac{\partial \delta\phi}{\partial \phi_{out}} = 1 \qquad [B.11]$$

and

$$\frac{\partial \delta\phi}{\partial \phi_{in}} = -1 \qquad [B.12]$$

therefore, equation [B.10] simplifies to,

$$U_{\delta\phi} = \left[U_{\phi_{out}}^2 + U_{\phi_{in}}^2 \right]^{1/2} \qquad [B.13]$$

The uncertainty in the humidity at the exit of the test cell is governed by the uncertainty of the Vaisala humidity sensor used to measure the exit humidity. The Vaisala sensor has an uncertainty of 1% for humidities from 0-90% and an uncertainty of 2% for humidities from 90-100%. According to Gibson (2000b) the uncertainty of this sensor can be decreased to 0.5% with in-situ calibration. The uncertainty of the humidity sensor is assumed to be 0.5% for this uncertainty analysis

The uncertainty in the humidity at the entrance of the test cell is governed by the uncertainty of the mass flow controllers that proportionally mix the incoming gas streams, and the concentration of those streams. The incoming concentration is given by,

$$C_{in} = \frac{Q_{dry} \cdot C_{dry} + Q_{sat} \cdot C_{sat}}{Q_{sat} + Q_{dry}} \qquad [B.14]$$

where C_{in} the concentration of the inlet stream [kg/m^3], Q_{dry} is the flow rate of the dry nitrogen [cm^3/min], Q_{sat} is the flow rate of the saturated nitrogen [cm^3/min], C_{dry} is the concentration of the dry nitrogen [kg/m^3], and C_{sat} is the concentration of the saturated nitrogen [kg/m^3]. The uncertainty in the incoming concentration is given by,

$$U_{C_{in}} = \left[\begin{array}{l} \left(\frac{\partial C_{in}}{\partial Q_{sat}} \cdot U_{Q_{sat}} \right)^2 + \left(\frac{\partial C_{in}}{\partial Q_{dry}} \cdot U_{Q_{dry}} \right)^2 \\ + \left(\frac{\partial C_{in}}{\partial C_{sat}} \cdot U_{C_{sat}} \right)^2 + \left(\frac{\partial C_{in}}{\partial C_{dry}} \cdot U_{C_{dry}} \right)^2 \end{array} \right]^{1/2} \qquad [B.15]$$

where the uncertainty in Q_{sat} and Q_{dry} are both equal to 0.8% of the full scale or 16 cm^3/min, and the uncertainty in C_{dry} and C_{sat} is assumed to be 1%.

The humidity of the incoming stream is calculated using the ideal gas law and the definition of humidity given by,

$$\phi_{in} = \frac{C_{in} \cdot R \cdot T}{p_{sat} M_w} \qquad [B.16]$$

The uncertainty in the incoming humidity is given by,

$$U_{\phi_{in}} = \left[\left(\frac{\partial \phi_{in}}{\partial C_{in}} \cdot U_{C_{in}} \right)^2 + \left(\frac{\partial \phi_{in}}{\partial T} \cdot U_T \right)^2 + \left(\frac{\partial \phi_{in}}{\partial p_{v,sat}} \cdot U_{p_{v,sat}} \right)^2 \right]^{1/2} \qquad [B.17]$$

where the uncertainty of all parameters have already been determined.

The uncertainty of the incoming humidity is substituted into equation [B.13] to determine the uncertainty in the humidity difference. This uncertainty is then substituted into equation [B.6] to obtain the uncertainty in the mass flux.

Neglecting the boundary layer uncertainty, the uncertainty in the resistance is given by,

$$U_{R_s} = \left[\left(\frac{\partial R_s}{\partial \Delta \bar{C}} \cdot U_{\Delta \bar{C}} \right)^2 + \left(\frac{\partial R_s}{\partial \dot{m}''} \cdot U_{\dot{m}''} \right)^2 \right]^{1/2} \qquad [B.18]$$

where the uncertainty of the log mean concentration difference is given by,

$$U_{\Delta \bar{C}} = \left[\left(\frac{\partial \Delta \bar{C}}{\partial \Delta C_a} \cdot U_{\Delta C_a} \right)^2 + \left(\frac{\partial \Delta \bar{C}}{\partial \Delta C_b} \cdot U_{\Delta C_b} \right)^2 \right]^{1/2} \qquad [B.19]$$

where, for parallel flow, ΔC_a is the difference of the inlet flows and ΔC_b is the difference of the outlet flows. The uncertainty of the inlet flows are given by equation [B.15] and the uncertainty of the outlet flows are governed by the uncertainty of the Vaisala sensors.

Substituting the uncertainties of the inlet and outlet flows into equation [B.19], the uncertainty of the log mean concentration difference is calculated. The log mean concentration uncertainty and the mass flux uncertainty of equation [B.6] are then substituted into equation [B.18] to determine the overall uncertainty in the vapour diffusion resistance.

APPENDIX C
NUMERICAL MODEL OF FAN ET AL. (2005)

The steady-state operating condition for the RAEE system occurs when the total heat and mass transfer rates in the exhaust and supply exchangers are balanced, i.e. when energy and mass are balanced. The following assumptions are used in the numerical model of Fan (2005).

- The heat and mass transfer processes are in steady state and only in the z direction normal to each membrane (Figure 1.5).
- The channel flow and the heat and mass transfer processes are fully developed throughout the exchanger.
- Heat gain or loss due to the latent heat from the phase change of water at the membrane occurs only in the liquid component.
- Heat and mass transfer occurs only within each exchanger (i.e., no heat and mass transfer between the exchangers or connecting piping and ambient air).
- The bulk mean coupling fluid temperature and water concentration at the exit of one exchanger can be used for the entrance to the downstream exchanger.
- Pumping energy for the liquid side and fan energy for the air side considered negligible.

To begin the simulation, the initial conditions of the air supply and exhaust return are input by the user. In this thesis, these conditions are always the ARI summer test conditions given in Table 2.4. The simulation begins with an arbitrary temperature and concentration of the incoming liquid on the supply side. The simulation then starts iterating the physical properties, the parameters of the inlet and outlet conditions for each exchanger, and the balance of heat and mass in the loop of the RAEE.

The energy balance equations for the heat and mass at any point on the air side of a single exchanger is given by,

$$2NTU_{m,Air}(W_{Air} - W_{Sol}) = -\frac{\partial W_{Air}}{\partial x^*} \quad [C.1]$$

and

$$2NTU_{Air}\left(T_{Air} - T_{Sol}\right) = -\frac{\partial T_{Air}}{\partial x^*} \quad [C.2]$$

where W is the humidity ratio [$g_{water\ vapour}$ /$kg_{dry\ air}$], T is the temperature [K], x* is the dimensionless co-ordinate of x and NTU_{air} is given by,

$$NTU_{Air} = \frac{Ux_0y_0}{\left(\dot{m}c_p\right)_{Air}} \quad [C.3]$$

and $NTU_{m,air}$ is given by,

$$NTU_{m,Air} = 2 \cdot \frac{U_m x_0 y_0}{\dot{m}_{Air}} \quad [C.4]$$

where x_o and y_o are the dimensions of the exchanger [m], $\dot{m}$ is the mass flow rate of air [kg/s], c_p is the specific heat capacity of air [J/(g K)], and the overall heat transfer coefficient, U, is given by,

$$U = \left[\frac{1}{g_{Sol}} + \frac{\Delta z}{k} + \frac{1}{g_{Air}}\right]^{-1} \quad [C.5]$$

and the overall coefficient of mass transfer, U_m, is given by,

$$U_m = \left[\frac{1}{g_{m,Sol}} + \frac{\Delta z}{k_m} + \frac{1}{g_{m,Air}} \right]^{-1} \qquad [C.6]$$

where Δz is the membrane thickness [m], k is the thermal conductivity of the membrane material [W/(m K)], g_{sol} and g_{air} are the convective heat transfer coefficients of the solution and air respectively [W/ (m^2 K)], k_m is the vapour permeability of the membrane [kg/(m s)], and $g_{m,sol}$ and $g_{m,air}$ are the convective mass transfer coefficients [kg/(m^2 s)].

The convective heat transfer coefficients are determined from the Nussult number for fully developed laminar flow between infinite plates. The convective mass transfer coefficients are determined from the convective heat transfer coefficients using the Chilton-Colburn analogy.

Similarly, the energy balance equations for any point of a single exchanger on the solution side are given by,

$$2NTU_{m,Sol}(W_{Air} - W_{Sol}) = \frac{\partial X_{Sol}}{\partial y^*} \qquad [C.7]$$

and

$$2NTU_{Sol}\left(T_{Air} - T_{Sol}\right) = \frac{\partial T_{Sol}}{\partial y^*} - \frac{2U_m x_0 y_0}{\left(\dot{m} c_p\right)_{Sol}}(W_{Air} - W_{Sol}) \cdot h_{fg} \qquad [C.8]$$

where X is the concentration of the solution [kgw/kgd], y* is a dimensionless coordinate in y, and NTU_{sol} is given by,

$$NTU_{Sol} = \frac{U_m x_0 y_0}{\left(\dot{m} c_p\right)_{Sol}} \qquad [C.9]$$

and $NTU_{m,sol}$ is given by,

$$NTU_{m,Sol} = 2 \cdot \frac{U_m x_0 y_0}{\dot{m}_{Sol}} \qquad [C.10]$$

To couple two individual exchangers into a run-around loop the energy and mass must be conserved throughout the liquid loop. The equations for energy and mass transfer rates are given by the following equations where for the supply exchanger, the energy transfer rate between the air and liquid is

$$\begin{aligned} q_{Sup} &= \left(\dot{m}c_p\right)_{AirSup,in} T_{AirSup,in} - \left(\dot{m}c_p\right)_{AirSup,out} T_{AirSup,out} + \dot{m}_{Supply} \cdot h_{fg} \\ &= \left(\dot{m}c_p\right)_{LiquidSupply,out} T_{LiquidSupply,out} - \left(\dot{m}c_p\right)_{LiquidSupply,in} T_{LiquidSupply,in} \end{aligned} \qquad [C.11]$$

and the mass transfer rate between the air and liquid is

$$\begin{aligned} \dot{m}_{membrane} &= \dot{m}_{Salt}(X_{LiquidSupply,out} - X_{LiquidSupply,in}) \\ &= \dot{m}_{Air}(W_{AirSupply,in} - W_{AirSupply,out}) \end{aligned} \qquad [C.12]$$

The heat and mass transfer balance in the exhaust exchanger is given by the same equations with the appropriate exhaust temperatures and heat capacities.

The run-around system is considered balance when the heat transfer rate and the mass transfer rate of the supply and exhaust exchangers are within the tolerance limits set in the computer simulation.

The most important property in terms of quantifying the results of the RAEE is the total effectiveness of the exchanger. The effectiveness of the exchanger is given the following general definition,

$$\varepsilon = \frac{\text{Actual heat transfer rate}}{\begin{array}{l}\text{Maximum possible heat transfer rate of an exchanger with} \\ \text{an infinite heat transfer area and the same operating conditions}\end{array}} \quad [C.13]$$

From the definition of equation [C.13] the following effectiveness values of the RAEE system are defined. Assuming that the air mass flow rate of the supply and exhaust streams are equal. The sensible effectiveness is given by,

$$\varepsilon_{sen} = \frac{T_{AirSupply,in} - T_{AirSupply,out}}{T_{AirSupply,in} - T_{AirExhaust,in}} = \frac{T_{AirExhaust,out} - T_{AirExhaust,in}}{T_{AirSupply,in} - T_{AirExhaust,in}} \quad [C.14]$$

similarly, the latent effectiveness of the RAEE is,

$$\varepsilon_{lat} = \frac{W_{AirSupply,in} - W_{AirSupply,out}}{W_{AirSupply,in} - W_{AirExhaust,in}} = \frac{W_{AirExhaust,out} - W_{AirExhaust,in}}{W_{AirSupply,in} - W_{AirExhaust,in}} \quad [C.15]$$

and the total effectiveness of the RAEE is,

$$\varepsilon_{tot} = \frac{H_{AirSupply,in} - H_{AirSupply,out}}{H_{AirSupply,in} - H_{AirExhaust,in}} = \frac{H_{AirExhaust,out} - H_{AirExhaust,in}}{H_{AirSupply,in} - H_{AirExhaust,in}} \quad [C.16]$$

.